

Dynamic Wireless Access Methods with Applications to eHealth Services

by

Phond Phunchongharn

A Thesis Submitted to the Faculty of Graduate Studies of
the University of Manitoba
in Partial Fulfillment of the Requirements for the Degree of

DOCTOR OF PHILOSOPHY

Department of Electrical and Computer Engineering
University of Manitoba
Winnipeg

© Phond Phunchongharn, 2012

Supervisor: Prof. E. Hossain

ABSTRACT

For opportunistic spectrum access and spectrum sharing in cognitive radio networks, one key problem is how to develop wireless access schemes for secondary users so that harmful interference to primary users can be avoided and quality-of-service (QoS) of secondary users can be guaranteed. In this research, dynamic wireless access protocols for secondary users are designed and optimized for both infrastructure-based and ad-hoc wireless networks.

Under the infrastructure-based model, the secondary users are connected through a controller (i.e., an access point). In particular, the problem of wireless access for eHealth applications is considered. In a single service cell, an innovative wireless access scheme, called electromagnetic interference (EMI)-aware prioritized wireless access, is proposed to address the issues of EMI to the medical devices and QoS differentiation for different eHealth applications. Afterwards, the resource management problem for multiple service cells, specifically, in multiple spatial reuse time-division multiple access (STDMA) networks is addressed. The problem is formulated as a dual objective optimization problem that maximizes the spectrum utilization of secondary users and minimizes their power consumption subject to the EMI constraints for active and passive medical devices and minimum throughput guarantee for secondary users. Joint scheduling and power control algorithms based on greedy approaches are proposed to solve the problem with much less computational complexity.

In an ad-hoc wireless network, the robust transmission scheduling and power control problem for collision-free spectrum sharing between secondary and primary users in STDMA wireless networks is investigated. Traditionally, the problem only considers the average link gains; therefore, QoS violation can occur due to improper power allocation with respect to instantaneous channel gain realization. To overcome this problem, a robust power control problem is formulated. A column generation based algorithm is proposed to solve the problem by considering only the potential subset

of variables when solving the problem. To increase the scalability, a novel distributed two-stage algorithm based on the distributed column generation method is then proposed to obtain the near-optimal solution of the robust transmission schedules for vertical spectrum sharing in an ad-hoc wireless network.

Table of Contents

Abstract	ii
Table of Contents	iv
List of Figures	x
List of Tables	xiii
List of Abbreviations	xiv
Acknowledgement	xvii
Dedication	xviii
1 Introduction	1
1.1 Infrastructure vs. Ad-hoc Networks	2
1.2 Cognitive Radio	3
1.3 Potential Wireless Devices and Technologies for Cognitive Radio Environment	4
1.3.1 Wireless Devices for Cognitive Radio Environment	4
1.3.2 Wireless Networking Technologies and Services for Cognitive Radio Environment	5
1.4 Healthcare Environment	7
1.4.1 Challenges in a Clinical Environment	7
1.4.1.1 Human Error	7
1.4.1.2 Information Accessibility	7
1.4.1.3 Service Accessibility	8
1.4.1.4 Continuous Monitoring	8
1.4.1.5 Time Efficiency	8

1.4.2	Examples of Healthcare Applications and Their Technical Requirements	9
1.4.2.1	Electronic Medical Record (EMR)	9
1.4.2.2	Patient Monitoring System	9
1.4.2.3	Clinician Notifier	10
1.4.2.4	Telemedicine	10
1.4.2.5	Wireless Medicine (Wireless Meds)	10
1.4.2.6	Tracking System	11
1.4.2.7	Intelligent Emergency Management System	11
1.4.2.8	Advanced Physical Rehabilitation System	11
1.4.3	Electronic Medical Devices: Examples and Classifications	13
1.5	Issues Involved in Using Wireless Technology in a Hospital Environment	13
1.5.1	Electromagnetic Interference (EMI)	15
1.5.1.1	Impact of EMI on Biological Systems	16
1.5.1.2	Electromagnetic Interference Caused to Medical Devices	17
1.5.2	Electromagnetic Compatibility (EMC)	17
1.5.2.1	Electromagnetic Compatibility for Medical Devices	18
1.5.2.2	Electromagnetic Compatibility for Wireless Transmitters	21
1.6	Requirements for Wireless Communications Systems Used in eHealth Applications	23
1.7	Contributions of the Thesis	24
1.7.1	EMI-aware Prioritized Wireless Access Protocol for a Single Service Cell in an Infrastructure-based Wireless Network	25
1.7.2	EMI-aware Transmission Scheduling and Power Control for Multiple Service Cells in an Infrastructure-based Wireless Network	26
1.7.3	Robust Scheduling and Power Control for an Ad-hoc Cognitive STDMA Wireless Network	27
1.7.4	Distributed Robust Scheduling and Power Control for an Ad-hoc Cognitive STDMA Wireless Network	28

2	EMI-Aware Prioritized Wireless Access Scheme for a Single Service Cell	29
2.1	Related Work	30
2.2	EMI-Aware Prioritized Wireless Access Scheme	32
2.2.1	System Overview	32
2.2.2	System Architecture for EMI-Aware Prioritized Wireless Access	33
2.2.3	EMI-Aware Prioritized Wireless Access Scheme	35
2.2.3.1	Common Control Broadcasting	37
2.2.3.2	EMI-Aware RTS-CTS Protocol for Uplink Request Transmission	40
2.2.3.3	EMI-Aware RTS-CTS Protocol for Downlink Request Transmission	41
2.2.3.4	Prioritized Queue Management and Data Transmission	42
2.3	Queuing Analysis of the Prioritized Wireless Access Scheme	43
2.3.1	Queuing Model and Assumptions	44
2.3.2	Discrete-Time Markov Chain (DTMC) Model	45
2.3.3	Performance Measures	47
2.3.3.1	Average Transmission Delay of High-priority Users .	47
2.3.3.2	Loss Probability of Low-priority Users	48
2.4	System Performance Optimization and Prediction	48
2.4.1	Optimization of Blocking Probabilities for EMI-Aware Priori- tized Wireless Access Scheme	49
2.4.2	Exponential Moving Average Prediction Model	50
2.5	Performance Evaluation	51
2.5.1	Simulation Setup	52
2.5.1.1	Evaluation Scenario	52
2.5.1.2	System Configurations for EMI-Aware Prioritized Wire- less Access System	53
2.5.2	Performance Evaluation of the EMI-Aware RTS-CTS Protocol	54
2.5.3	Performance Evaluation of EMI-Aware Prioritized Wireless Access Protocol	56
2.5.3.1	Effects of Transmission Durations	56

2.5.3.2	Effects of Blocking Probabilities	58
2.5.3.3	Comparison with Other Scheduling Schemes	60
2.5.4	Performance Evaluation of EMI-Aware Prioritized Wireless Access Protocol Integrated with EMA Prediction Model	62
2.5.5	Summary of the Results and Discussions	64
2.6	Implementation of the EMI-Aware Prioritized Wireless Access Scheme	65
2.7	Conclusion	66

3	EMI-Aware Transmission Scheduling and Power Control for Multi- ple Service Cells	67
3.1	Related Work	69
3.2	System Model and Assumptions	70
3.2.1	Primary and Secondary Network Models	70
3.2.2	Wireless Transmission Model	72
3.2.3	Wireless Channel Model	73
3.3	Optimization Formulation for Transmission Scheduling and Power Control	73
3.3.1	Interference Modeling for Protected Users	73
3.3.2	Interference Modeling for Primary Users	74
3.3.3	QoS Modeling for Secondary Users	74
3.3.4	Formulation of the Dual-Objective Optimization Problem	75
3.4	Proposed Algorithms	76
3.4.1	Joint Scheduling and Power Control Algorithm Based on Trans- mit Power Minimization	76
3.4.2	Enhanced Greedy Algorithm Based on Interference Minimization	79
3.5	Performance Evaluation	80
3.5.1	Simulation Parameters	80
3.5.2	Simulation Results	82
3.5.2.1	Spectrum utilization by secondary networks	85
3.5.2.2	Power consumption of secondary networks	86
3.5.2.3	Electromagnetic interference level	88
3.5.2.4	Computation time for the proposed algorithms	88
3.6	Conclusion	89

4	Robust Scheduling and Power Control for an Ad-Hoc STDMA Wireless Network	92
4.1	Related Work and Key Contributions of the Chapter	94
4.2	System Model and Assumptions	96
4.2.1	Network and Channel Model	96
4.2.2	Feasible Access Patterns	97
4.3	Formulation of the Robust Transmission Scheduling and Power Control Problem	98
4.3.1	The Nominal Problem	98
4.3.2	Modeling Channel Uncertainty	99
4.3.3	Modeling Traffic Demand Uncertainty	100
4.3.4	Complexity of the Robust Scheduling and Power Control Problem	101
4.4	A Stabilized Column Generation-Based Algorithm for Transmission Scheduling and Power Control	102
4.4.1	Classical Column Generation Method	102
4.4.2	Stabilized Column Generation Method	103
4.5	Pricing Problem for Robust Scheduling and Power Control	106
4.5.1	Pricing Problem	106
4.5.2	A Heuristic Algorithm to Solve the Pricing Problem	108
4.5.3	Initial Feasible Access Patterns	110
4.6	Performance Evaluation	111
4.6.1	Heuristic Pricing Algorithm	111
4.6.2	Stabilized Column Generation	113
4.6.3	Robust Scheduling and Power Control	115
4.7	Conclusion	119
5	Distributed Robust Scheduling and Power Control for an Ad-Hoc Cognitive STDMA Network	120
5.1	System Model and Assumptions	123
5.1.1	Network Model	123
5.1.2	Feasible Access Patterns	124
5.2	Nominal and Robust Transmission Scheduling and Power Control Problem Formulations	125

5.2.1	Nominal Problem Formulation	125
5.2.2	Robust Problem Formulation with Ellipsoidal Uncertainty Set	126
5.3	Classical Column Generation and Distributed Column Generation Methods For Robust Transmission Scheduling and Power Control Prob- lem	129
5.3.1	Classical Column Generation Method	129
5.3.2	Distributed Column Generation Method	130
5.3.2.1	A Distributed Algorithm to Solve the Restricted Mas- ter Problem	130
5.3.2.2	A Distributed Algorithm to Solve the Pricing Problem	131
5.3.3	Convergence of the Distributed Algorithms	138
5.4	Bounds on the SINR Constraint Violation and Expected Number of Transmission Length for Secondary Users	139
5.4.1	Probabilistic Bound on the SINR Constraint Violation	139
5.4.2	Bounds on the Expected Number of Transmission Length	142
5.5	Performance Evaluation	144
5.5.1	Simulation Parameters	144
5.5.2	Simulation Results	144
5.5.2.1	Impact of $\zeta^{(th)}$ on the Proposed Distributed Algorithm	144
5.5.2.2	Distributed Transmission Scheduling and Power Con- trol Based on Column Generation Method	145
5.5.2.3	Validation of the Probabilistic Bound on the SINR Constraint Violation	148
5.5.2.4	Bound on the Expected Transmission Length	150
5.6	Conclusion	151
6	Summary and Discussions	154
6.1	Summary of Contributions	154
6.2	Future Work	158
	Bibliography	160
	Appendix A Inner Matrix $\mathbf{A}_{k,k-1}$, $\mathbf{A}_{k,k}$, and $\mathbf{A}_{k,k+x_1}$	170

List of Figures

Figure 2.1	EMI-aware prioritized wireless system for eHealth in a hospital environment.	34
Figure 2.2	Flowchart of EMI-aware prioritized wireless access scheme for uplink request transmission.	36
Figure 2.3	Flowchart of EMI-aware RTS-CTS protocol for downlink transmission.	42
Figure 2.4	Queuing model for the EMI-aware prioritized wireless access system.	44
Figure 2.5	Interference probability over 9 service areas.	55
Figure 2.6	Outage probability over 9 service areas.	56
Figure 2.7	Performance evaluation with variations of β_1 and β_2	57
Figure 2.8	Performance evaluation with variations of P_{d1} and P_{d2}	59
Figure 2.9	Performance evaluation compared with other scheduling schemes	61
Figure 2.10	Overall throughput compared with other scheduling schemes.	62
Figure 2.11	The probability of violation.	63
Figure 3.1	A multiple service cell scenario in a hospital environment.	68
Figure 3.2	Percentage of spectrum utilization versus the total required time slots per frame.	85
Figure 3.3	Average power consumption per time slot versus the total required time slots per frame.	87
Figure 3.4	Minimum SINR of primary users.	87
Figure 3.5	Maximum electric fields experienced by the protected users.	88
Figure 3.6	Optional caption for list of figures	90
Figure 4.1	The block diagram of the robust transmission scheduling and power control framework.	94

Figure 4.2	The flowcharts for the classical column generation and stabilized column generation methods.	104
Figure 4.3	The flowchart of the Weighted Interference Criterion Greedy (WICG) algorithm.	109
Figure 4.4	Average number of secondary removal links and the total number of secondary links.	112
Figure 4.5	Average computation time in seconds and the total number of secondary links.	113
Figure 4.6	Average number of iteration and the bounds of slack and surplus variables \mathbf{e}	114
Figure 4.7	Average transmission length and the bounds of slack and surplus variables \mathbf{e}	114
Figure 4.8	Variation in the average transmission length with the robustness parameter for channel uncertainty, τ	116
Figure 4.9	Variation in the probability of secondary traffic demand violation with the robustness parameter for traffic demand uncertainty, ϵ	117
Figure 4.10	Variation in the average transmission length with the robustness parameter for traffic demand uncertainty, ϵ	118
Figure 5.1	The column generation method.	122
Figure 5.2	The frame structure.	124
Figure 5.3	Average transmission length with $\zeta^{(th)}$	145
Figure 5.4	Comparison with the centralized scheduling in terms of average transmission length.	146
Figure 5.5	Comparison with other distributed schemes in terms of average transmission length.	147
Figure 5.6	Comparison with other distributed schemes in terms of average number of iterations.	147
Figure 5.7	Power evolution of secondary links during the first phase for solving the pricing problem.	149
Figure 5.8	Comparison between the probabilistic bound on P^v and the simulation results with variation of ϵ	149

Figure 5.9 Comparison between the probabilistic bound on P^v and the simulation results with variation of σ 150

Figure 5.10 Bound on the expected transmission length and the simulation results. 151

Figure 5.11 Variation in the expected transmission length and the simulation results. 152

List of Tables

Table 1.1	Requirements of eHealth applications [4]	12
Table 1.2	Applications of wireless technologies in eHealth applications . .	13
Table 1.3	Classification of medical devices [31]-[34]	14
Table 1.4	Electromagnetic spectrum [35]	15
Table 1.5	Electromagnetic compatibility requirements for medical devices and standards for test methods and equipments [43]	20
Table 1.6	Limits for the maximum radio frequency energy exposure [35] .	22
Table 3.1	Key notations	71
Table 3.2	Protected users in the simulation setup	83
Table 3.3	Primary and secondary users in the simulation setup	84
Table A.1	Events that can occur during an RTS time slot	171
Table A.2	Elementary matrices of $\mathbf{U}\mathbf{1}_k^{(j)}$	173
Table A.3	Elementary matrices of $\mathbf{V}_k^{(j,j)}$	174

List of Abbreviations

3G	Third Generation
ACK	Acknowledge
ARQ	Automatic Repeat reQuest
BAN	Body Area Network
CCU	Critical Care Unit
CDMA	Code-Division Multiple Access
CPR	Cardiopulmonary Resuscitation
CPU	Central Processing Unit
CSCR	Combined Sum Criterion Removal
CSMA/CA	Carrier Sense Multiple Access with Collision Avoidance
CTS	Clear-to-Send
DCF	Distributed Coordination Function
DCPC	Distributed Constrained Power Control
DIFS	DCF Inter-Frame Space
DSA	Dynamic Spectrum Access
ECG	Electrocardiograph
EDD	Earliest Due Date
EDS	Electrostatic Discharge
EEG	Electroencephalography
EFT	Electrical Fast Transients
eHealth	Electronic Health
EM	Electromagnetic
EMA	Exponential Moving Average
EMC	Electromagnetic Compatibility
EMG	Electromyography
EMI	Electromagnetic Interference
EMR	Electronic Medical Record

FAF	Floor Attenuation Factor
FCC	Federal Communications Commission
FCFS	First-Come-First-Served
FDA	Food and Drug Administration
FDMA	Frequency-Division Multiple Access
HIS	Hospital Information System
ICU	Intensive Care Unit
ID	Identification
IEC	International Electrotechnical Commission
IP	Integer Programming
IR	Infrared
ISM	Industrial, Scientific and Medical
IT	Information Technology
LED	Light Emitting Diode
LOS	Line-of-Sight
LP	Linear Programming
LTE	Long Term Evolution
MAC	Medium Access Control
MADWIFI	Multiband Atheros Driver for Wi-Fi
MICS	Medical Implant Communications Service
MIP	Mixed-Integer Programming
NMSE	Normalized Mean Square Error
NP	Nondeterministic Polynomial Time
OFDM	Orthogonal Frequency-Division Multiplexing
OR	Operating Room
PCF	Point Coordination Function
PDA	Personal Digital Assistants
QoS	Quality of Service
RAC	Radio Access Controller
RAM	Random Access Memory
RF	Radio Frequency
RFID	Radio-Frequency Identification
RTS	Request-to-Sent

SIFS	Short Inter-Frame Space
SINR	Signal-to-Interference-plus-Noise Ratio
STDMA	Spatial-Reuse Time-Division Multiple Access
TDMA	Time-Division Multiple Access
UNII	Unlicensed National Information Infrastructure
UWB	Ultra Wide-Band
VoWLAN or VoWiFi	Voice over WLAN
WICG	Weighted Interference Criterion Greedy
WLAN	Wireless Local Area Network
WMTS	Wireless Medical Telemetry Service
WPAN	Wireless Personal Area Network
WWAN	Wireless Wide Area Network

Acknowledgement

First and foremost, I would like to express my deep gratitude to my supervisor, Dr. Ekram Hossain, for his continuing guidance, support, and encouragement throughout my Ph.D. program. He is a great academic mentor with very understanding, open-minded, and tremendous patient characteristics. He has not only opened my mindset to a new research direction but also taught me how to complete the work properly. My great appreciation goes to Dr. Simon Haykin, Dr. Rasit Eskicioglu, Dr. Robert McLeod, and Dr. Jun Cai for being my committees. Their invaluable suggestions have helped me to improve this thesis. I am also very grateful to Dr. Sergio Camorlinga for his insightful guidance, which has helped me a lot in my research work. My sincere thanks go to Dr. Dusit Niyato, Dr. Long Le, and Dr. Kaewon Choi for their helpful feedbacks when we collaborated on the conference and journal papers which are parts of this thesis.

I would like to acknowledge Telecommunications Research Laboratory (*TRLabs*) and Natural Sciences and Engineering Research Council of Canada (NSERC) for the financial supports. Many thanks go to the rest of the faculty members and all of the staff members in the ECE department and *TRLabs* for their help and support. In particular, Judy, Amy, and Patricia have always kindly facilitated me and took care of my paperwork in all occasions. I also sincerely thank my colleagues, especially, P’Pan, Ming and Bharat for their help in many occasions. Many thanks go to my friends in Winnipeg, particularly Thai friends, for their friendship and support. My gratitude also goes to my Canadian friends and family, the Rempels (my Canadian family), the Khaus, and Alice, for their help and warmth hearts. I am thankful to my best friend forever, Beow (K), for his care and encouragement that have enabled me to hurdle the difficult situations throughout my life and study.

Last but not least, I would like to express my deepest appreciation to my parents, Sarn and Lamai Phunchongharn for their unconditional love and many sacrifices they have made for me. I am also grateful to my sister and brothers, Vilai Saerayossakul, Ekkasit Phunchongharn, and Sarun Phunchongharn, for always believing in me. I would not have been able to complete this thesis without the support from all my family members. This thesis is dedicated to them.

To my family

Chapter 1

Introduction

During the last few years, the demand for wireless services has dramatically increased. This has in turn created the demand for more radio spectrum and improved radio spectrum utilization for the existing wireless communications systems. However, the traditional wireless communications systems statically utilize the frequency bands and hence lack adaptability. With the static spectrum allocation, some frequency bands are not efficiently utilized. To enhance the spectrum efficiency, the concept of cognitive radio has been introduced. A cognitive wireless node can adaptively transmit and receive data in a dynamic radio environment through dynamic spectrum access. For the next generation wireless networks, cognitive radio based on dynamic spectrum access has emerged as a new spectrum licensing paradigm. The objective is to maximize the utilization of the limited radio bandwidth, while accommodating more services and applications to wireless networks. The new spectrum licensing paradigm is more flexible by allowing low-priority (or secondary) users to opportunistically access the spectrum as long as the high-priority (or primary) users are not harmfully interfered. Dynamic spectrum access is the key approach in a cognitive radio network for improving the spectrum utilization and enhancing the performance of the wireless system under the controlled interference environment.

In healthcare environments, wireless technologies have been employed for electronic Health (eHealth) applications to provide mobility and service availability. Example eHealth applications which utilize wireless technology include electronic medical record, remote patient monitoring, telemedicine etc. [1],[2]. Despite its numerous benefits, an extensive use of wireless communications can interfere with electromagnetic interference (EMI)-sensitive medical devices. The interference can cause malfunctioning of those medical devices [3] (e.g., automatic shutdown, automatic restart,

waveform distortion and howling), which can potentially be harmful to patients using healthcare services. Furthermore, wireless transmissions from secondary eHealth applications can cause harmful interference to communications of wireless medical devices. Consequently, wireless communications systems to be used for eHealth applications, especially in healthcare centers such as in a hospital or a clinic, have to be carefully designed to avoid this EMI problem. Unfortunately, the traditional IEEE 802.11-based wireless local area networks (WLANs) do not take this EMI issue into account. Also, different medical applications have different requirements. Again, the conventional systems for nonmedical applications may not be able to support QoS guarantees (e.g., delay and loss probability) for medical applications [4].

Motivated by these problems, in this thesis, we aim at developing dynamic wireless access methods and related techniques for secondary users in eHealth services. We first give an overview of infrastructure and ad-hoc network models which are the potential network models employed in the healthcare services. Next, cognitive radio concept and potential wireless devices and technologies are described. We further provide an overview of the healthcare environment. Challenges and requirements involved in using wireless communications systems in eHealth services are then described. Finally, we briefly introduce the main contributions of this thesis.

1.1 Infrastructure vs. Ad-hoc Networks

There are two types of configurations in wireless network which are infrastructure and ad-hoc model. The infrastructure mode connects the wireless devices through a common controller (i.e., access point) while ad-hoc mode allows the devices to connect directly [5]. The benefits of the infrastructure mode are as follows:

- Expanding the wired network with the wireless capability: An access point allows the communication among the wired and wireless devices.
- Increasing the range of the wireless network: The network range can be increased by adding more access points.
- Exploiting roaming ability: the wireless devices can roam from one area to another area without connection loss when multiple access points are installed in those areas.

On the other hand, an ad-hoc network, also called a peer-to-peer network is simple to set up and inexpensive due to no need of an access point. Moreover, the throughput rates between two wireless nodes directly connected in the ad-hoc network is twice faster than using the infrastructure network because the infrastructure mode takes time to send the signal to and from the access point rather than directly send to its destination. However, spectrum sharing in both wireless network modes requires efficient spectrum access techniques to maximize the system throughput, increase spectrum utilization and satisfy the QoS requirements of secondary users and interference constraints of primary users.

1.2 Cognitive Radio

Cognitive radio is a communications system with self-awareness of the radio environment (e.g., spectrum usage, power spectral density, and wireless protocol signalling) that efficiently uses spectrum in an intelligent way. The cognitive radio was first introduced in [6]-[8]. Since the radio spectrum in the traditional wireless systems is underutilized and the spectrum demands from emerging wireless applications increase, the new generation of wireless communications requires the development of new spectrum allocation policies. The new spectrum allocation policies should realize a flexible and efficient usage of the spectrum. This allows the secondary users (i.e., lower priority users) to opportunistically exploit the spectrum without causing any harmful performance degradation (due to the interference) in the primary users (i.e., higher priority users) by using cognitive radio technology. A cognitive radio is implemented based on the concept of dynamic spectrum access (DSA). DSA can be grouped into two types, namely, horizontal spectrum sharing and vertical spectrum sharing. In the former case, all users/nodes have equal priority, while in the latter case, user/nodes have different priorities to access the spectrum. In this thesis, the vertical spectrum sharing in a cognitive radio network is emphasized.

The cognitive ways that secondary cognitive users exploit the spectrum can be categorized into three types [9] as follows:

- Interference avoidance (spectrum interweave): The secondary users can coexist with the primary users by being orthogonal to each other. They may access

the spectrum with any collision-free scheme (e.g., time-division multiple access (TDMA), frequency-division multiple access (FDMA)). The cognition in the interference avoidance is the ability to accurately detect the presence of other wireless devices, detect the white space (i.e., spatial, temporal, and spectral gaps), and adjust their transmissions to fill in the spectral void.

- Interference control (spectrum underlay): The secondary and primary users can coexist in the same spectrum in the way that the interference at the primary receivers is controlled below an acceptable threshold which can be derived from the QoS requirements of primary users. The cognition in the interference control is the knowledge of the acceptable interference threshold and the interference gains caused by cognitive transmitters at the primary users in the transmission ranges.
- Interference mitigation (spectrum overlay): The secondary and primary users can coexist in the same spectrum with the additional knowledge of the channels between primary and secondary users. The additional cognition in the interference mitigation is the knowledge about the primary system and its operation (e.g., the primary user's codebooks) so that the secondary users can decode primary users' transmissions or primary users' message in certain cases. Then, opportunistic interference cancellation and asymmetrically cooperating cognitive radio channels can be used by the cognitive secondary users.

1.3 Potential Wireless Devices and Technologies for Cognitive Radio Environment

1.3.1 Wireless Devices for Cognitive Radio Environment

- Cellular (mobile) telephones are the most widely-used wireless devices in today's communications. Generally, cellular phones provide voice communication, short message service (SMS), and multimedia message service (MMS). In the new generation cellphones, Internet services are also provided for web browsing, instant messaging, and email.
- Personal digital assistants (PDAs) are portable devices that possess high com-

putation power. PDAs can be used as calculators, document processors, audio and video players, and gaming consoles. Most of recent PDAs are also equipped with wired and wireless connectivity. A PDA can be used as a mobile phone to host voice communication sessions and/or as a computer to access the Internet. These devices usually require a stylus pen or a keyboard as an input.

- Smartphones are handheld devices integrating the traditional cellular phone and PDA while mainly focusing on the cellular phone part. Smartphones provide information storage, e-mail, and program installation services along with functions in the cellular phones. The features of a Smartphone are more oriented to a cellular phone than that of a PDA. Smartphones are expected to play an important role in eHealth applications.
- Radio-frequency identification (RFID) [10, 11] technology can be used to identify, track, and store item information. An RFID system consists of three parts: RFID tags, RFID reader and a data management system. An RFID tag contains an identification code, while an RFID reader is an electronic device which can be used to retrieve identification codes. Data management system stores application information associated with the identification codes. In general, an RFID reader connects to the data management system in order to retrieve information associated with RFID tags.

RFID is a radio wave innovation operating on low-frequency (30 KHz to 500 KHz), high-frequency (13.56 MHz), or ultra high frequency (850 MHz to 950 MHz, and 2.4 GHz to 2.5 GHz) bands. With low frequency, the system cost is low, but it has a short operating range. On the other hand, the system which operates in high frequency incurs a higher cost, but it has a longer reading range.

1.3.2 Wireless Networking Technologies and Services for Cognitive Radio Environment

- Wireless Wide Area Network (WWAN) technology such as a cellular technology [12, 13] provides wireless services over large geographical areas. Each base station (cell site) covers approximately 800 meters in urban areas and 8 kilo-

metres in rural areas.

- Wireless Local Area Networks (WLANs) is a class of wireless networks which has an operating range of 30-50 meters for indoor and up to 900 meters for outdoor. Currently, most of the WLAN devices communicate using the IEEE 802.11 standard [14], which specifies physical and MAC layer protocols. Since the operating range is relatively small, IEEE 802.11 specifies low transmission power (< 10 mW) in order to reduce interference and to save energy.
- Wireless Personal Area Networks (WPANs) support short-range (within 10 meters) connections, and operate at a very low power transmission. WPAN is implemented in most mobile phones to provide connectivity to neighboring devices such as, laptops or hands-free headsets. Most of the WPAN devices (e.g., Bluetooth, ultra wide-band (UWB), and ZigBee devices [15, 16, 17]) are based on the IEEE 802.15 standard [18].
- Wireless Medical Telemetry Service (WMTS) is an important service to remotely monitor patients' vital signs (e.g., body temperature, heart rate, blood pressure, and respiratory rate among others) [19]. WMTS consists of two main components – wireless wearable sensors and central monitoring stations. These sensors monitor patients' vital signs and then transmit the data to a central monitoring station. WMTS provides mobility to patients and permits remote monitoring of several patients at the same time.

Prior to establishment of the WMTS, medical telemetry devices operated as secondary users on vacant television channels 7-13 (174-216 MHz) and 14-46 (470-668 MHz) and on 460-470 MHz, which the Federal Communications Commission (FCC) has specified for hand-held devices (2 Watts or higher) and other mobile transmitters operated by police, ambulances, firefighters, emergency teams, taxis and commercial trucks [20]. If there are more intense usage of primary services (e.g., hand-held devices), the potential risk of interference to medical telemetry devices can be increased.

In order to guard the telemetry from the radio frequency (RF) interference, FCC established WMTS and also allocated certain frequencies and rules for this service. There are 14 MHz of spectrum bands (e.g., 608-614 MHz, 1395-1400 MHz, and 1429-1432 MHz) which have been allocated for use by licensed physicians,

healthcare facilities and certain trained and supervised technicians. Therefore, the medical telemetry devices can operate without interference because they are operating in these channels as primary users.

- Medical Implant Communications Service (MICS) is similar to WMTS but medical implant devices are used inside the human body, for example, cardiac pacemakers and implanted defibrillators that transmit conditions of patients' heart with ultra-low power to support of diagnostic or therapeutic functions. FCC has proposed the 402-405 MHz band for MICS [19]. This service is an unlicensed wireless radio service which permits users to employ medical implant devices without causing interference to other wireless devices.

1.4 Healthcare Environment

This section emphasizes key requirements in healthcare applications and the wireless technology features which could help meet the requirements. Also, we provide a classification of different medical devices used in a healthcare environment.

1.4.1 Challenges in a Clinical Environment

1.4.1.1 Human Error

In the United States, human errors in clinical environments account for 45,000-90,000 deaths per year and approximately 770,000 injuries every year [21]. Statistics in [22] show that such human errors are caused by healthcare miscommunications. Wireless technology can be used to reduce the human errors in the information processing and gathering process. The doctors may prescribe via a PDA, and the prescription may be transmitted to the pharmacy through a wireless network [22, 23].

1.4.1.2 Information Accessibility

Information accessibility helps expedite medical care processes and reduce human error mentioned earlier. Medical information can be classified into the following: 1) patient information, 2) technical information, and 3) facility information. Patient information is the specific patient details such as allergies, blood type, and medical

history. Technical information refers to medical details such as main effects, side effects, and efficacy. This information also includes knowledge about various diseases and how to deal with different symptoms. Facility information specifies resources available at the facility such as equipment and drug inventory, list of registered specialists and availability of operating rooms. Wireless technology acts as a quick and convenient way to access this medical information. Physicians may use a wireless device to retrieve patient information at the point of care.

1.4.1.3 Service Accessibility

Wireless technology can help connect small clinics in remote or rural areas to a hospital. Operating at a small point of care, doctors may call for a consultation from specialists in a hospital by using wireless connections.

1.4.1.4 Continuous Monitoring

Continuous monitoring is required for a special class of patients [1]. For example, patients suffering from chronic diseases (e.g., memory loss, heart disease, diabetes) have to be continuously monitored and taken care of in hospitals, which can be costly and inconvenient for some patients. Also, it could be fairly laborious for a caregiver to continuously monitor the patients. Wireless technology can be used for monitoring patients. Patients may have implanted wireless sensors or external sensors to monitor their physical conditions such as glucose level, blood pressure, blood temperature or heart rate.

1.4.1.5 Time Efficiency

According to [22], a nurse walks 5 miles on average between the patient's bedside and nurse stations and spends 50 minutes per day to communicate with physicians over a phone. Also, medical staffs spend a large portion of their time trying to locate medical equipment. Wireless technology can help reduce unnecessary activities and improve time efficiency of healthcare services. Electronic prescription eliminates the ambiguity of hand-written prescriptions, and helps reduce the time that nurses require to confirm the prescription with doctors. Furthermore, RFID-based tracking and inventory management systems help locate medical assets in real-time. Time

management in a hospital would be more efficient with the introduction of wireless technology.

1.4.2 Examples of Healthcare Applications and Their Technical Requirements

This section shows a few healthcare application examples which use wireless technologies.

1.4.2.1 Electronic Medical Record (EMR)

EMR refers to an information system customized for hospital environments, also called hospital information system (HIS). The main functionalities of EMR are to collect medical data (including patient data, technical data, and facility data), to process and store data in a given format, and to present users (e.g., medical staffs) with the data in a readable format. Wireless technology provides medical staffs with a quick and convenient access to EMR.

Doctors can use cellular phones, PDAs, or Smartphones to retrieve patient information when they are on their way to the hospital, and can start treating the patient as soon as they reach the hospital. Containing facility information, EMR can also help improve managing hospital operations such as inventory management and scheduling treatments [1, 2, 21, 23].

1.4.2.2 Patient Monitoring System

A patient monitoring system helps caregivers monitoring patients who need continuous care [1, 2, 24]. Wireless implant and external sensors are used to monitor a patient's condition such as blood pressure, temperature, heart rate, or glucose level. These sensors can be programmed to send an alarm signal to the nearest point of care terminal upon detection of a predefined condition such as high blood pressure. This wireless network is also called wireless sensor network or body area network (BAN).

1.4.2.3 Clinician Notifier

A clinician notifier system provides real-time retrieval of vital signals (e.g., electrocardiograph (ECG), blood pressure, or sugar level) of patients for physician or supervising medical staffs [25]. The clinician notifier applications can be supported by effective patient monitoring applications. The vital signals from the monitoring devices are transmitted to the central server. When an abnormal condition is detected, an alarm will be sent to a supervising medical staff. Once the medical staffs receive the alarm, they will transmit a request to retrieve the real-time vital signals of the patients.

1.4.2.4 Telemedicine

Telemedicine addresses the service accessibility issue. It provides healthcare delivery to patients in remote areas. For example, telemedicine applications include remote consultations, remote diagnosis, and patient information transfers. Healthcare professionals in a remote area can discuss with a specialist about patients' symptoms using WWAN services. The professionals in a remote area can also ask the specialist to see inside a patient's ear with a tele-otoscope, or to hear the patient's heartbeat with a tele-stethoscope and provide advice. In prehospital triage, when a patient in a remote area needs to be transferred to a hospital, patient information can be transmitted to the hospital in advance. The hospital can prepare a treatment when the patient is on the way and can start treating the patient upon arrival [26, 27, 28].

1.4.2.5 Wireless Medicine (Wireless Meds)

Wireless Meds incorporates bar-coding and wireless technologies into healthcare services in order to reduce human errors due to miscommunications. Here, the doctor starts to issue a prescription via a PDA. The prescription is sent from the PDA to a pharmacy via WLAN. At the pharmacy, drug packages are bar-coded according to the prescription. The bar-code contains drug information as well as patient's information. At the patient's bedside, nurses check whether the medicine bar-codes match with the bar-code associated with a patient before giving the medicine to the patient. This protocol assures that the patient receives the right drug with the right dose at the right time. However, if there is any mismatch with the bar-code, the nurses may

use a voice over WLAN (VoWLAN or VoWiFi) communications to consult with the doctor.

1.4.2.6 Tracking System

The main objective of a tracking system is to gain visibility over hospital resources such as patient information, equipment, and drug inventory. Tracking systems utilize two key technologies, RFID and WLAN. They operate as follows: An RFID tag or a WLAN transceiver is attached to the resource to be tracked. RFID readers such as WLAN access points are installed throughout the hospital. As the resource roams in a hospital, it passes through RFID readers or various WLAN access points. Tracking systems gather the location information collected by RFID readers or WLAN access points, and feed the information to the EMR. Then, users can obtain the real-time object location through EMR user interfaces. In a hospital, a tracking system can be used to locate equipment such as IV pump [22, 29]. It can also be used for remote patient monitoring to track patient locations [26].

1.4.2.7 Intelligent Emergency Management System

An intelligent emergency management system is designed to deal with emergency events. It consists of two parts. The first part ensures that only one request is sent to the rescue units. The main idea is to collect location information from emergency reporting. Reporting entries with the same incident location tend to correspond to the same event. The second part uses road traffic information to compute the best driving route for the rescue units [26].

1.4.2.8 Advanced Physical Rehabilitation System

Advanced physical rehabilitation systems use specially designed exercise routines and equipment to help patients regain physical ability. During a rehabilitation exercise routine, sensors are attached to various parts of patients to measure physical conditions such as heart rate. Traditionally, these sensors are connected to rehabilitation equipment using cables. Recently, wireless wearable sensors are introduced to replace traditional sensors [30].

Table 1.1. *Requirements of eHealth applications [4]*

Applications	Bandwidth	Latency	Packet loss probability	Reliability	Security
Electronic medical record	1-10 Mbps	≤ 1 s	$\leq 10^{-2}$	Moderate	Very high
Telemedicine, wireless meds, and intelligent emergency management system	10 kbps -1 Mbps	10-250 ms	$\leq 10^{-4}$	Moderate	High
Patient monitoring, clinician notifier, and physical rehabilitation system	10-100 kbps	≤ 300 ms	10^{-6}	Very high	High
Tracking System	$\ll 1$ kbps	$\leq 3-5$ s	0	Very high	Moderate

Advanced physical rehabilitation systems utilize technologies such as wireless wearable sensors, PDAs, and WPAN. In the simplest form, patients can start exercise routines by following the instructions provided by specialists through PDAs. Wireless wearable sensors provide the system with greater flexibility. These sensors form a WPAN as soon as a patient gets close to rehabilitation equipment. Wearing wireless wearable sensors, patients no longer have to change the sensors when switching the equipment.

Wireless wearable sensors can also be incorporated in a so-called “biofeedback” system. Here, the measured physical condition is fed to the monitoring center. The monitoring center uses the collected information to adaptively recommend patients for their next set of exercise routines. When the measured physical condition shows serious physical abnormality, the monitoring center may dispatch the information to a health professional for immediate care. Also, when the exercise is prescheduled, the monitoring center may send out a message to alert the patient of a coming exercise session.

The eHealth applications mentioned above require different performance measures, address different challenges in a clinical environment, and utilize different wireless technologies. These features are summarized in Table 1.1 and Table 1.2.

Table 1.2. *Applications of wireless technologies in eHealth applications*

eHealth applications	Medical challenges	Wireless devices and technologies
Electronic medical record	Human error, Information accessibility	Cellular phone, PDA, WWAN, WLAN, WPAN
Patient monitoring	Continuous monitoring	WLAN, WPAN, WMTS, MICS
Clinician notifier	Information accessibility	WWAN, WLAN
Telemedicine	Service accessibility	WWAN, WLAN
Wireless meds	Human error, time efficiency	PDA, WLAN
Tracking system	Information accessibility, continuous monitoring, Time efficiency	RFID, WLAN
Intelligent emergency management system	Information accessibility, time efficiency	Cellular phone, WLAN, WWAN
Physical rehabilitation system	Continuous monitoring, time efficiency	PDA, WLAN, WPAN, WMTS, MICS

1.4.3 Electronic Medical Devices: Examples and Classifications

Different medical devices can be classified based on functions, physical properties, and locations as shown in Table 1.3.

1.5 Issues Involved in Using Wireless Technology in a Hospital Environment

Although wireless technology provides many advantages for healthcare services, it can cause undesirable Electromagnetic Interference (EMI) in a hospital environment. This section presents the effect of EMI on the medical environment and Electromagnetic Compatibility (EMC) requirements in a healthcare environment.

Table 1.3. *Classification of medical devices [31]-[34]*

Medical devices	Classification based on		
	Functions	Physical properties	Locations
Incubators	Life-supporting equipment	Passive	Neonatal care
Hearing aids	Life-supporting equipment	Passive	Home care
Pacemakers	Life-supporting equipment	Active or passive	Home care
Infusion pumps	Therapy devices	Passive	Ambulance, ICU, Neonatal care
Foetal heart monitors	Diagnostic equipment	Passive	Examination room
Electrocardiograph (ECG) monitors	Diagnostic equipment	Active or passive	Emergency room, ICU, examination room, neonatal care
Anesthesia machines	Therapy devices	Passive	Operating room
Defibrillators	Life-supporting equipment	Passive	Ambulance, emergency room, operating room, ICU, neonatal care
Capnometers	Diagnostic equipment	Active or passive	Emergency room, ICU, examination room, neonatal care
Pulse oximeters (SO_2)	Diagnostic equipment	Active or passive	Emergency room, ICU, examination room, neonatal care
Electroencephalography (EEG) monitors	Diagnostic equipment	Active or passive	Emergency room, ICU, examination room, neonatal care
Electromyography (EMG) monitors	Diagnostic equipment	Active or passive	Emergency room, ICU, Examination room, Neonatal care
Hematology analyzers	Diagnostic equipment	Active or passive	Emergency room, ICU, examination room, neonatal care
Holter monitors	Diagnostic equipment	Active or passive	Emergency room, ICU, examination room, neonatal care, home care
Telemetry monitors	Diagnostic equipment	Active	Emergency room, ICU, examination room, neonatal care, home care

Table 1.4. *Electromagnetic spectrum [35]*

Electromagnetic spectrum	Frequency (Hz)	Energy (electron-volt, eV)
Non-ionizing radiation		
Power lines	$10 - 10^4$	$10^{-14} - 10^{-9}$
Radio and television	$10^4 - 10^8$	$10^{-10} - 10^{-7}$
Cellular radio	$10^8 - 10^9$	$10^{-6} - 10^{-5}$
Microwave	$10^8 - 10^{12}$	$10^{-6} - 10^{-3}$
Infra-red	$10^{12} - 10^{15}$	$10^{-3} - 1$
Visible light	10^{15}	$1 - 10$
Ultra-violet	$10^{15} - 10^{17}$	$1 - 10^3$
Ionizing radiation		
X-rays	$10^{17} - 10^{20}$	$10^3 - 10^5$
Gamma rays	$10^{20} - 10^{26}$	$10^5 - 10^{12}$

1.5.1 Electromagnetic Interference (EMI)

Electromagnetic waves are self-propagating waves that consist of electric and magnetic field components [35]. Table 1.4 shows various types of electromagnetic waves classified based on the frequency as well as energy. Electromagnetic waves are classified into ionizing radiating waves and non-ionizing radiating waves. The key difference between these two types is that ionizing radiating waves are characterized by high frequency and energy while non-ionizing radiating waves are characterized by low frequency and energy. The radiation energy is given by (1.1), where EV is defined as the radiation energy (eV), h is the fraction of the Planck constant ($\sim 4.136 \times 10^{-15} eV \cdot s$), and f is the frequency in cycles per second (s^{-1}) [36]. Ionizing radiating waves are able to strip electrons off the molecule of the exposed object. This is called the ionization process.

$$EV = hf. \quad (1.1)$$

Wireless communications use electromagnetic waves as information carriers, and therefore, inevitably create Electromagnetic Interference (EMI). EMI is an undesired electromagnetic wave, which can cause adverse effects on data transmissions, biological systems, and medical devices [37]. For example, EMI causes power line voltage drops and interruptions, electrical fast transients (EFTs), electrostatic discharges, and radiated and conducted emission among others. Therefore, EMI is an important issue for wireless technology applications in healthcare environments.

1.5.1.1 Impact of EMI on Biological Systems

Biological effects are defined as the measurable response of a biological system to a stimulus or a change in the environment [35, 38], which can be either harmful or harmless. For example, increasing heart rate due to coffee drinking is a harmless biological effect, while liver cirrhosis caused by chronic alcohol drinking is a harmful biological effect. Harmful biological effects can be also caused by ionizing EMI. Ionizing electromagnetic waves can cause a thermal effect, heated tissues and increased body temperature. The eyes and the testicles are notably vulnerable to the thermal effect [35].

Most of the wireless communications use non-ionizing radiation waves which have far less energy and cause small thermal effects to the human body. Although some researchers believed that non-ionizing EMI can lead to cancers and tumors, there is no significant evidence suggesting association between the radio frequency/microwave electromagnetic field exposure and some common brain tumors such as Glioma and Meningioma [39].

The potential risk of EMI is still a controversial health issue. World Health Organization [38] reports that the low frequency exposure from mobile phones results in minor changes in brain activities, reaction time, and sleep patterns. Consequently, the United States Food and Drug Administration (FDA) agency has suggested people to limit the duration of cell phone or other wireless device usage, and encourages the use of hands-free devices to increase the distance between the antenna and the user [40].

1.5.1.2 Electromagnetic Interference Caused to Medical Devices

EMI can cause medical equipment malfunctions such as display distortion, waveform distortion, howling, automatic restart, and/or automatic shut down. Depending on types of EMI and medical equipment, these malfunctioning effects could be reversible or irreversible. For example, EMI from mobile phones could stop an external cardiac pacemaker to stimulate pulses and syringe pump to generate alarms. While the pacemaker starts operating in its normal condition as soon as EMI is reduced (i.e., when the mobile phones move away), the syringe pump does not. A clinician needs to reset the syringe pump, after it is exposed to EMI. The adverse effects from which the medical devices can and cannot return to their normal condition in absence of EMI without human intervention are called *reversible* and *irreversible* malfunctions, respectively [3].

Several events and experiments showed that EMI can cause medical equipment malfunctions. For example, digital TV broadcasting systems can cause disruption to wireless heart monitoring devices [41]. [42] reported experiments on EMI caused by cellular phones using the 900 MHz and 1800 MHz on medical devices.

The following recommendations were made in [3]:

- Cell phones should *not be present* in the operating rooms, ICU (Intensive Care Unit) rooms, and CCU (Critical Care Unit) rooms.
- Cell phones should *not be present* within one meter range of medical devices.
- Cell phones *should be switched off* in examination rooms and in-patient rooms.

1.5.2 Electromagnetic Compatibility (EMC)

Since EMI can cause medical device malfunctions and can lead to devastating impacts on healthcare services, active electromagnetic devices must be compatible to medical devices in an electromagnetic sense. According to [37, 43], a device is said to be “electromagnetically compatible” if it can operate under its intended EM environment and does not introduce excessive EMI which may interfere with other devices. This section focuses on the EMC of medical devices and wireless communications devices.

1.5.2.1 Electromagnetic Compatibility for Medical Devices

The International Electrotechnical Commission (IEC) established two important standard series for medical electrical devices EMC: the IEC 60601-1 and the IEC 61000-4 standard series. IEC 60601-1 series specify general requirements for safety of medical equipments. IEC 61000-4 series recommend testing and measurement techniques for EMC. The readers are referred to [44]-[50] for the testing and measurement techniques. The following discussions are based on IEC 60601-1-2 standard within the IEC 60601-1 series which deals with the requirements for medical electrical devices EMC [51]-[52].

IEC 60601-1-2, which is sometimes referred to as IEC 601-1-2 or EN 60601-1-2, defines the immunity standard level and compliance level for medical equipments [43]. Immunity level is the maximum EM disturbance level in which medical devices can operate without performance degradation. Compliance level is the EM disturbance level which is below or equal to the immunity level. The standard defines seven types of EM disturbances for EMC as follows:

- *Electrostatic discharge*: Medical devices must withstand electrostatic charge transfer from/to another object with different electrostatic potential. The minimum electrostatic voltage that medical devices must be able to withstand and the EM environment guidance are shown in Table 1.5. Testing and measurement techniques are specified in IEC 61000-4-2 [44].
- *Radiated RF electromagnetic fields*: Although EM waves contain both electric and magnetic components, the electric component is more detrimental to medical devices. The requirement for this category is defined for the electric field (measured in *volts/meter* or V/m) only. Medical devices must operate normally in an anechoic chamber with an electric field generator. The electric field requirement for life supporting and non-life supporting equipment and the EM environment guidance are given in Table 1.5. The testing and measurement techniques are specified in IEC 61000-4-3 [45].
- *Electrical fast transients*: When an induction load is connected or disconnected to a wire, an electric surge is generated. An inductive load can be an electrical device plugged into a line or be an input/output to a signal line. The minimum electric surge that medical devices must withstand and the EM environment

guidance are shown in Table 1.5. Testing and measurement techniques are provided in IEC 61000-4-4 [46].

- *Surges*: EM pulses can cause fast and short duration electrical transients in power line voltage, also called a voltage spike. The minimum requirement of surges for AC power lines to ground and AC power lines to lines of medical devices and the EM environment guidance are given in Table 1.5. IEC 61000-4-5 [47] specifies testing and measurement techniques.
- *Conducted RF disturbances*: Intended RF emission in the range 150 kHz up to 80 MHz can generate undesired voltage on medical devices' external wires and cables. The minimum RF voltages that non-life supporting and life supporting medical devices must be able to withstand inside and outside the ISM (Industrial, Scientific and Medical) band and the EM environment guidance are given in Table 1.5. The ISM band frequencies are 6.765 MHz-6.795 MHz, 13.553 MHz-13.567 MHz, 26.957 MHz-27.283 MHz, and 40.66 MHz-40.70 MHz. IEC 61000-4-6 [48] specifies the testing and measurement techniques.
- *Voltage dips*: refer to short interruptions and voltage variations on power supply input lines. Voltage dips are generated by abrupt increasing in load or source impedances in power lines. The immunity requirement measured in percentages of voltage dips over the A.C. main voltage prior to application of the test level (U_T) and the EM environment guidance are shown in Table 1.5. This requirement is for all life supporting equipment with rated input power of 1 kVA. or less and non-life supporting equipment with rated power greater than 1 kVA. but the rated input current less than or equal 16 A per phase. Testing and measurement techniques are specified in IEC 61000-4-11 [49].
- *Power frequency magnetic field*: refers to magnetic disturbance at A.C. power frequencies 50 and 60 Hz which can cause problems for medical devices especially devices using CRT displays and Hall effect sensors. Table 1.5 shows the minimum magnetic field (measured in *amperes/meter* or A/m) that medical devices must be able to withstand and the EM environment guidance. IEC 61000-4-8 [50] specifies testing and measurement techniques.

Table 1.5. *Electromagnetic compatibility requirements for medical devices and standards for test methods and equipments [43]*

Immunity requirements	Immunity level	Electromagnetic environment guidance
Electrostatic discharge (ESD) - Non-conductive parts - Conductive parts	± 8 KV ± 6 KV	The devices should operate on wood, concrete or ceramic tile floors. The relative humidity is required at least 30% when the floors are covered with synthetic material.
Radiated RF electromagnetic fields (at 80 MHz to 2.5 GHz) - Non-life supporting · 80 MHz to 800 MHz · 800 MHz to 2.5 GHz - Life supporting · 80 MHz to 800 MHz · 800 MHz to 2.5 GHz	3 V/m 3 V/m 3 V/m 10 V/m	RF communication device should be used to used within the separation distance (d) which can be calculated as follows: $[3.5/E]^* \sqrt{P}^{**}$ m $[7/E] \sqrt{P}$ m $[12/E] \sqrt{P}$ m $[23/E] \sqrt{P}$ m
Electrical fast transients - Power lines - Signal lines	± 2 KV ± 1 KV	The device should operate with main power quality of a typical commercial or hospital environment.
Surges - A.C. power lines to ground - A.C. power lines to lines	± 2 KV ± 1 KV	The device should be operate with main power quality of a typical commercial or hospital environment.
Conducted RF disturbance (at 150 kHz to 80 MHz) - Non-life supporting - Life supporting · Outside ISM band · Inside ISM band	3 VRMS 3 VRMS 10 VRMS	RF communication device should be used to used within the separation distance (d) which can be calculated as follows: $[3.5/V]^{***} \sqrt{P}$ m $[3.5/V] \sqrt{P}$ m $[12/V] \sqrt{P}$ m
Voltage dips (% dip in U_T) - 0.5 cycles - 5 cycles - 25 cycles - 5 sec	> 95% 60% 30% > 95%	The device should be operate with main power quality of a typical commercial or hospital environment. An uninterruptible power supply or a battery is required when the device is required to continuously operate during power main interruption.
Power frequency magnetic field	3 A/m	The device should operate in power frequency magnetic field which is at level characteristic of a location in a typical commercial or hospital environment.

Note that * E is actual radiated RF immunity levels of the medical device (V/m), ** P is maximum output power of transmitter in Watt, *** V is actual conducted RF immunity levels of the medical device.

1.5.2.2 Electromagnetic Compatibility for Wireless Transmitters

FCC proposed a guideline of radio frequency energy exposure for wireless transmitters as shown in Table 1.6. The guideline limits the maximum exposure in term of electric and magnetic field strength and power density at different frequency range from 300 kHz to 100 GHz. At the far-field zone (i.e., more than several wavelengths distance from the RF source), power density can be used to characterize the field strength with the relation $PS = \frac{E^2}{3770} = 37.7M^2$ where PS is the power density, E is the electric field and M is the magnetic field [53]. However, at the near-field measurement, the physical relationships between electric and magnetic components are complex. Therefore, both electric and magnetic fields are necessary to be determined to completely characterize the RF environment. Electric and magnetic fields are more meaningful for the lower frequencies which have the longer wavelengths. On the other hand, the limits of higher frequencies are determined in terms of power densities. There are two types of RF exposures: controlled and uncontrolled. Controlled or occupational exposure limits are applied in the cases when people around the transmitter are fully aware of the potential of its exposure due to their employment and can protect themselves from the exposure. On the other hand, uncontrolled or general population exposure is applied in the cases when people (e.g., general public) around the transmitter are unaware of the potential of its exposure and cannot protect themselves from the exposure [35].

Table 1.5 and Table 1.6 show that at the same frequency, a wireless transmitter can cause the maximum electric field much greater than the radiated RF immunity standard of medical devices. For example, at 80-300 MHz, the wireless transmitters can generate a maximum electric field of 27.5 and 64.1 V/m for uncontrolled and controlled exposure, respectively, while the minimum radiated RF immunity requirement of the IEC 60601-1-2 standard is only 3 V/m for both non-supporting and supporting life equipment. These two standards are not conforming to each other. Furthermore, the IEC 60601-1-2 standard does not apply to the older versions of medical equipment, and the wireless transceivers can produce electric field strengths in the order of hundreds of V/m when it moves closer to the medical equipments. Therefore, the medical devices may fail due to RF interference.

Table 1.6. *Limits for the maximum radio frequency energy exposure [35]*

Frequency (MHz)	Controlled exposure				Uncontrolled exposure			
	Electric field (V/m)	Magnetic field (A/m)	Power density (mW/cm ²)	Averaging time (minutes)	Electric field (V/m)	Magnetic field (A/m)	Power density (mW/cm ²)	Averaging time (minutes)
0.3 - 1.34	614	1.63	100	6	614	1.63	100	30
1.34 - 3.04	614	1.63	100	6	$824/f$	$2.19/f$	$180/f^2$	30
3.0 - 30	$1842/f$	$4.89/f$	$900/f^2$	6	$824/f$	$2.19/f$	$180/f^2$	30
30 - 300	61.4	0.163	1.0	6	27.5	0.073	0.2	30
300 - 1500	-	-	$f/300$	6	-	-	$f/1500$	30
1500 - 100000	-	-	5	6	-	-	1.0	30

Note that f denotes frequency in MHz.

1.6 Requirements for Wireless Communications Systems Used in eHealth Applications

- *Electromagnetic compatibility (EMC) and electromagnetic interference (EMI) requirement:* Many medical devices in healthcare environments are sensitive to EMI. Therefore, all wireless communications systems to be used in eHealth applications need to satisfy the EMC requirements. For example, the wireless devices used in eHealth applications must limit the transmission power to avoid harmful interference to the medical devices in their vicinity. In this case, the transmission parameters of the wireless devices (e.g., frequency and transmission power) can be determined from the IEC 60601-1-2 standard [43] which describes the EMI immunity levels of the medical devices. In wireless communications, two crucial EM disturbances are the radiated RF electromagnetic field and conducted RF disturbance which can be induced by RF radiation. Therefore, the transmission parameters of the non-medical wireless devices should take these two EM disturbances into consideration.
- *QoS provisioning for eHealth applications:* EHealth applications can be classified into four classes based on their communications requirements as shown in Table 1.1. Loss and delay are two major communications QoS performance measures for these applications. For example, a cardiac patient could be continuously monitored through a real-time patient monitoring application. If the transmission of critical physiological data is delayed, the patient may not receive prompt aid when an abnormal condition arises. IEEE 802.11e is one of wireless technologies which has been adopted in eHealth applications with QoS support [54]. IEEE 802.11e provides different privilege for channel access by fixing different backoff window sizes to different classes of applications. However, this may not be able to support QoS guarantee for medical applications.
- *Coexistence of different wireless technologies for eHealth applications:* Several wireless technologies are used in the same area (e.g., in the hospital). For example, IEEE 802.11-based WLAN and IEEE 802.15.4a/ultra wide-band (UWB)-based WPAN technologies can be used for eHealth applications with high bandwidth requirements, e.g., telemedicine and electronic medical record applica-

tions. Bluetooth and ZigBee can be used in body sensor networks for patient monitoring and physical rehabilitation applications. Many of these technologies operate on the same or overlapping frequency bands (e.g., IEEE 802.11b/g, Bluetooth, and ZigBee use 2.4 GHz ISM band), and therefore, interference and spectrum management are crucial [4].

- *Seamless connectivity*: Wireless communications can greatly improve the mobility of the eHealth applications. The bio-signal data can be continuously monitored when the patient moves. The mobile medical staff should be able to access different healthcare and patient monitoring applications in an online manner. To support seamless service and to achieve better performance for the eHealth applications, mobility management (i.e., roaming and handoff) is necessary.
- *Security of healthcare data*: Healthcare data (including patient data, service data, and facility data) is security-sensitive. The system should have zero tolerance to unauthorized eavesdropping and intrusion. Therefore, strong authentication and encryption mechanisms are required for eHealth applications. For example, in a WLAN, IEEE 802.11i-based key distribution and 802.1x-based authentication methods can be used [54].

1.7 Contributions of the Thesis

In a healthcare environment, there exist both passive and active medical devices. Passive medical devices, also referred to as *protected users* (e.g., incubators, electrocardiograph (ECG) monitors, and defibrillators), do not transmit any wireless signal but their electronic components are sensitive to EMI. The protected users can be categorized into non-life-supporting and life-supporting devices. Life-supporting devices (e.g., defibrillators and incubators) provide artificial biological function to patients while non-life-supporting devices (e.g., infusion pumps and ECG monitors) can be used for either therapy or diagnostic.

On the other hand, active medical devices, also referred to as *primary users* (e.g., telemetry monitors, wireless holter monitors, wireless ECG monitors), can transmit data wirelessly. Transmissions of these active medical devices can be interfered by

wireless transmissions from other devices using eHealth applications such as hospital information system (HIS) applications. The transmissions from these eHealth devices should not cause harmful interference to the protected and primary users. Therefore, these devices, also referred to as *secondary users* in this thesis, must opportunistically transmit their data. For eHealth applications in a hospital environment, where different locations (e.g., emergency room, operating room, examination room) have different medical devices, dynamic wireless access techniques can be used to avoid interference to active and passive medical devices and simultaneously improve the radio spectrum utilization.

In the first part of this thesis, we deal with the problem of dynamic wireless access of secondary users under an infrastructure wireless network where secondary users are connected through a cognitive radio controller. We consider the network scenarios involving both a single service cell and multiple service cells. In the latter part, we consider an ad-hoc wireless network where secondary users are directly connected to each other. We propose both centralized and distributed schemes for robust scheduling and power control in a cognitive Spatial-Reuse Time-Division Multiple Access (STDMA) wireless network.

1.7.1 EMI-aware Prioritized Wireless Access Protocol for a Single Service Cell in an Infrastructure-based Wireless Network

In Chapter 2, we first introduce an EMI-aware prioritized wireless access protocol for a single service cell. This protocol jointly addresses two critical challenges (i.e., EMI for both protected and primary users and QoS provisioning for secondary users) in wireless communications systems for eHealth applications in hospital environments. System architecture for this protocol is first designed and described. We then propose an EMI-aware RTS/CTS protocol which takes IEC 60601-1-2 standard for passive medical devices and signal-to-interference-plus-noise ratio (SINR) threshold of active medical devices into account. Furthermore, a prioritized wireless access scheme is proposed to provide QoS guarantee for different types of eHealth applications (i.e., primary and secondary users). Then, we develop a Markov chain model to analyze the performance of the proposed access scheme in terms of the average transmission

delay and loss probability. The analytical model is also used to obtain the optimal system parameter (i.e., blocking probability) to guarantee the QoS of eHealth applications while maximizing the system throughput. We further propose an exponential moving average (EMA) prediction to obtain one-step-ahead values of the blocking probabilities based on the various system parameters (e.g., the number of users in the network, channel access patterns, and the presence of EMI-sensitive medical devices).

1.7.2 EMI-aware Transmission Scheduling and Power Control for Multiple Service Cells in an Infrastructure-based Wireless Network

To generalize the problem, we consider a scenario of multiple service cells in Chapter 3. The deployment of eHealth applications has been done through the IEEE 802.11 technology [54]. Most commodity 802.11 WLAN interface products deploy DCF (Distributed Coordination Function) mode which uses carrier sense multiple access with collision avoidance (CSMA/CA) with binary exponential backoff algorithm. This mode can support only best-effort service and may not be able to provide QoS guarantee (e.g., delay and loss probability) for medical applications [4]. IEEE 802.11 standard also provides the PCF (Point Coordination Function) mode that supports a centralized polling scheme for scheduling transmissions based on the users' bandwidth requirements and priorities. Wireless access through PCF is similar to time-division multiple access (TDMA) technique that provides per-connection QoS guarantee and maximizes the channel utilization. Moreover, there exists a software-based TDMA protocol over IEEE 802.11 DCF WLAN interfaces [55]. From the QoS perspective, either IEEE 802.11 PCF or software-based TDMA over IEEE 802.11 DCF is more suitable for eHealth applications. This motivates us to focus on the TDMA-based wireless access for both primary and secondary networks in hospital environments.

In Chapter 3, we focus on transmission scheduling and power control of secondary users in multiple STDMA networks. STDMA is a generalization of time-division multiple access (TDMA) where time slots in a channel assigned to different wireless nodes in a geographical area can be reused by other nodes in another geographical area as long as the concurrent transmissions do not cause interference to each other. With STDMA networks, the secondary and primary users from different networks

can transmit data simultaneously if the EMI level to primary and protected users is maintained below the maximum threshold. The objective is to maximize the spectrum utilization of secondary users and minimize their power consumption subject to the EMI constraints for active and passive medical devices and minimum throughput guarantee for secondary users. The multiple-access problem is formulated as a dual objective optimization problem, which is shown to be NP-complete. We propose a joint scheduling and power control algorithm based on a greedy approach to solve the problem with much lower computational complexity. To this end, an enhanced greedy algorithm is proposed to improve the performance of the greedy algorithm by finding the optimal sequence of secondary users for scheduling. Using extensive simulations, the tradeoff in performance in terms of spectrum utilization, energy consumption, and computational complexity is evaluated for both algorithms.

1.7.3 Robust Scheduling and Power Control for an Ad-hoc Cognitive STDMA Wireless Network

In wireless communications, the system information (e.g., channel gains, number of users, SINR measurement) is typically inaccurate, time-varying, or uncertain. Resource allocation without taking care of these uncertain issues may lead to poor or even infeasible solutions to the realization. Over the last decade, robust optimization has emerged to undertake optimization problems with data uncertainty. The robust optimization seeks a solution that is near-optimal but remains feasible under the perturbation of parameters in the optimization problem without uncertainty (i.e., nominal problem).

Chapter 4 addresses robust transmission scheduling and power control problem for spectrum sharing between secondary and primary users in an STDMA network where secondary users are communicated in an ad-hoc fashion. The objective is to find a robust minimum-length schedule for secondary users (in terms of time slots) subject to the interference constraints for primary users and the traffic demand of secondary users. We consider the fact that power allocation based on average (or estimated) link gains can be improper since actual link gains can be different from the average link gains. Therefore, transmission of the secondary links may fail and require more time slots. We also consider this demand uncertainty arising from channel gain uncertainty.

We then propose a centralized algorithm based on a column generation method to solve the scheduling and power control problem for secondary users.

The column generation method breaks the problem down to a restricted master problem and a pricing problem. However, the classical column generation method can have convergence problem due to primal degeneracy. We propose an improved column generation algorithm to stabilize and accelerate the column generation procedure by using the perturbation and exact penalty methods. Furthermore, we propose an efficient heuristic algorithm for the pricing problem based on a greedy algorithm.

1.7.4 Distributed Robust Scheduling and Power Control for an Ad-hoc Cognitive STDMA Wireless Network

Since the centralized schemes may not be suitable when the network is large due to high complexity (i.e., lack scalability), dynamic spectrum access schemes should operate in a distributed way. In Chapter 5, we investigate the distributed robust transmission scheduling and power control problem in a cognitive STDMA network. In particular, we address the problem of minimizing the transmission length of the secondary links under their minimum QoS requirements without violating the maximum tolerable interference for the primary receivers.

To provide robustness, our problem formulation takes an ellipsoidal form of channel gain uncertainty into account. Since an optimal solution cannot be obtained due to the NP-completeness of the problem, we propose a novel distributed two-stage algorithm based on the distributed column generation method to obtain the near-optimal solution for the robust transmission schedules in an ad-hoc cognitive radio network. To demonstrate its relative efficiency, our algorithm is compared with previously proposed algorithms. For the proposed algorithm, we also derive the bounds on the probability of signal-to-noise-plus-interference ratio (SINR) constraint violation and the expected additional number of time slots required to satisfy the traffic demand requirements of secondary links.

Chapter 2

EMI-Aware Prioritized Wireless Access Scheme for a Single Service Cell

In this chapter, we address jointly the EMI and QoS provisioning issues in radio frequency (RF) WLAN for eHealth applications in a single service cell. We first design system architecture for EMI-aware prioritized wireless access. An EMI-aware RTS/CTS (Request to Send/Clear to Send) protocol which complies with IEC 60601-1-2 standard is designed to avoid EMI to sensitive medical devices and a prioritized channel access scheme is developed to provide QoS guarantee for different eHealth applications. We consider two types of eHealth applications, namely, clinician notifier application and electronic medical record (EMR) application. The clinician notifier application provides real-time retrieval of vital signals (e.g., electrocardiograph (ECG), blood pressure, or sugar level) of patients for physician or supervising medical staffs while the EMR application provides storage, retrieval and processing of medical records for medical users. Clinician notifier applications (e.g., real-time critical applications) are sensitive to packet delay and loss whereas EMR applications (e.g., medical IT applications) are only sensitive to packet loss. Therefore, the users of clinician notifier applications are defined as high-priority users to have higher privilege to access the network while the users of EMR applications are defined as low-priority users.

We then develop a Markov chain model to derive the performance metrics of the proposed access scheme including the average transmission delay of high-priority users and the loss probability of low-priority users. The analytical model is also used to

optimize system parameters (e.g., blocking probabilities) to guarantee the QoS performances for wireless access by eHealth applications while maximizing the system throughput (i.e., the number of users who can successfully transmit their data). A target blocking probability is contributed by two factors: one is the requirement to avoid EMI and the other is the requirement to avoid congestion (i.e., satisfy the QoS requirements). The effective blocking for congestion avoidance should be increased before the network becomes highly congested to provide QoS guarantee. Moreover, the effective blocking to avoid congestion should be reduced when the network becomes lightly loaded to avoid unnecessary throughput degradation. Therefore, the blocking probabilities due to congestion effect should be obtained in advance. We propose an exponential moving average (EMA) prediction model to forecast the one-step-ahead values of the blocking probabilities based on the various parameters (e.g., the number of high-priority and low priority users in the network, channel access pattern of high-priority and low-priority users, and the presence of EMI-sensitive medical devices).

2.1 Related Work

Recently, there have been few studies on applications of WLANs in medical environments. An infrared (IR) LAN was proposed in [56] to gather information from monitoring devices in the operating room (OR). This wireless network can increase the mobility and reduce the problem of cabling infrastructure especially when the layout of the OR is changed. Moreover, IR used in this network can avoid the EMI problem to life-sustaining devices in the OR. The concept of illuminating network was also proposed to address the EMI problem in [57]. This network uses high brightness LED as a transmitter. However, the use of both light and IR as the carrier does not allow seamless mobility and the transmissions can be easily interrupted by obstacles (e.g., medical devices or people moving in the hospital).

On the contrary, radio frequency (RF) is more suitable for wireless communication in this respect. There exist two main technologies in the deployment of RF wireless medical telemetry systems which are the proprietary networks in the allocated WMTS bands and the IEEE 802.11 wireless networks in the unlicensed bands

(e.g., Industrial Scientific Medical (ISM) bands in 2.4 GHz or Unlicensed National Information Infrastructure (UNII) bands at 5 GHz). Even though WMTS bands was dedicated to ensure that wireless medical telemetry devices can operate free of harmful interference, the WMTS telemetry systems especially in dense metropolitan areas are restricted by the limited bandwidth. In contrast, an IEEE 802.11-based network can provide the large bandwidth in unlicensed bands with inexpensive cost by the standard deployment. Moreover, WMTS-based network is restricted to support patient telemetry only and cannot be used for generalized medical applications [54]. The authors in [4] also discussed the opportunity of exploiting WPAN and WLAN technologies in medical environment. These technologies can support diverse health-care applications which can be classified in to four categories according to their QoS requirements, i.e., office/medical IT, real-time noncritical applications, real-time critical applications, and remote control applications. One of the main communications problems of using IEEE 802.11-based network in medical environments is how to provide efficient spectrum utilization while guaranteeing the QoS requirements of the applications, especially for life-critical applications.

In [58], a fully-distributed contention control mechanism was designed to support a medical-grade QoS WLAN. The proposed design is based on the modifications of IEEE 802.11e MAC standard which defines a set of QoS enhancements for WLAN applications. The medical traffic is classified into four categories based on their criticality, which are alarm signal (AC0, the highest priority), real-time monitoring traffic (AC1), other medical applications (AC2), and non-medical applications (AC3, the lowest priority). The proposed protocol can control the channel access of each class by adjusting the contention window (CW). To guarantee the QoS of AC0 and AC1 applications, the CW value of AC0 applications is fixed to CW_MIN to ensure the highest priority channel access while that of AC1 applications is updated with a granularity of one inversely proportional to the access probability. The performance of AC1 applications under the proposed access mechanism is better than that under the conventional IEEE 802.11e MAC. A QoS support mechanism was also proposed in [59] implemented in *CareNet*. This is a wireless sensor system for remote health care. To ensure the QoS requirements of all the data transmissions be satisfied, the number of users that can be supported by the current system resource are first deter-

mined by using Linear Programming (LP) techniques. Then, the admitted users are queued and scheduled to transmit based on their priorities in the queue. The packet with the highest delay priority is scheduled and transmitted first. Therefore, the users who have higher reliability and delay priorities (i.e., critical condition) achieve higher throughput, lower delay, and lower drop rate. However, these medical-grade QoS wireless networks do not take EMI issue into account. This can be risk to EMI-sensitive medical devices when deploying these wireless networks in the healthcare environments.

In our work, we deal with the problem of designing a wireless communications protocol for eHealth applications by considering two critical issues in healthcare environments: EMI to medical devices and QoS of eHealth applications. To handle the EMI problem, our EMI-prioritized RTS/CTS protocol adapts the transmission power of wireless transmitter to avoid causing the EM field to passive medical devices in its vicinity greater than the requirements specified in IEC 60601-1-2 standard. Moreover, the proposed protocol also provide admission control which comply with the standard and the QoS requirements specified in [4] and differentiated scheduling and queue management which enables data with higher priority to enjoy a better treatment in the network.

2.2 EMI-Aware Prioritized Wireless Access Scheme

This section describes the system architecture of an EMI-aware prioritized wireless system for eHealth applications in hospital environments. This system addresses the EMI problem with an EMI-aware RTS/CTS protocol and performs QoS provisioning with a prioritized wireless access scheme.

2.2.1 System Overview

We consider two types of eHealth applications and the corresponding users are referred to as *high-priority* and *low-priority* users. The low-priority users utilize the radio resources only when the high-priority users are not present. However, the wireless access protocol must provide quality of service (QoS) guarantee to both types of users. Also, the wireless access protocol must be aware of EMI constraints to medical

devices which are referred to as *protected* users. Electronic medical devices can be classified either as passive or active devices. The passive devices (e.g., electrocardiograph (ECG) monitors, blood pressure monitors, infusion pumps, and defibrillators) do not transmit any radio signal for communications. However, these medical devices can experience EMI from wireless transmissions. On the other hand, the active medical devices (e.g., telemetry monitors, wireless holter monitors, and wireless ECG monitors) can transmit radio signals. Wireless transmissions of these medical devices can be also interfered by other wireless non-medical devices. The method to avoid EMI to these protected users will be described in Section 2.2.3.

The proposed system operates on two channels under unlicensed spectrum bands. One is the control channel used for transmitting control signals and the other channel (i.e., data channel) is used to transmit data. A time-division multiple access (TDMA) scheme is used for wireless access. We assume that the active medical transmitters also transmit data in the same channel as data channel of the proposed system.

2.2.2 System Architecture for EMI-Aware Prioritized Wireless Access

Fig. 2.1 illustrates a healthcare scenario in a cardiac department that consists of active medical devices applied in a remote patient monitoring system, passive medical devices, and our EMI-aware prioritized wireless access system. Details of this figure are presented in Section 2.5.1.1. The proposed system is composed of three main components: the inventory system, the radio access controller (RAC), and the clients (i.e., high-priority and low-priority users). The clients communicate with the RAC over wireless link while the RAC is connected to the inventory system with wired infrastructure. The key functions of these components are as follows:

- The *inventory system* is used to gather the information of all electronic medical devices in the hospital (e.g., status ON-OFF, locations, EMI immunity levels, and signal-to-interference-plus-noise ratio (SINR) thresholds). This system can be supported by an effective tracking system to maintain the locations of active and passive medical devices and wireless eHealth devices in a hospital environment. For example, a tracking system utilizing the RFID technology [29] can be used for this purpose.

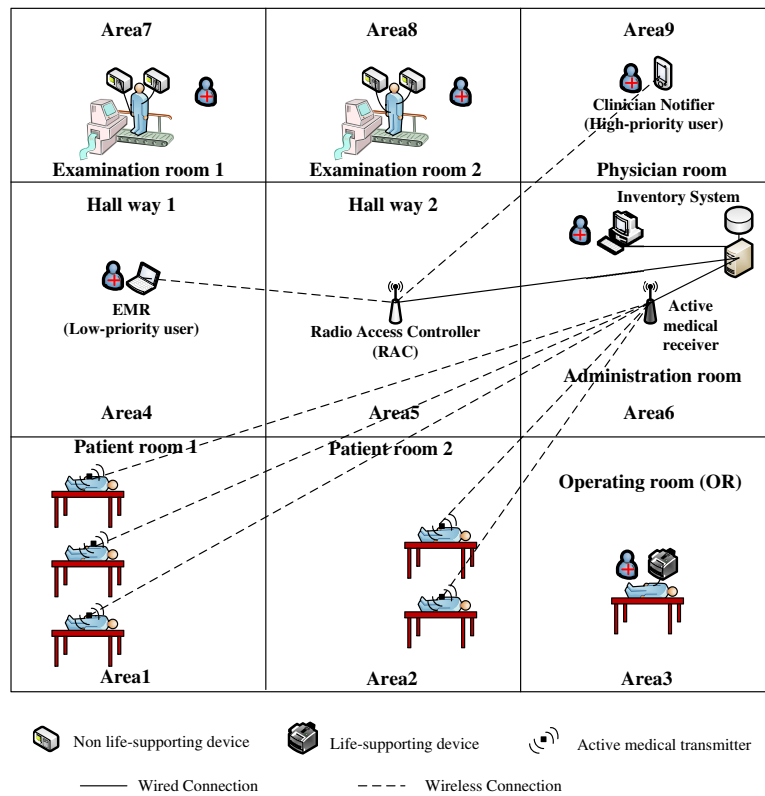


Figure 2.1. *EMI-aware prioritized wireless system for eHealth in a hospital environment.*

- The *radio access controller* (RAC) is used to effectively control and manage dynamic spectrum sharing among various clients by using the updated information from the inventory system. The RAC defines safe transmission parameters (i.e., transmission power) for the clients to avoid harmful EMI to the medical devices. At the same time, the RAC also guarantees the QoS of different clients. The RAC can perform effective channel allocation and control wireless access of the clients using an EMI-aware prioritized wireless access scheme. The details of this protocol will be described in Section 2.2.3.
- The *clients* are wireless non-medical devices using high-priority and low-priority eHealth applications. These users/devices can transmit/receive data through the RAC (i.e., infrastructure mode of communications) by adaptively tuning the transmission power.

The RAC is equipped with two radio transceivers (i.e., one for common control channel and the other for data channel). Consequently, it can access both channels simultaneously. On the other hand, the clients are equipped with a single multichannel radio transceiver which can access only one channel at a time (i.e., either the common control channel or the data channel).

2.2.3 EMI-Aware Prioritized Wireless Access Scheme

In the infrastructure mode, the high-priority and low-priority users first connect to the RAC in the common control channel by using a time-slotted RTS (request to send)-CTS (clear to send)-based channel access mechanism. The users perform carrier sensing before transmitting RTS message to avoid collision with other users. The transmission of both high-priority and low-priority users must not cause any interference to the protected users. The wireless access mechanism consists of two steps, i.e., common control broadcasting and EMI-aware prioritized wireless access protocol (including EMI-aware RTS-CTS protocol and prioritized queue management and data transmission). The transmissions in both uplink and downlink are considered. The common control broadcasting for these uplink and downlink transmissions is the same while the EMI-aware prioritized wireless access mechanisms are slightly different. The operation of the entire wireless access procedure for uplink transmission is shown in Fig. 2.2.

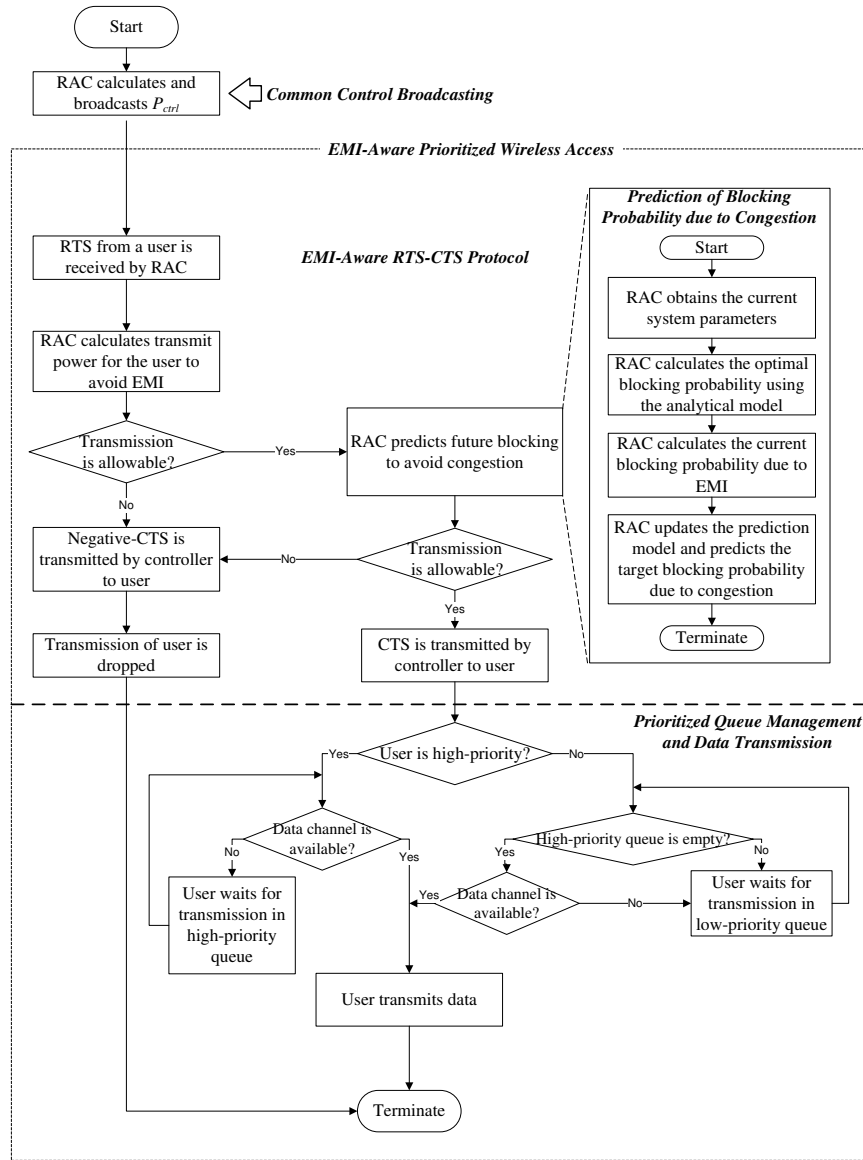


Figure 2.2. Flowchart of EMI-aware prioritized wireless access scheme for uplink request transmission.

2.2.3.1 Common Control Broadcasting

This step is used to broadcast p_{ctrl} which is the maximum transmission power for transmitting either RTS or CTS message by a client on the control channel without causing too much EMI to the protected users. Each user has different p_{ctrl} depending on the locations of users. The upper-bound on transmission power of active medical devices (i.e., p_A) and transmission power of passive non-life-supporting and life-supporting devices (i.e., p_{NLS} and p_{LS} , respectively, can be obtained as follows.

- Active medical devices: The interference from the other wireless users should not cause SINR of the active medical devices to fall below the required threshold. By simplifying the SINR equations, the upper-bound on transmission power by a transmitter of eHealth applications that active medical user/device x can tolerate ($p_A(x)$) can be obtained from

$$p_A(x) = \frac{\frac{p_t(x)g(D_x(x))}{\gamma(x)} - \sum_{\chi=1, \chi \neq x}^X p_t(\chi)g(D_\chi(x)) - N(x)}{g(D_A(x))} \quad (2.1)$$

where $p_t(x)$ is the transmission power of the active medical transmitter x in watts. $D_x(x)$ is the distance between the transmitter and the receiver of active medical device x . $\gamma(x)$ and $N(x)$ are the SINR threshold and the background noise of the active medical receiver x in watts, respectively. $D_A(x)$ is the distance between the user and the active medical receiver x . $g(d)$ is the channel gain where $g(d) = 10^{-L(d)/10}$ and $L(d)$ is the total indoor propagation path loss. $L(d)[dB]$ is given as $L(d)[dB] = L(d_0)[dB] + 10n_{SF}\log(\frac{d}{d_0}) + FAF[dB]$ [60], where d_0 is the reference distance, FAF is the average floor attenuation factor, and n_{SF} is the exponent value for the same floor measurement. The RAC can retrieve locations of the transmitter and receiver and SINR threshold of the active medical device x from the inventory system. $\sum_{\chi=1, \chi \neq x}^X p_t(\chi)g(D_\chi(x))$ is the aggregate interference from other active wireless transmitters to the active receiver x where X is the number of active wireless transmitters that simultaneously transmit data at a time slot. Since active medical devices have to comply with the EMC standard, we assume that active medical devices do not interfere with passive medical devices. In this case, the level of EM energy from the transmissions of active medical devices must not exceed the EMI immunity level to which the passive medical devices were designed and tested for.

- Passive medical devices: RF emission of the transmitter of eHealth applications should not cause the EM field to passive medical devices greater than their EMI immunity level. Let $p_{NLS}(y)$ and $p_{LS}(z)$ be the upper-bound on transmission power by a transmitter of eHealth applications that non-life-supporting device y and life-supporting device z can tolerate. $p_{NLS}(y)$ and $p_{LS}(z)$ can be obtained from

$$\begin{aligned}
 p_{NLS}(y) &= \left(\frac{D_{NLS}(y)}{7} E_{NLS}(y) - D_{NLS}(y) \sum_{\chi=1}^X \sqrt{p_t(\chi)/D_\chi(y)} \right)^2 \\
 p_{LS}(z) &= \left(\frac{D_{LS}(z)}{23} E_{LS}(z) - D_{LS}(z) \sum_{\chi=1}^X \sqrt{p_t(\chi)/D_\chi(z)} \right)^2. \quad (2.2)
 \end{aligned}$$

Note that (2.2) [43] holds for the radio frequency spectrum in the range from 800 MHz to 2.5 GHz. This equation is calculated from the basic relationship between radiated power and electric field (i.e., $E = Z_0 \frac{\sqrt{P}}{D}$). The constant Z_0 comes from the free-space impedance where $(Z_0)^2$ has unit of Ohms (Ω). D is the distance between the wireless transmitter and the medical device. $D_{NLS}(y)$ and $D_{LS}(z)$ are the distances from the non-life-supporting device y to the user and from the life-supporting device z to the user, respectively. $E_{NLS}(y)$ and $E_{LS}(z)$ are the EMI immunity (i.e., the radiated RF immunity) levels of non-life-supporting device y and life-supporting device z , respectively. The EMI immunity level here is defined in terms of the electric field (measured in volts per meter or V/m) for which the medical devices can operate properly. $p_t(\chi)$ is the transmission power of the active medical device χ . Therefore, the aggregate transmission power of the active medical devices and the wireless transmitter will not cause the EM energy to rise above the EMI immunity levels of the passive medical devices. Again, the RAC can retrieve these EMI immunity levels and locations of the passive medical devices from the inventory system.

The maximum transmission power for a user can be obtained by solving (2.3).

$$p_{max} = \min \left\{ \min_x (p_A(x)), \min_y (p_{NLS}(y)), \min_z (p_{LS}(z)) \right\}. \quad (2.3)$$

However, multiple users can transmit at the same time. In such a case, p_{ctrl} should be calculated by considering the aggregate transmission power when multiple users

simultaneously transmit RTS messages on the control channel. Therefore, p_{ctrl} can be computed as follows:

$$p_{ctrl}^H = \sum_{n_1=0}^{T_1-1} \binom{T_1-1}{n_1} \alpha_1^{n_1} (1 - \alpha_1)^{(T_1-1-n_1)} \quad (2.4)$$

$$p_{ctrl}^L = \sum_{n_2=0}^{T_2} \binom{T_2}{n_2} \alpha_2^{n_2} (1 - \alpha_2)^{(T_2-n_2)} \frac{p_{max}}{n_1 + n_2 + 1} \quad (2.5)$$

$$p_{ctrl}^L = \sum_{n_1=0}^{T_1} \binom{T_1}{n_1} \alpha_1^{n_1} (1 - \alpha_1)^{(T_1-n_1)} \quad (2.5)$$

$$\sum_{n_2=0}^{T_2-1} \binom{T_2-1}{n_2} \alpha_2^{n_2} (1 - \alpha_2)^{(T_2-1-n_2)} \frac{p_{max}}{n_1 + n_2 + 1}$$

where p_{ctrl}^H and p_{ctrl}^L denote p_{ctrl} of a high-priority and low-priority user, respectively. T_1 and T_2 are the total number of high-priority and low-priority users, respectively. α_1 and α_2 are the arrival probabilities of a high-priority and low-priority user at a certain time slot, respectively. Details of obtaining α_1 and α_2 will be described in Section 2.3.1. Considering when a high-priority user is transmitting on the data channel, $T_1 - 1$ in (2.4) and T_1 in (2.5) will be replaced by $T_1 - 2$ and $T_1 - 1$, respectively, and $n_1 + n_2 + 1$ in both (2.4) and (2.5) can be substituted by $n_1 + n_2 + 2$. On the other way, if a low-priority user is transmitting on the data channel, T_2 in (2.4) and $T_2 - 1$ in (2.5) will be replaced with $T_2 - 1$ and $T_2 - 2$, respectively, and $n_1 + n_2 + 1$ in both (2.4) and (2.5) will be replaced by $n_1 + n_2 + 2$.

The ON-OFF status and locations of medical devices and locations of clients (i.e., high-priority and low-priority users) can change dynamically over time. Therefore, the RAC computes and broadcasts p_{ctrl} when the state of a medical device changes. We assume that the status of the medical devices is always updated in the inventory system. If a device is switched on or off, the inventory will update this to the RAC. The RAC will calculate a new value for p_{ctrl} for every user and then broadcast it as follows. Similar to IEEE 802.11 standard, at the beginning of each time slot, each user will wait until the channel (i.e., control or transmission channel) is sensed idle for a DCF inter-frame space (DIFS) before transmitting an RTS message or a data packet. If the RAC has to update p_{ctrl} , it will broadcast a new message of p_{ctrl} after a short inter-frame space (SIFS) in both control and data channels. Since the SIFS is shorter than the DIFS, all users can detect the broadcasting and stop their transmissions

so that the users can synchronize to the RAC. With this mechanism, the RAC can always capture the change of the hospital environment and does not cause EMI to the medical devices.

2.2.3.2 EMI-Aware RTS-CTS Protocol for Uplink Request Transmission

After common control channel broadcasting, a user can transmit its transmission requests by using an EMI-aware RTS-CTS protocol on the control channel. The protocol works as follows (Fig. 2.2). Before transmitting data, the user transmits an RTS message to the RAC by using p_{ctrl} . If a high-priority user suffers collision, it will wait for a random time based on a constant backoff window while a low-priority user will wait for a random time based on exponential backoff window. In this case, the users are said to be in the imaginary orbit and will retransmit the RTS message in near future. Note that the information about the user type will be indicated in the request message of the EMI-aware RTS-CTS protocol.

Once the RTS message is successfully received by the RAC, it calculates the upper-bound transmission power for the user on the data channel in the same way as p_{ctrl} . If the RAC cannot find the feasible transmission power which meets the EMI constraints of the medical devices and satisfies the minimum QoS requirements (i.e., minimum data rate) of the user, the request for data transmission of the user will be dropped. The probabilities that the dropping event occur are P_{d1}^{EMI} and P_{d2}^{EMI} for high-priority and low-priority users, respectively. Please note that the user who can cause the EMI problem to the medical devices will be not allowed to transmit on the data channel and be certainly dropped where P_d^{EMI} represents the probability that the users will cause the EMI problem and be dropped. In addition, to avoid congestion, the RAC will randomly drop the transmission requests with probabilities P_{d1}^{cong} and P_{d2}^{cong} for high-priority and low-priority users, respectively. These probabilities can be determined for each time slot from an analysis (i.e., prediction) of future system performance. Details to obtain P_d^{cong} are described in Section 2.4. Therefore, transmissions of high-priority and low-priority users can be dropped with P_{d1} and P_{d2} , respectively, where $P_d = P_d^{EMI} + P_d^{cong}$. Please note that the user who can cause the EMI problem to the medical devices will be not allowed to transmit on the data channel and be certainly dropped where P_d^{EMI} represents the probability that the users will cause the EMI

problem and be dropped.

If the transmission request of a user is dropped, a negative CTS message is transmitted to the user by the RAC. Otherwise, the RAC will transmit a CTS message with the maximum allowable transmission power. The user can adaptively tune its transmission power on the data channel accordingly. Once the CTS message is successfully received by the user, the user will immediately transmit an acknowledge (ACK) message to the RAC within the same time slot. A time slot of CTS transmission is composed of the CTS transmission period and the ACK transmission period. If the RAC does not receive the ACK message at the end of the time slot, it will automatically repeat the CTS transmission (e.g., using Automatic Repeat reQuest (ARQ) protocol) in the next time slot. Note that, this protocol deals with transmission in the link layer where the ACK message is the acknowledgement of transmission between two nodes (i.e., single-hop transmission). It is different from acknowledgement at TCP (Transmission Control Protocol) layer which considers end-to-end transmission (i.e., may need more than one hop for a transmission). Furthermore, the acknowledgement of TCP layer is recognized as data at the link layer.

Similar to the broadcasting, each user waits until the common control channel is sensed idle for a DIFS before transmitting an RTS message. Upon receiving an RTS message, the RAC will immediately transmit a CTS message to the user after an SIFS during the CTS time slot.

2.2.3.3 EMI-Aware RTS-CTS Protocol for Downlink Request Transmission

The flowchart of the EMI-aware RTS-CTS protocol for downlink request transmission is shown in Fig. 2.3. Once the RAC has a request from a user/device, it retrieves the location of the user and calculates the feasible transmission power to avoid the EMI. If the RAC cannot find the feasible transmission power, the transmission request will be dropped with probabilities P_{d1}^{EMI} and P_{d2}^{EMI} for high-priority and low-priority users, respectively. To avoid congestion, the downlink transmission request can be also dropped with probabilities P_{d1}^{cong} and P_{d2}^{cong} for high-priority and low-priority users, respectively. If the transmission request is allowable, the RAC will transmit an RTS message along with the feasible transmission power on the data channel to

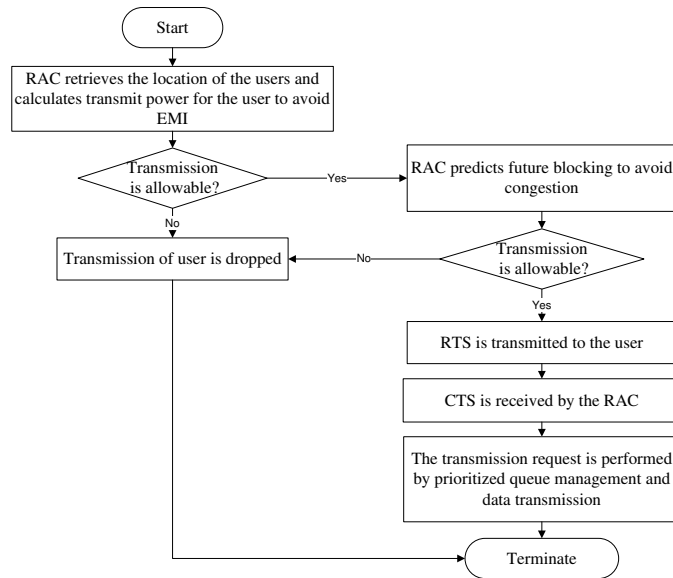


Figure 2.3. *Flowchart of EMI-aware RTS-CTS protocol for downlink transmission.*

the user after an SIFS to avoid collision with RTS message from other users. Upon receiving the RTS message, the user will respond with a CTS message after an SIFS period. In the same time slot of the CTS transmission, the RAC will immediately transmit an ACK message to the user. An ARQ mechanism is also used to recover from erroneous transmissions.

Although the RTS/CTS protocol incurs overhead in data transmission, it can be used to avoid harmful interference to the medical devices, and the hidden terminal problem. In practice, RTS and CTS transmission lengths are very small (e.g., 18 ms each) while the duration of data transmissions of high-priority and low-priority users are several hundred milliseconds (e.g., 250 ms for high-priority and 810 ms for low-priority users). Compared with the data transmission length, the overhead caused by the RTS/CTS protocol is negligible.

2.2.3.4 Prioritized Queue Management and Data Transmission

Upon receiving the CTS message for uplink transmission or RTS message for downlink transmission, the user will switch its radio from the control channel to the data channel. The user will wait in the data channel until the RAC transmits a message to allow the user to transmit/receive data when the data channel is available for the

user. The duration of a time slot is assumed to be fixed during which one packet can be transmitted. This transmission time slot is composed of the data transmission period and the ACK transmission period. We also assume that an ARQ protocol is used in the data channel for error control.

Two priority queues at the RAC are used to store the transmission requests of the high-priority and low-priority users separately. The sizes of these queues are finite. If the transmission queues are full, the RAC will transmit a negative CTS message to the user. The user will wait in the orbit and retransmit the request.

High-priority users are always allowed to transmit if there is any request in the transmission queue. The low-priority users have to wait in the queue until the queue for the high-priority users is empty. Then, the RAC allows a low-priority user to transmit. Moreover, the low-priority queue is a preemptive queue. If a low-priority user is in service, the low-priority user's service will be interrupted at once if a transmission request of a high-priority user arrives the transmission queue, and will not be resumed until there is no high-priority user in the queue.

Due to channel fading, the message to allow a transmission from the RAC to a user may be lost. After a finite number of retransmissions (e.g., based on the ARQ protocol), the RAC will give up and remove the request from its transmission queue. On the other hand, if the user does not receive this message within a finite time out period, it will restart the entire process.

2.3 Queuing Analysis of the Prioritized Wireless Access Scheme

This section presents a queuing model for the proposed prioritized wireless access scheme. We assume that the RAC will transmit data to the users only if the requests from the users are received. This analysis considers only uplink request transmissions. We assume that there is no packet loss due to channel fading. Since the data is transmitted based on TDMA using equal-length time slots, a discrete-time queuing model is developed. Two performance metrics, namely, the average transmission delay of high-priority users and the loss probability of low-priority users are derived.

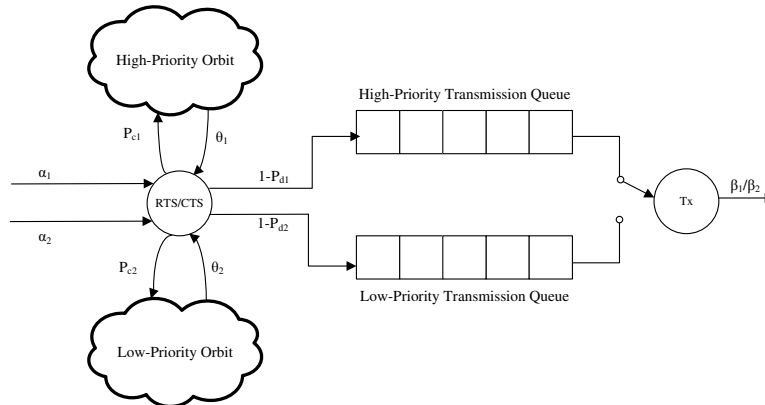


Figure 2.4. *Queuing model for the EMI-aware prioritized wireless access system.*

2.3.1 Queuing Model and Assumptions

The queuing model for the EMI-aware prioritized wireless access scheme consists of two tandem servers (i.e., one for the control channel and the other for the data channel), two orbits and two buffers (i.e., each one for high-priority users and low-priority users) as shown in Fig. 2.4. We consider a scenario where an RTS request arrives at the server in the control channel according to independent Bernoulli processes with arrival probabilities α_1 and α_2 for high-priority users and low-priority users, respectively. For eHealth applications, α_1 and α_2 can be defined from the number of events occurring over a time period. For example, an EMR application has 60 events per hour. If a time slot is 18 ms, $\alpha = \frac{60 \times 18}{60 \times 60 \times 1000} = 0.0003$. When a collision occurs, the users will go to the orbits. A high-priority user in the orbit retransmits the RTS message with probability θ_1 and a low-priority user will retry with probability θ_2 . θ_1 and θ_2 can be computed using (2.6) [61] and (2.7) [62], respectively, as follows:

$$\theta_1 = \frac{2}{W_1 + 1} \quad (2.6)$$

where W_1 is the constant backoff window size of high-priority users, and

$$\theta_2 = \frac{2}{W_2 P_{c2} \sum_{j=0}^{m-1} (2P_{c2})^j + W_2 + 1} \quad (2.7)$$

where W_2 is the minimum backoff window size of low-priority users. Here m is the maximum backoff stage and P_{c2} is the collision probability of the low-priority users when transmitting RTS messages. P_{c2} can be computed as $P_{c2} = 1 - P_{nc2}$, where

P_{nc2} is the probability that the collision of low-priority users does not occur during an RTS time slot. P_{nc2} is obtained from

$$P_{nc2} = \begin{cases} (n_2)\alpha_2(1 - \alpha_2)^{n_2-1}(1 - \theta_2)^{o_2}(1 - \alpha_1)^{n_1}(1 - \theta_1)^{o_1} \\ + (o_2)\theta_2(1 - \theta_2)^{o_2-1}(1 - \alpha_2)^{n_2}(1 - \alpha_1)^{n_1}(1 - \theta_1)^{o_1} \\ + (1 - \alpha_2)^{n_2}(1 - \theta_2)^{o_2} \end{cases} \quad (2.8)$$

where o_1 and o_2 are the number of high-priority and low-priority users in the orbits, respectively. n_1 and n_2 are the number of high-priority and low-priority users remaining in the control channel (i.e., not including the users waiting in the orbit and in the data channel), respectively. The first and the second terms denote, respectively, the probabilities that a low-priority user remaining in the control channel and in the orbit successfully transmits an RTS message. The last term is the probability that there is no RTS transmission of low-priority users. The size of the orbit for RTS requests of high priority users is not limited while that of low-priority users is bounded to N in order to control the collision to high-priority users.

The EMI-aware RTS-CTS process in the control channel requires two time slots (i.e., one time slot for RTS message and the other slot for CTS or negative CTS message). Hereafter, CTS refers to both CTS and negative CTS message. To avoid EMI and congestion effect, the transmission requests from users can be blocked with probabilities P_{d1} and P_{d2} for high-priority and low-priority users, respectively.

Moreover, the sizes of the buffers for high-priority and low-priority users are B_1 and B_2 , respectively. We also assume that the event of the user to finish its data transmission is assumed to be geometrically distributed with parameter β_1 for high-priority users and β_2 for low-priority users. β_1 and β_2 characterize the variable size of medical files (e.g., ECG files, patient profiles) for each eHealth application.

2.3.2 Discrete-Time Markov Chain (DTMC) Model

The state space of DTMC is given by $\mathcal{S} = \{(k, j, i, h, g, f); k = 0, 1, 2, \dots, T_1; j = 0, 1, 2, \dots, N; i = 0, 1, 2, \dots, B_1; h = 0, 1, 2, \dots, B_2; g = 0, 1, 2; f = 0, 1, 2, 3, 4\}$. Here, k represents the number of high-priority users in the orbit which is limited by the total number of high-priority users in the system T_1 . Also, j represents the number of low-priority users in the orbit which is limited to N . i and h refer to the number

of transmission requests waiting in the high-priority and low-priority buffers, respectively, plus one in service. i and h are limited by $B1$ and $B2$. g represents the status of the server on the data channel for $g = 0$ referring to the idle server (i.e., the buffers are empty), $g = 1$ referring to that a high-priority user is transmitting/receiving, and $g = 2$ referring to that a low-priority user is transmitting/receiving (i.e., there is no transmission request in the high-priority buffer). f represents the status of the server on the control channel where $f = 0$ referring to the idle server, $f = 1$ referring to that an RTS of a high-priority user is transmitting, $f = 2$ referring to that an RTS of a low-priority user is transmitting, $f = 3$ referring to that a CTS of a high-priority is transmitting, and $f = 4$ referring to that a CTS of a low-priority user is transmitting. Assuming that successful RTS, CTS, and data packet transmissions occur at the end of an equally-spaced discrete-time slot, a transition of the system from one state to another can be triggered by either 1) a collision, or 2) an RTS successfully arriving at the RAC on the control channel, or 3) a CTS transmitted from the RAC on the control channel, or 4) a user finishing its transmission on the data channel. We show the transition probability matrix \mathbf{P} of the DTMC in (2.9). $\mathbf{A}_{k,k-1}$, $\mathbf{A}_{k,k}$, and $\mathbf{A}_{k,k+x_1}$ are the transition probability matrices that the number of high-priority users in the orbit will be changed from k to $k - 1$, from k to k , and from k to $k + x_1$, respectively. The details of each inner matrix $\mathbf{A}_{k,k-1}$, $\mathbf{A}_{k,k}$, and $\mathbf{A}_{k,k+x_1}$ are shown in Appendix A.

$$\mathbf{P} = \begin{bmatrix} \mathbf{A}_{0,0} & \mathbf{A}_{0,1} & \mathbf{A}_{0,2} & \mathbf{A}_{0,3} & \cdots & \mathbf{A}_{0,T_1-1} & \mathbf{A}_{0,T_1} \\ \mathbf{A}_{1,0} & \mathbf{A}_{1,1} & \mathbf{A}_{1,2} & \mathbf{A}_{1,3} & \cdots & \mathbf{A}_{1,T_1-1} & \mathbf{A}_{1,T_1} \\ \mathbf{0} & \mathbf{A}_{2,1} & \mathbf{A}_{2,2} & \mathbf{A}_{2,3} & \cdots & \mathbf{A}_{2,T_1-1} & \mathbf{A}_{2,T_1} \\ \mathbf{0} & \mathbf{0} & \mathbf{A}_{3,2} & \mathbf{A}_{3,3} & \cdots & \mathbf{A}_{3,T_1-1} & \mathbf{A}_{3,T_1} \\ \vdots & \vdots & \vdots & \vdots & \cdots & \vdots & \vdots \\ \mathbf{0} & \mathbf{0} & \mathbf{0} & \mathbf{0} & \cdots & \mathbf{A}_{T_1,T_1-1} & \mathbf{A}_{T_1,T_1} \end{bmatrix}. \quad (2.9)$$

After obtaining the transition probability matrix \mathbf{P} , we can compute the stationary probability vector π by solving (2.10) [63]

$$\pi = \pi\mathbf{P}, \quad \pi\mathbf{1} = 1 \quad (2.10)$$

where π is a row vector with dimension $[(T_1 - B_1 + 1) \times (N + 1) \times (B_1 + 1) \times (B_2 + 1) \times 5] + \sum_{ii=1}^{B_1} [(N + 1) \times ii \times (B_2 + 1) \times 5]$, and $\mathbf{1}$ is a column vector of ones, with the same dimension. Here, $\pi_k^{(j,i,h)}$ represents the stationary probability that there are k users in

the high-priority orbit, j users in the low-priority orbit, i users in the high-priority queue, and h users in the low-priority queue. The structure of stationary probability vector π is as follows:

$$\begin{aligned}
\pi &= [\pi_0 \cdots \pi_k \cdots \pi_{T_1}] \\
\pi_k &= [\pi_k^{(0)} \cdots \pi_k^{(j)} \cdots \pi_k^{(N)}] \\
\pi_k^{(j)} &= [\pi_k^{(j,0)} \cdots \pi_k^{(j,i)} \cdots \pi_k^{(j,B_1)}] \\
\pi_k^{(j,i)} &= [\pi_k^{(j,i,0)} \cdots \pi_k^{(j,i,h)} \cdots \pi_k^{(j,i,B_2)}] \\
\pi_k^{(j,0,0)} &= [\pi_k^{(j,0,0,0)}], h = 0; i = 0 \\
\pi_k^{(j,0,h)} &= [\pi_k^{(j,0,h,2)}], h > 0; i = 0 \\
\pi_k^{(j,i,h)} &= [\pi_k^{(j,i,h,1)}], h \geq 0; i > 0 \\
\pi_k^{(j,i,h,g)} &= [\pi_k^{(j,i,h,g,0)} \pi_k^{(j,i,h,g,1)} \pi_k^{(j,i,h,g,2)} \pi_k^{(j,i,h,g,3)} \pi_k^{(j,i,h,g,4)}]
\end{aligned}$$

where $k \in \{0, 1, \dots, T_1\}$, $j \in \{0, 1, \dots, N\}$, $i \in \{0, 1, \dots, B_1\}$, $h \in \{0, 1, \dots, B_2\}$, and $g \in \{0, 1, 2\}$. By partitioning π in this manner, each element of π can be mapped to each state in the state space \mathcal{S} .

2.3.3 Performance Measures

Two performance metrics, namely, *the average transmission delay* of high-priority users and *the loss probability* of low-priority users are derived as follows:

2.3.3.1 Average Transmission Delay of High-priority Users

The average transmission delay accounts for the time from when a high-priority user transmits an RTS message on the control channel to when it successfully transmits all packets. Therefore, the average transmission delay of high-priority users can be computed as follows:

$$\bar{D} = \bar{D}_{orbit} + RTS + CTS + \bar{D}_{queue} \quad (2.11)$$

where \bar{D}_{orbit} is the average waiting time in the orbit until the user successfully transmits the RTS message. RTS and CTS are the average time to transmit RTS and

CTS messages, respectively, each of which requires one time slot. \bar{D}_{queue} is the average waiting time for transmission in the queue until the user successfully transmits all packets. \bar{D}_{orbit} and \bar{D}_{queue} can be obtained from Little's theorem [63] as follows:

$$\bar{D}_{orbit} = \frac{\bar{o}_1}{\alpha_{orbit}^e}, \quad \bar{D}_{queue} = \frac{\bar{q}_1}{\alpha_{queue}^e} \quad (2.12)$$

where \bar{o}_1 and α_{orbit}^e are the average number of transmission requests of high-priority users in the orbit and the effective arrival probability of high-priority users to the orbit, respectively. \bar{q}_1 and α_{queue}^e are the average number of transmission requests of high-priority users waiting in the transmission queue and the effective arrival probability to the queue, respectively. \bar{o}_1 can be expressed as $\bar{o}_1 = \sum_{k=0}^{T_1} k\pi_k$ and \bar{q}_1 is given by $\bar{q}_1 = \sum_{k=0}^{T_1} \sum_{j=0}^N \sum_{i=0}^{B_1} i\pi_k^{(j,i)}$.

α_{orbit}^e is given by the probability of collision with high-priority users (P_{c1}) which can be computed in a way similar to that of P_{c2} as defined in (2.8). α_{queue}^e is the probability that an RTS message is successfully transmitted by a high-priority user and the transmission request is allowable. α_{queue}^e can be expressed as $\alpha_{queue}^e = (1 - P_{d1}) \times \sum_{k=0}^{T_1} \sum_{j=0}^N \sum_{i=0}^{B_1} \sum_{h=0}^{B_2} \sum_{g=0}^2 \pi_k^{(j,i,h,g,1)}$.

2.3.3.2 Loss Probability of Low-priority Users

Since we assume that the size of the orbit for high-priority users unlimited, the transmission requests of high-priority users will never be lost. However, to limit the collisions between high-priority and low-priority users, the size of the low-priority orbit is limited to N . When the transmission requests of low-priority users in the orbit reaches N , any new transmission request of low-priority users on the control channel is dropped. Therefore, the loss probability of low-priority users (P_L) is given by

$$P_L = \sum_{k=0}^{T_1} \sum_{i=0}^{B_1} \sum_{h=0}^{B_2} \sum_{g=0}^2 \sum_{f=0}^4 \pi_k^{(N,i,h,g,f)}. \quad (2.13)$$

2.4 System Performance Optimization and Prediction

In this section, we optimize the system parameters (i.e., blocking probability P_{d1} and P_{d2}) by using the performance measures obtained from the queuing analysis.

Optimal blocking probabilities can be selected to maximize the system throughput while the QoS requirements for wireless access by eHealth applications are satisfied. The optimal blocking probability (P_d) is contributed by two factors: one is the EMI effect (P_d^{EMI}) and the other is the congestion effect (P_d^{cong}).

2.4.1 Optimization of Blocking Probabilities for EMI-Aware Prioritized Wireless Access Scheme

The system throughput is defined as the ratio of the number of users that successfully transmit their data over the total number of users that successfully transmit RTS message on the control channel. Therefore, the system throughput can be expressed as $1 - P_d$. Given the system parameters (i.e., α_1 , α_2 , W_1 , W_2 , m , β_1 , β_2 , T_1 and T_2), a two-stage optimization problem can be formulated as follows:

$$\text{Minimize : } P_{d1} \quad (2.14)$$

$$\text{Subject to : } \bar{D}(P_{d1}) \leq D^{(req)} \quad (2.15)$$

$$\text{Minimize : } P_{d2} \quad (2.16)$$

$$\text{Subject to : } P_L(P_{d1}, P_{d2}) \leq P_L^{(req)} \quad (2.17)$$

where $D^{(req)}$ and $P_L^{(req)}$ are the QoS requirements of eHealth applications in term of the average transmission delay of high-priority users and the loss probability of low-priority users, respectively. $\bar{D}(P_{d1})$ and $P_L(P_{d1}, P_{d2})$ can be computed as shown in (2.11) and (2.13) by using queuing analysis as described in Section 2.3. In the first stage, an optimal P_{d1} is selected to maximize the throughput of high-priority users while the average transmission delay of the users is satisfied as defined in (2.14) and (2.15). In the second stage (defined by (2.16) and (2.17)), an optimal P_{d2} is selected to maximize the throughput of low-priority users while maintaining the loss probability of the users below an acceptable level. The optimal P_{d1} obtained from the first stage is used to computed the loss probability of low-priority users as shown in (2.17). The optimization formulation in (2.14)-(2.17) can be solved numerically.

2.4.2 Exponential Moving Average Prediction Model

The prediction process is shown in Fig. 2.2. In each time slot, the optimal P_{d1} and P_{d2} can be computed by using the two-stage optimization formulation described above for the given system parameters. At the same time, the RAC calculates the blocking probabilities due to EMI (P_{d1}^{EMI} and P_{d2}^{EMI}). Since, the blocking probabilities due to the congestion should be greater than or equal to zero, they can be computed as follows:

$$P_{d1}^{cong} = \max(P_{d1} - P_{d1}^{EMI}, 0) \quad (2.18)$$

$$P_{d2}^{cong} = \max(P_{d2} - P_{d2}^{EMI}, 0). \quad (2.19)$$

The effective P_{d1}^{cong} and P_{d2}^{cong} should be increased before the network becomes congested and be reduced before unnecessary throughput degradation occurs. Therefore, P_{d1}^{cong} and P_{d2}^{cong} should be obtained in advance. In this case, one-step ahead values of P_{d1}^{cong} and P_{d2}^{cong} can be obtained by using an exponential moving average (EMA) filter. With an EMA filter, the predicted value of H at time slot $t + 1$, i.e., $\hat{H}(t + 1)$, is computed based on its value in time slot t , i.e., $\hat{H}(t)$ as follows:

$$\hat{H}(t + 1) = \hat{H}(t) + a(H(t) - \hat{H}(t)) \quad (2.20)$$

where $H(t)$ is the measured value at time slot t and a is a constant smoothing factor between 0 and 1. The accuracy of EMA depends on the smoothing factor a . Therefore, we can adjust the performance of EMA by setting the appropriate value of the smoothing factor a . Given a training data set, we can define the appropriate value of a to minimize the least normalized mean square error (NMSE). The NMSE is used to measure the accuracy of a prediction model. The NMSE can be computed as follows:

$$NMSE = \frac{\sum_{t=1}^S (\hat{H}(t) - H(t))^2}{S \times var(H)} \quad (2.21)$$

where S is the number of samples in the training data set, $var(H)$ is the variance of the measured values of H .

In each time slot, based on the current conditions (i.e., the measured values), the RAC first predicts the values of optimal P_{d1} , the optimal P_{d2} , P_{d1}^{EMI} and P_{d2}^{EMI} by

using (2.20). Then, the one-step ahead values of P_{d1}^{cong} and P_{d2}^{cong} can be obtained from (2.18) and (2.19) according to the prediction values. The prediction algorithm of blocking probabilities due to congestion avoidance is presented in Algorithm 1.

Algorithm 1 Prediction of blocking probabilities for congestion avoidance

- 1: Initialize $P_{d2} = 0$.
 - 2: Obtain optimal P_{d1} by solving the problem defined in (2.14) and (2.15) given the system parameters $\alpha_1, \alpha_2, W_1, W_2, m, \beta_1, \beta_2, T_1$ and T_2 .
 - 3: Obtain optimal P_{d2} by solving the problem defined in (2.16) and (2.17) given the system parameters $\alpha_1, \alpha_2, W_1, W_2, m, \beta_1, \beta_2, T_1, T_2$, and optimal P_{d1} .
 - 4: Obtain P_{d1}^{EMI} and P_{d2}^{EMI} from the observations.
 - 5: Predict P_{d1} and P_{d2} for the next time slot by solving (2.20) given the current optimal P_{d1} and P_{d2} .
 - 6: Predict P_{d1}^{EMI} and P_{d2}^{EMI} for the next time slot by solving (2.20) given the current observation P_{d1}^{EMI} and P_{d2}^{EMI} .
 - 7: Obtain P_{d1}^{cong} and P_{d2}^{cong} for the next time slot by solving (2.18) and (2.19) given the prediction values of $P_{d1}, P_{d2}, P_{d1}^{EMI}$, and P_{d2}^{EMI} .
 - 8: Make a decision to drop a request of a user according to P_{d1}^{cong} and P_{d2}^{cong} when a user requests to transmit data.
-

2.5 Performance Evaluation

We consider two eHealth applications, namely, clinician notifier and electronic medical record (EMR) applications. The clinician notifier applications (defined as high-priority applications) are used by physicians or medical staffs to retrieve real-time vital signals of patients when they receive an alarm notification. These applications have average delay requirement of 300 ms. EMR applications (defined as low-priority applications) are used by medical staffs to add, retrieve, and update medical data (e.g., patient profile, patient historical medications, and normal ECG recording files). EMR applications require loss probability less than 0.01 [4].

2.5.1 Simulation Setup

2.5.1.1 Evaluation Scenario

We consider a service section over 27×22 square meters in a cardiac department of a hospital including one operating room, two examination rooms, two patient rooms, an administration room, a physician room and a hall way. The service section is divided into nine areas as shown in Fig. 2.1. The RAC is located at the center of the service section.

We consider one life-supporting medical device (i.e., a defibrillator), four non-life-supporting medical devices (i.e., two electrocardiograph monitors and two blood pressure monitors), and one active medical receiver with five active medical transmitters. The locations of RAC, passive medical devices, and active medical receiver are fixed, while the locations of active medical transmitters and the users of high-priority and low-priority applications are uniformly random.

The defibrillator is used for cardiopulmonary resuscitation (CPR) for a patient of cardiac arrest while the non-life-supporting medical devices are used for treadmill exercise tests. The EMI susceptibility of the defibrillator, the ECG monitors, and the blood pressure monitors conform to the IEC 60601-1-2 standard [43]. The EMI immunity level of the defibrillator is specified to 10 V/m while the EMI immunity levels of ECG and blood pressure monitors are 3 V/m. The active medical devices are used for an in-hospital patient monitoring application which continuously monitors electrocardiograph (ECG) signals of five patients with cardiac diseases. The active medical receiver is based on IEEE 802.11g technology which has the requirement of SINR threshold equal to 16dB to guarantee 11 Mb/s transmission rate [64]. We assume that the background noise is negligible. Five active medical transmitters are scheduled to transmit the ECG signals to the active medical receiver in a round-robin manner. Therefore, only one transmitter can transmit data in each time slot. The controller is assumed to have perfect knowledge of locations and status of all medical devices. The location information of high-priority and low-priority users can be also retrieved from the inventory system.

For the patient with cardiac arrest, the defibrillator is operated once and the arrival time is uniformly random. The duration of ON status is normally distributed with mean 4.68 minutes and standard deviation 5.27 [65]. The treadmill exercise tests

are scheduled for two simultaneous tests every hour. Each test takes 10 to 15 minutes to set up, 10 to 15 minutes to operate, and 10 to 15 minutes to observe [66]. Two electrocardiograph (ECG) monitors and two blood pressure monitors used in the test are operated every hour. Moreover, the in-hospital patient monitoring application operates all time. The simulation is run for 12 hours.

The receiver of the RAC is based on IEEE 802.11b technology which requires the received signal strength of -94dBm to guarantee 1 Mb/s transmission rate [67]. We assume that both high-priority and low-priority users require the data rate of 1 Mb/s. The transmission power is attenuated due to indoor propagation path-loss and floor attenuation factor. Both high-priority and low-priority users operate in 2.4 GHz. The average indoor path loss is obtained as described in 2.2.3.1. The floor attenuation factor through one floor (FAF) is 16.2 dB [60], the measured line-of-sight (LOS) path loss at $d_0 = 1m$ is 37.7 dB (i.e., $L(d_0) = 37.7$ dB), and obstructed path loss exponent (n_{SF}) is 3.3 [68]. Based on this information, the RAC can calculate the appropriate transmission power for each user and then compute the received signal strength from the appropriate transmission power. A transmission is dropped due to EMI when the received signal strength at the receiver (either the RAC or the users) is less than -94 dBm.

2.5.1.2 System Configurations for EMI-Aware Prioritized Wireless Access System

For the clinician notifier application, the ECG signals from the monitoring devices are transmitted to the central server. When an abnormal condition is detected, an alarm will be sent to a supervising medical staff. Once the medical staffs receive the alarm, they will transmit a request to retrieve the real-time ECG signals of the patients as high-priority users in the system. A sampling rate of 250 Hz with 8-bit resolution is used to capture ECG data [69]. The ECG signals captured for 120s on average (i.e., $250 \times 8 \times 120 = 240$ *kbits*) will be transmitted to the high-priority application users. The clinician notifier applications are assumed to run 40 times an hour on average.

For EMR, the medical data size ranges from 10 kBytes (i.e., patient profile) to 100 kBytes (i.e., normal ECG recording files). A medical staff is assumed to access an EMR application 60 times in an hour on average.

The maximum size of low-priority orbit is $N = 3$. The maximum queue size for high-priority and low-priority users is $B_1 = B_2 = 3$. Both high-priority and low-priority users have the same backoff window sizes equal to 32 (i.e., $W_1 = W_2 = 32$). The maximum backoff stage for low-priority users is $m = 5$.

Based on the above scenario, the arrival probabilities for a high-priority user (α_1) and low-priority user (α_2) are 0.0002 and 0.0003, respectively. The probability that a user finishes its transmission in one time slot is 0.0714 for high-priority users (β_1) and 0.0222 for low-priority users (β_2). The simulation results obtained using MATLAB are averaged over five simulation runs.

2.5.2 Performance Evaluation of the EMI-Aware RTS-CTS Protocol

We consider the uplink transmission scenario on the data channel in which only one user can transmit data at a time. Two performance measures, namely, the *interference probability* and the *outage probability* are studied. The interference probability is the probability that the user causes EMI to the medical devices when the transmission power is higher than the acceptable level while the outage probability is the probability that the received signal strength at the RAC is less than -94 dBm.

Fig. 2.5 shows the interference probability over 9 service areas for the EMI-aware protocol and the traditional CSMA/CA protocol with transmission power fixed at 10 dBm, 0 dBm, and -5 dBm. As expected, the proposed protocol never causes EMI while the traditional CSMA/CA protocol does cause the interference to medical devices. The higher the transmission power, the more the probability of interference is. The traditional protocol can cause severe interference to the medical devices especially in area 6 since the active medical receiver is located in this area. It can also cause interference to the passive medical devices in areas 3, 7, and 8. However, the passive devices operate occasionally while the active devices operate all the time. Therefore, there are more chances that the wireless device causes interference to the active medical devices. The average interference probabilities of the traditional protocol with transmission power of 10dBm, 0dBm, and -5dBm are 81.96%, 43.73%, and 25.50%, respectively.

However, the outage probability of the EMI-aware protocol is greater than that

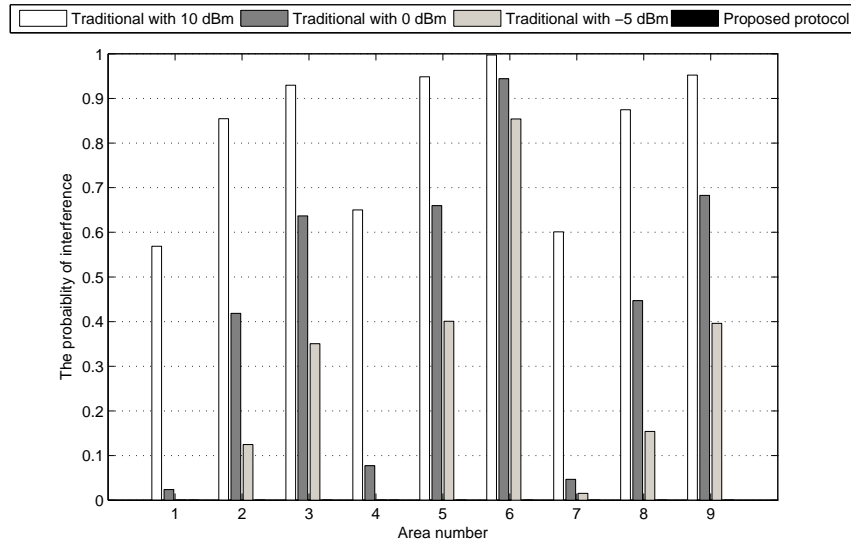


Figure 2.5. *Interference probability over 9 service areas.*

due to the traditional protocol with transmission power of 10 dBm and 0 dBm in most of the areas (Fig. 2.6). This is due to the fact that the EMI-aware protocol limits the transmission power of an active device/user to avoid the EMI to the medical devices in the vicinity. The outage probabilities around area 6 are high to avoid the EMI to the active medical receiver. However, the EMI-aware RTS-CTS protocol can adaptively increase the transmission power in the different areas according to the presence and the activity of the medical devices. Consequently, with the EMI-aware RTS-CTS protocol, the outage probability in these areas is less than that due to the traditional protocol with transmission power of 0dBm and -5dBm. The traditional protocol with transmission power of 10dBm never has the outage problem due to high transmission power but it causes the highest interference probability. The average outage probability for the traditional protocol with transmission power of 0dBm and -5dBm is 1.01% and 33.51%, respectively, while that due to the EMI-aware protocol is 18.71%.

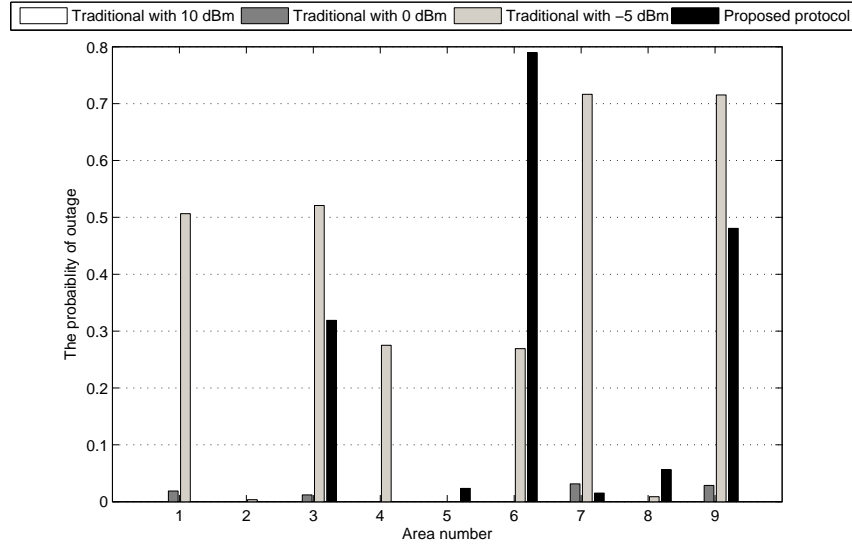


Figure 2.6. Outage probability over 9 service areas.

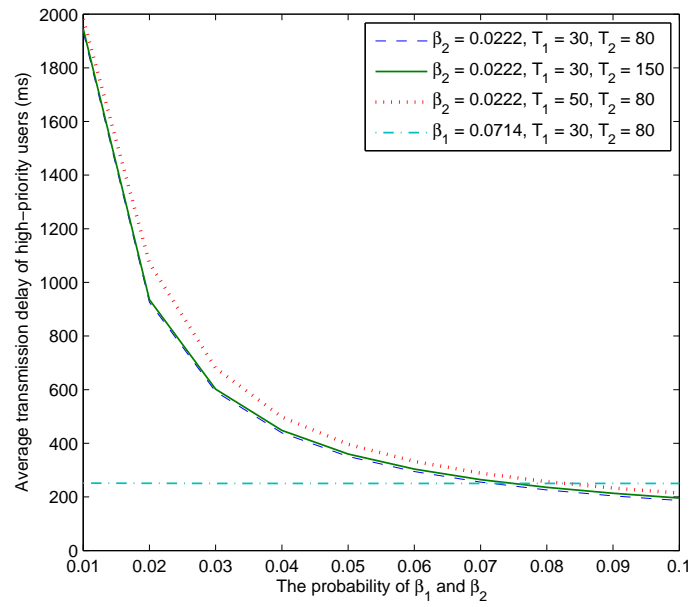
2.5.3 Performance Evaluation of EMI-Aware Prioritized Wireless Access Protocol

We investigate the performance of high-priority and low-priority users in the EMI-aware prioritized wireless access protocol. We study two performance metrics, namely, the *average transmission delay* of high-priority users (\bar{D}) and the *loss probability* of low-priority users (P_L).

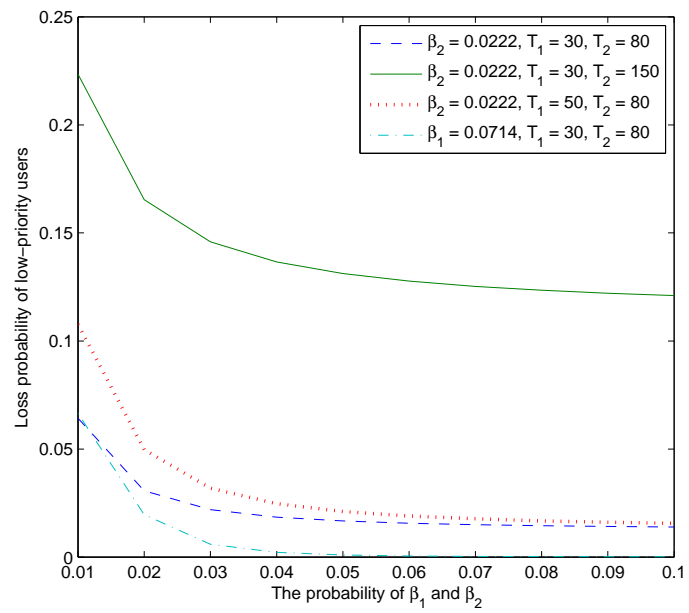
2.5.3.1 Effects of Transmission Durations

We first study the effect of transmission durations of high-priority and low-priority users on the performance of the proposed protocol. The transmission durations are based on the probabilities that users finish their transmissions in a certain time slot (β_1 and β_2). We fix the blocking probabilities of high-priority and low-priority users to 0.1972 and 0.2012, respectively, which are the blocking probabilities of high-priority and low-priority users (P_{d1}^{EMI} and P_{d2}^{EMI}) due to EMI effect. The average transmission delay of high-priority users (\bar{D}) and the loss probability of low-priority users (P_L) obtained from the queuing model are shown in Fig. 2.7.

Clearly, as the transmission duration of high-priority users decreases (i.e., β_1 increases), \bar{D} decreases. The average transmission duration of low-priority users (i.e.,



(a)



(b)

Figure 2.7. (a) Average transmission delay of high-priority users, and (b) loss probability of low-priority users versus β_1 and β_2 .

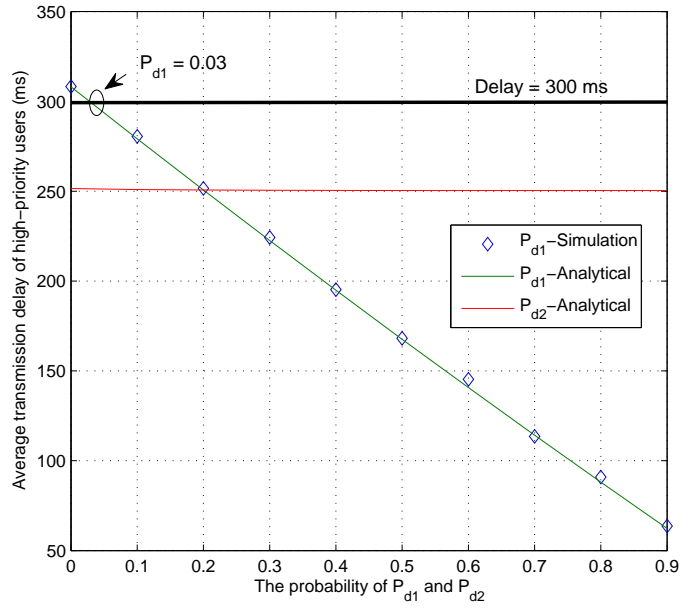
$1/\beta_2$) does not affect the performance of high-priority users. Moreover, \bar{D} also increases when the number of high-priority and low-priority users increases. As the number of users increase, the chance that a collision occurs also increases. Therefore, the high-priority users have to spend more time in the orbit. As shown in Fig. 2.7(b), it is evident that P_L is sensitive to β_1 , β_2 , and number of users in the system.

2.5.3.2 Effects of Blocking Probabilities

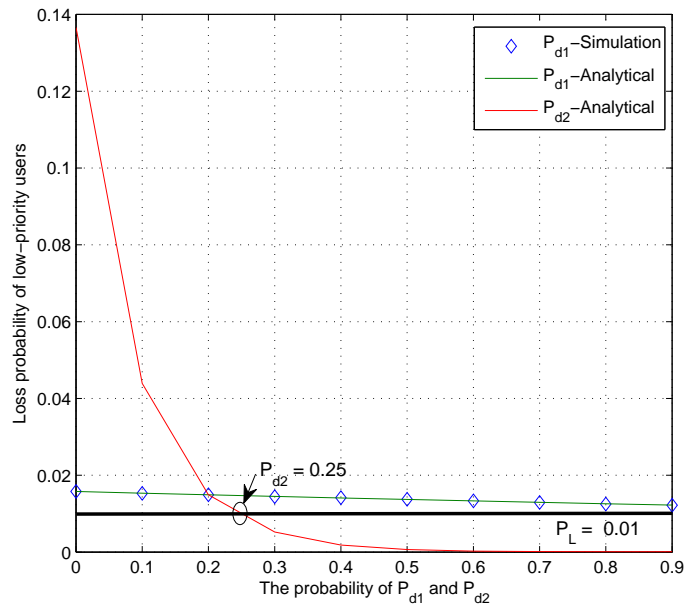
We also investigate the impact of blocking probabilities of high-priority and low-priority users (P_{d1} and P_{d2}). We fix the number of high-priority and low-priority users to 30 and 80, respectively. We also fix P_{d1} at 0.1972 while P_{d2} is varied. Alternatively, P_{d2} is fixed at 0.2012 while P_{d1} is varied. We show the analytical and simulation results on \bar{D} and P_L in Fig. 2.8.

As expected, the average transmission delay \bar{D} decreases when P_{d1} increases. As P_{d1} increases, the average number of requests from high-priority users in the queue decreases. Note however that \bar{D} is not sensitive to P_{d2} . In Fig. 2.8(b), as P_{d1} increases, low-priority users have higher probability to transmit their data and the probabilities that the queue and the orbit of low-priority users are full are smaller. Therefore, P_L decreases as P_{d1} increases. Similarly, when P_{d2} increases, the average number of requests from low-priority users in the queue decreases. In this case, there is a high probability that the requests from low-priority users in the orbit are transmitted, and therefore, the number of low-priority users in the orbit significantly decreases. Consequently, when P_{d2} increases, P_L decreases.

Based on the above results, the RAC can optimize the blocking probabilities to guarantee the QoS of users in the system while maximizing the system throughput. In Fig. 2.8, P_{d1} should be equal to 0.03 to guarantee \bar{D} below 300 ms while P_{d2} should be equal to 0.25 which is the minimum P_{d2} to maintain P_L below 0.01. However, since P_{d1}^{EMI} is 0.1972, P_{d1}^{cong} should be zero. On the other hand, since P_{d2}^{EMI} is 0.2012, P_{d2}^{cong} is fixed at 0.0488 (i.e., $0.25 - 0.2012$). In this way, the system can achieve both the maximum throughput and guarantee QoS while avoiding EMI to medical devices at the same time.



(a)



(b)

Figure 2.8. (a) Average transmission delay of high-priority users, and (b) loss probability of low-priority users versus P_{d1} and P_{d2} .

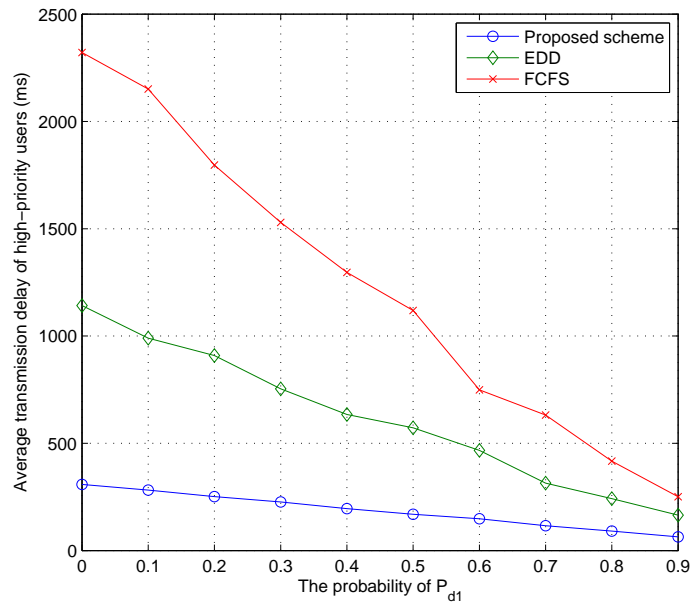
2.5.3.3 Comparison with Other Scheduling Schemes

We compare the performance of the proposed prioritized wireless access scheme with other centralized scheduling schemes via simulations. Two scheduling schemes, namely, First-Come-First-Served (FCFS) and Earliest Due Date (EDD) schemes, are considered. The FCFS scheme serves the requests of the users following the sequence of arrival whereas the EDD algorithm serves the user who has the shortest deadline or the shortest time to extinction first. In this case, we define the maximum delay (i.e., time to extinction) equal to 300 ms and 1s for high-priority and low-priority users, respectively.

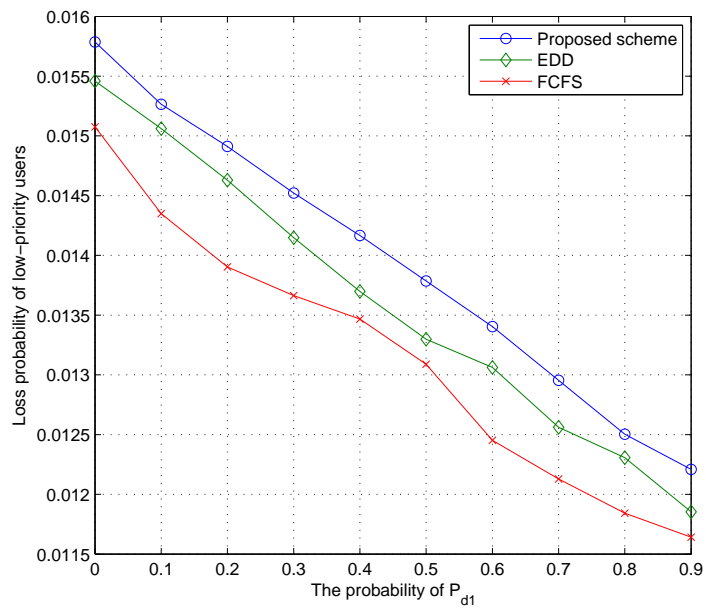
Fig. 2.9(a) shows average transmission delay ($Delay$) of the proposed scheme compared to EDD and FCFS scheduling schemes. The proposed scheme outperforms the two other scheduling schemes due to the prioritized transmission. Since high-priority users always have the privilege to transmit their data first, \bar{D} of the proposed scheme is always lower than those of EDD and FCFS scheduling schemes. Although the EDD scheme also provides high privilege to high-priority users, occasionally, it has to give higher privilege to low-priority users when they are close to be extinct. With the FCFS scheme, the high-priority users may have to wait in the transmission queue until the transmission of low-priority users finishes. Moreover, the lengths of transmission of low-priority users are longer than those of high-priority users. Therefore, \bar{D} for the FCFS scheme is always larger than that for the EDD and the proposed schemes.

A comparison of loss probability (P_L) is shown in Fig. 2.9(b). The proposed scheme always gives the privilege to high-priority users that could result in packet loss for low-priority users. EDD and FCFS schemes can provide lower P_L to low-priority users. However, these schemes also cause relatively large $Delay$ to high-priority users at the same time. The proposed scheme can improve the average delay by 70.08% and 84.90% compared to those of EDD and FCFS schemes, respectively, while the loss probability increases by 2.52% and 6% compared to EDD and FCFS schemes, respectively. Note that the proposed scheme can provide delay and loss guarantee for high and low-priority users, respectively. The EDD and FCFS schemes may not be able to provide these QoS guarantee.

In addition, a comparison among overall throughput of the three schemes (i.e.,



(a)



(b)

Figure 2.9. (a) Average transmission delay of high-priority users, and (b) loss probability of low-priority users compared with other scheduling schemes.

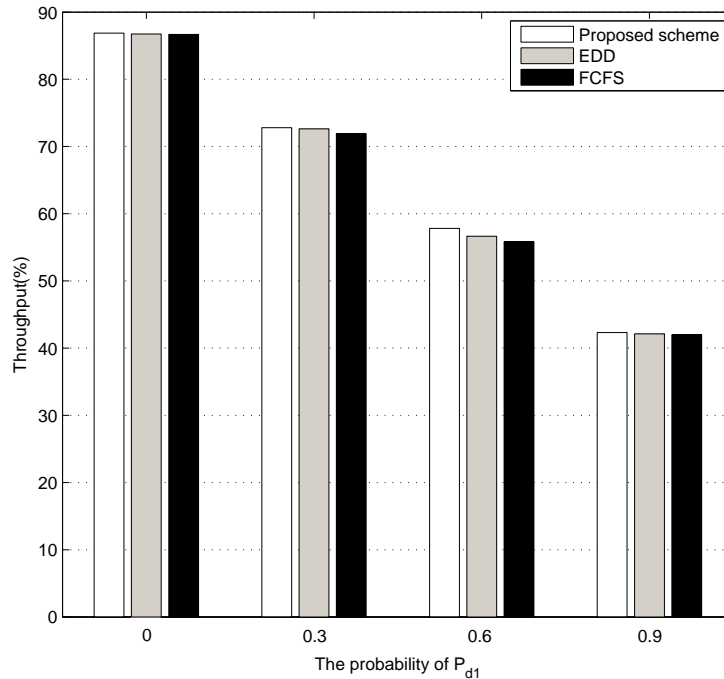


Figure 2.10. Overall throughput compared with other scheduling schemes.

the proposed scheme, EDD, and FCFS) is shown in Fig. 2.10. The proposed scheme can provide higher throughput than EDD and FCFS since the proposed scheme can serve more high-priority users which have the shorter transmission lengths than low-priority users. The proposed scheme can improve the overall throughput by 0.95% and 1.11% compared to those of EDD and FCFS schemes. Therefore, the proposed scheme achieves service differentiation between high-priority and low-priority users while improving the overall network utilization.

2.5.4 Performance Evaluation of EMI-Aware Prioritized Wireless Access Protocol Integrated with EMA Prediction Model

We also evaluate the performance of the EMA prediction model when it is used to support the EMI-aware prioritized wireless access protocol to predict the values of P_{d1}^{cong} and P_{d2}^{cong} . In the evaluation scenario, the initial number of high-priority users is set to 300, and this number decreases by 50 every two hours. The performance

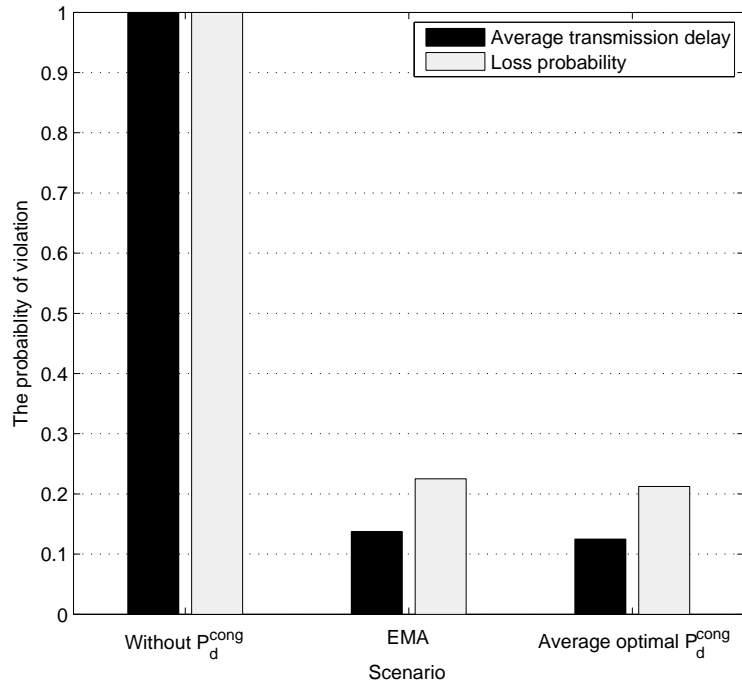


Figure 2.11. *The probability of violation.*

of the proposed prediction model is measured in terms of probability of violating the delay requirement (i.e., the probability that the average delay of high-priority users is greater than 300 ms) and the probability of violating the loss probability requirement (i.e., the loss probability of low-priority users is greater than 0.01). To obtain these probabilities, we first observe the average delay of high-priority users and loss probability of low-priority users every 30000 time slots. Then, the probability of violating QoS requirements is computed as the ratio of the number of violation occurrences to the overall observations. We compare these performance measures with two systems, i.e., the system without blocking to avoid the congestion, and the system with fixed blocking probability for congestion avoidance. Transmissions in the first system are dropped due to only the EMI effect, while transmissions in the second system are dropped due to both EMI effect and congestion effect. The congestion probability P_d^{cong} is fixed at the average of optimal blocking probabilities for every two hours. As the number of high-priority users is varied every two hours, P_d^{cong} is updated every two hours and then kept fixed for the system until the next update.

Fig. 2.11 shows the probabilities of violating the QoS requirements of three scenar-

ios. The system which does not use blocking to avoid congestion cannot guarantee the QoS requirements. On the other hand, the proposed system with EMA can adaptively perform and provide the results similar to the system with the blocking probabilities fixed at the average optimal values. Since the system parameters are random in nature, the QoS requirements will be violated occasionally. Compared to the system without blocking for congestion avoidance, the proposed system can reduce the probability of violation of average transmission delay and loss probability requirements by 86.25% and 77.50%, respectively.

2.5.5 Summary of the Results and Discussions

Based on the evaluation results, the key observations are as follows.

- The proposed EMI-aware prioritized wireless access protocol can protect biomedical devices from the harmful interference and adaptively adjust transmission power to achieve the transmission requirement (i.e., received sensitivity) based on the presence and status of medical devices.
- The proposed protocol can achieve service differentiation among different eHealth applications (i.e., clinician notifier and electronic medical record applications). The proposed protocol outperforms the other centralized scheduling schemes (e.g., FCFS and EDD schemes) to reduce the average transmission delay of high-priority users and improve the overall network utilization.
- The performance of those eHealth applications relies on several system parameters (e.g., the number of users, the average transmission durations, and the blocking probabilities). To optimize the system performance, the blocking probabilities can be adjusted to achieve the maximum throughput while satisfying the QoS requirements (i.e., the average transmission delay and loss probability).
- We observe that the effects of system parameters corresponding to low-priority users on the performance of high-priority users are not significant while the system parameters of high-priority users significantly affect the loss probability of low-priority users. Therefore, we can adaptively tune the performance of high-priority users by adjusting only the blocking probability of high-priority users. On the other hand, the performance of low-priority users is affected by

both the blocking probabilities of high-priority and low-priority users.

- With the EMA scheme, the proposed wireless access scheme can automatically adapt to the changes of the system conditions (i.e., the status and locations of medical devices and the number of users) by adaptively adjusting the blocking probabilities due to congestion avoidance. Performance evaluation results show that the proposed protocol integrated with EMA model can adaptively guarantee QoS.

2.6 Implementation of the EMI-Aware Prioritized Wireless Access Scheme

The proposed EMI-aware prioritized wireless access scheme can be implemented using off-the-shelf programmable IEEE 802.11 devices. For example, the MADWIFI (Multiband Atheros Driver for Wi-Fi) driver [70] is an open source Linux driver (implemented on kernel 2.4.20 or higher) to support wireless adapters using Atheros chipsets. With a loadable kernel module, the modified driver can be used without recompiling. MADWIFI driver also provides the wireless extension tool to easily configure the Atheros driver (e.g., setting frequency, sensitivity threshold, RTS/CTS threshold, transmission power, CW_min and CW_max).

To support common control broadcasting, a function to calculate p_{ctrl} should be added to the broadcast module of the driver. The same broadcasting method as that in IEEE 802.11 standard can be used.

Similar to the common control broadcasting, the IEEE 802.11 MAC should be modified to have functions to calculate the transmission power and make a decision (whether the transmission is allowable or not) depending on the transmission power to support EMI-aware RTS-CTS protocol. The feasible transmission power should be added in the CTS packet. The size of the backoff window should be set to a constant value for high-priority users while the exponential backoff scheme should be used for low-priority users. The users should be able to dynamically switch between control channel and data channel by setting the operating frequency via the wireless extension tool.

Finally, two buffers should be allocated to maintain the identification (ID) of the

users who are allowed to transmit data on the data channel. The Point Coordination Function (PCF) mode of IEEE 802.11 standard can be used for polling-based transmission on the data channel. However, the PCF mode should be modified to provide different priorities to users/devices for service differentiation.

2.7 Conclusion

We have proposed an EMI-aware prioritized wireless access scheme for eHealth applications. This scheme considers two major issues, namely EMI immunity to medical devices and QoS differentiation in healthcare environment. Two eHealth applications, namely clinical notifier and electronic medical record (EMR) applications have been considered. A queuing analytical model has been developed to study the behavior of the proposed scheme. Performance evaluation results have showed that the proposed scheme can protect the active and passive bio-medical devices from the harmful interference and also achieve service differentiation among different eHealth applications. Performances (i.e., delay and loss probability) of the proposed scheme can be optimized by adjusting the blocking probabilities. The results obtained from the queuing model can be used to optimize the blocking probabilities to maximize the system throughput while satisfying the QoS requirements of the eHealth applications. For adaptive performance tuning, we have proposed an exponential moving average (EMA) model to predict values of the blocking probabilities for congestion avoidance, based on the optimal blocking probabilities and the blocking probability due to EMI avoidance. The performance evaluation results have showed that the EMA scheme can accurately predict the blocking probabilities and guarantee QoS.

Chapter 3

EMI-Aware Transmission Scheduling and Power Control for Multiple Service Cells

In this chapter, we consider multiple STDMA infrastructure-based wireless networks as shown in Fig. 3.1, in which the secondary and primary users from different networks can transmit data simultaneously if the EMI level to primary (active medical devices) and protected (passive medical devices) users is maintained below the maximum threshold. We address the problem of dynamic wireless access for secondary networks using STDMA in hospital environments. The objectives are the followings: i) maximize spectrum utilization of the secondary networks, ii) minimize power consumption of the secondary users to increase battery life, iii) protect the medical devices from harmful interference considering the IEC 60601-1-2 standard, and iv) guarantee QoS performance of secondary users. To solve this problem for multiple STDMA wireless networks, we formulate a dual-objective optimization problem. The solution of the problem results in optimal transmission schedules, optimal channel allocations, and optimal transmission powers for the secondary users during each time slot. However, the exhaustive search used to find optimal solutions incurs huge computational complexity, and therefore, may not be suitable for online execution. Therefore, we propose an implementation-friendly *joint scheduling and power control algorithm* based on a greedy approach. However, the performance of the greedy algorithm can be improved by using the optimal sequence of secondary users that should be scheduled. With this additional stage, the spectrum utilization of secondary users can be increased and the interference to protected and primary users can be elimi-

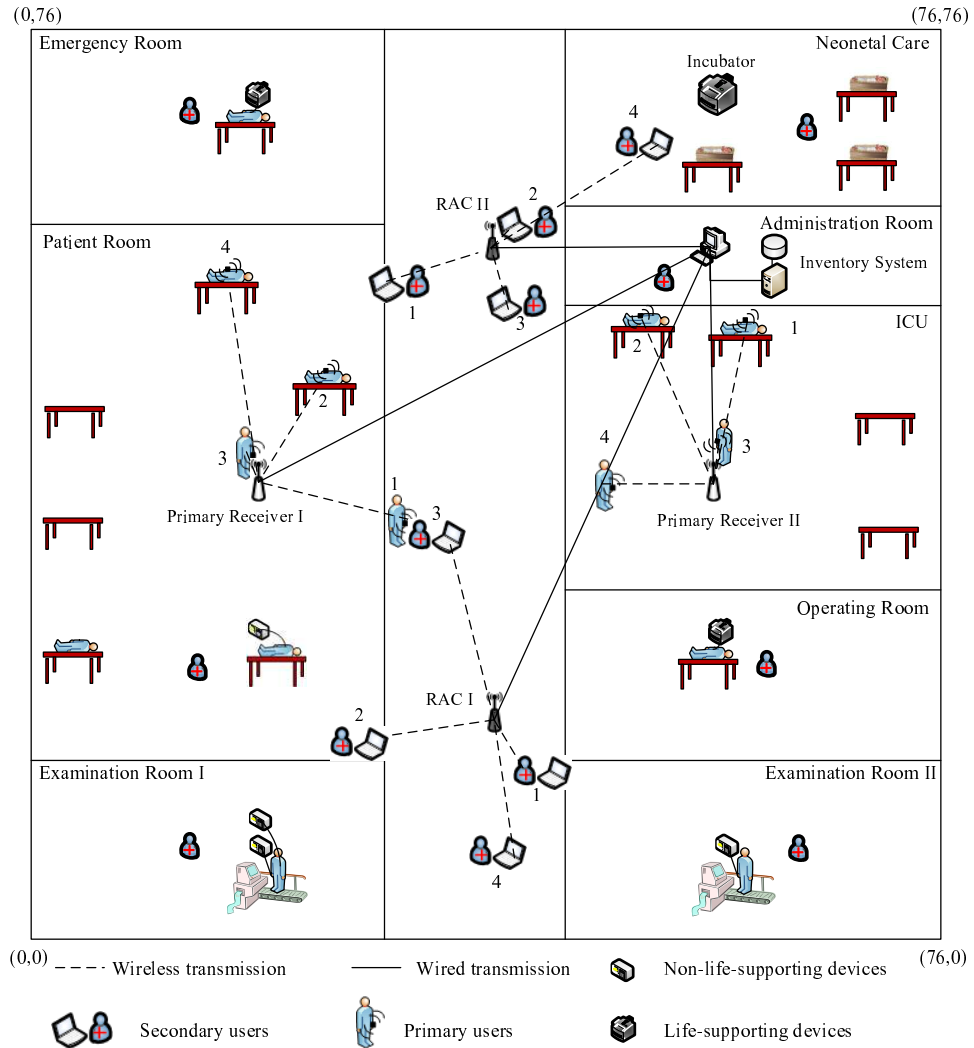


Figure 3.1. A multiple service cell scenario in a hospital environment.

nated. This is referred to as the *enhanced greedy algorithm*. The tradeoff between performance gain and computational complexity is evaluated for both the algorithms.

The proposed models for EMI-aware transmission scheduling and power control can be used for any wireless network using TDMA-type of wireless access. Therefore, in addition to IEEE 802.11 type network, the proposed algorithms can also be applied for IEEE 802.15.4 (i.e., ZigBee) networks, cellular, and WiMAX networks. For example, in the context of a cellular or WiMAX network, using the proposed algorithms, scheduling and power control for different users can be performed in a multi-cell basis.

3.1 Related Work

One of the main challenges of using IEEE 802.11-based network in medical environments is how to provide efficient spectrum utilization while guaranteeing the QoS requirements of the applications, especially for life-critical applications. To support medical-grade QoS in WLANs, the authors of [58] proposed a fully-distributed contention control mechanism with modifications to the IEEE 802.11e MAC (Medium Access Control) standard. A set of QoS enhancement methods for WLAN applications was defined to prioritize the medical traffic based on their criticality. To support QoS for remote health care, *CareNet* was designed in [59], where linear programming techniques were used for admission control and admitted users are prioritized, queued and scheduled to transmit data based on the criticality of their conditions. The authors of [71] proposed a QoS-aware network for remote ultrasound streaming by using the concept of cognitive radio. However, since these medical-grade QoS wireless networks do not consider the EMI issue, deploying these networks in a hospital or healthcare environment may cause risk to the EMI-sensitive medical devices.

To jointly address the EMI and QoS provisioning issues in RF WLAN for eHealth applications in hospital environments, in Chapter 2, we proposed a MAC protocol, namely, the EMI-aware prioritized wireless access protocol, which is based on the CSMA/CA method. To mitigate the EMI problem, we use power control (i.e., EMI-aware protocol) to avoid harmful interference to medical devices. This protocol, however, considers only one single service cell. In practice, there exist several service cells to provide coverage over large area in a hospital. The key challenge here is how to construct a spectrum access/sharing (i.e., scheduling) scheme such that primary users are protected from interference and the minimum QoS requirements of the secondary users are guaranteed.

To deal with the access problem of several concurrent transmissions, an optimal scheduling and power control scheme for TDMA-based point to multipoint wireless networks was introduced in [72]. The integration of scheduling and power control for wireless ad-hoc networks was also proposed in [73] in order to limit multi-user interference and increase single-hop throughput. The concept in [73] was extended for code-division multiple access (CDMA)-based cognitive radio networks [74].

Our work is different from the existing work on joint scheduling and power control

in the literature in the following aspects: First, we consider the problem of coexistence of multiple STDMA infrastructure-based wireless networks assuming a physical interference model (i.e., a signal-to-interference-plus-noise-ratio (SINR)-based model). Second, we consider spectrum sharing on multiple channels as opposed to only one channel. Third, we consider the EMI issue to protect the medical devices in the healthcare environment (to conform to the IEC 60601-1-2 standard) from the harmful interference. Fourth, we focus on the dual-objective of maximizing the spectrum utilization and minimizing energy consumption for dynamic wireless access, and we propose implementation-friendly algorithms to solve the scheduling and power control problem with low complexity.

3.2 System Model and Assumptions

The key notations used in this chapter are listed in Table 3.1.

3.2.1 Primary and Secondary Network Models

We consider STDMA-based transmissions by secondary users where \mathcal{L} secondary networks (i.e., service cells) coexist with \mathcal{K} primary networks and each network uses an infrastructure mode of operation. Each network consists of a controller (i.e., access point) and client devices/users – n_k users for primary network k and n_l users for secondary network l . Let $\{k, i\}$ denote primary user i in network k ($k \in \{1, 2, \dots, K\}$) and $\{l, j\}$ denote secondary user j in network l ($l \in \{1, 2, \dots, L\}$). The controllers of primary and secondary networks are connected through wire-line infrastructure. Each user is supported by an omni-directional antenna. We assume that there are \mathcal{C} channels ($c \in \{1, 2, \dots, C\}$) on which primary and secondary networks can coexist. To avoid co-channel interference, the neighboring primary networks operate on different channels. A secondary user is associated with the nearest radio access controller (RAC) (Fig. 3.1). To avoid collision during transmission, we assume that all users and controllers are synchronized to the same time reference. Time synchronization can be achieved by either centralized [75] or decentralized synchronization [76].

There exist \mathcal{M} protected devices (i.e., passive medical devices) in different locations where $m \in \{1, 2, \dots, M\}$. For all the protected devices, the locations and the

Table 3.1. Key notations

Notation	Physical meaning
\mathcal{K}	Set of all primary networks
\mathcal{L}	Set of all secondary networks
n_k	Number of users in primary network k
n_l	Number of users in secondary network l
\mathcal{C}	Set of all radio channels
\mathcal{M}	Set of all protected devices
T	Fixed frame length
$u_{l,j}^{req}$	Minimum bandwidth requirement of secondary user $\{l, j\}$
$p_{l,j}^{max}$	Maximum transmission power of secondary user $\{l, j\}$
$D_{h,f}^m$	Distance between transmitter $\{h, f\}$ and protected device m
$E_{h,f,c,t}^m$	Electric field from transmitter $\{h, f\}$ to protected device m on channel c at time t
ξ_m	Immunity level of the protected user m with the unit of V/m.
$D_{l,j}^{k,i}$	Distance between transmitter $\{l, j\}$ and receiver $\{k, i\}$
$g_{l,j}^{k,i}$	Channel gain from transmitter $\{l, j\}$ to receiver $\{k, i\}$
$N_{k,i}$	Thermal noise power of receiver $\{k, i\}$
$\mu_{k,i,c,t}^{(p)}, \mu_{l,j,c,t}^{(s)}$	SINR at primary receiver $\{k, i\}$ and that at secondary receiver $\{l, j\}$ on the channel c at time t , respectively
$\gamma_{k,i}^{(p)}, \gamma_{l,j}^{(s)}$	SINR requirement of primary receiver $\{k, i\}$ and that of secondary receiver $\{l, j\}$, respectively
$A_{k,i,c,t}^{(p)}, A_{l,j,c,t}^{(s)}$	Binary variables which are 1 if user $\{k, i\}$ and $\{l, j\}$ are selected to transmit on channel c at time t , respectively
$p_{k,i,c,t}^{(p)}, p_{l,j,c,t}^{(s)}$	Transmit power of secondary transmitter $\{k, i\}$ and $\{l, j\}$ on channel c at time t , respectively
$O_{l,j}$	A binary variable that is 1 if the total bandwidth of secondary user $\{l, j\}$ over all the slots is greater than $u_{l,j}^{req}$
\mathbf{V}	Set of unsatisfied secondary users whose acquired bandwidth is less than the required bandwidth
Ω	Set of transmission power of all unsatisfied secondary users in every channel
Ψ_t	Set of the secondary users that are admissible in time slot t

EMI immunity levels (defined in terms of electric field) are known via an inventory system (i.e., tracking system) [29]. This information is necessary for the transmitter to calculate the intensity of the electric field experienced by each protected device.

3.2.2 Wireless Transmission Model

The primary networks are assumed to be used for in-hospital patient monitoring for which the primary transmitters are scheduled to transmit bio-signal information to the primary controller in a round-robin manner. Therefore, only one user in each primary network can transmit data in each time slot. The access pattern of each primary network is assumed to be known to the secondary network controllers (i.e., RACs).

Time is divided into equal-size slots that are grouped into frames. The frame length (i.e., the schedule length) is fixed to T slots. T is selected based on the number of users in each network, network load, and QoS requirements. Each secondary user $\{l, j\}$ requires a minimum bandwidth of $u_{l,j}^{req}$ in a frame. $u_{l,j}^{req}$ can be obtained from the maximum delay requirement of the application of user $\{l, j\}$. In our case, the frame length is equal to the maximum of the total required bandwidth of all users in the secondary networks¹. Note that this assumption implies that a secondary user can transmit in a time slot without the interference from other secondary users (i.e. one time slot for one secondary user). Therefore, the frame length equals to the total time required bandwidth of all secondary users. This assumption is try to make the solution feasible when there is a critical interference problem in the network. There will be enough time slots to satisfy the bandwidth requirement of all secondary users. Otherwise, we need an admission control for secondary users to the networks. Transmission scheduling and power control are performed every frame, so that the secondary users can adapt to the change of the healthcare environment. With power control, the secondary users can share the same frequency band with the primary users in a *harmful-interference-free* manner. We assume a maximum transmission power, denoted as $p_{l,j}^{max}$ that user $\{l, j\}$ can use for wireless transmission.

¹For a given transmission rate in the radio channel, which depends on the specific radio technology being used, and a given duration of a time slot, the required amount of bandwidth for each user can be expressed in terms of number of time slots.

3.2.3 Wireless Channel Model

We consider an indoor propagation model. Let $L(D)$ denote the total indoor propagation path-loss at a distance D . $L(D_{l,j}^{k,i})$ is given as $L(D_{l,j}^{k,i})[dB] = L(D_0)[dB] + 10n_{SF}\log(\frac{D_{l,j}^{k,i}}{D_0}) + FAF[dB]$, where D_0 is the reference distance, $D_{l,j}^{k,i}$ is the distance between the receiving user $\{k, i\}$ from the transmitting user $\{l, j\}$, FAF is the average floor attenuation factor through one floor, and n_{SF} is the path-loss exponent value for the same floor measurement. We consider that FAF is 16.2 dB, the measured line-of-sight (LOS) path-loss at $d_0 = 1m$ is 37.7 dB (i.e., $L(D_0) = 37.7$ dB), and n_{SF} is 3.3 [68]. Let us denote the channel gain of receiving user $\{k, i\}$ from the transmitting user $\{l, j\}$ as $g_{l,j}^{k,i}$, where $g_{l,j}^{k,i} = 10^{-L(D_{l,j}^{k,i})[dB]/10}$. Since the mobility of users is low (i.e., pedestrian mobility), the link gain is assumed to remain the same during a frame.

3.3 Optimization Formulation for Transmission Scheduling and Power Control

3.3.1 Interference Modeling for Protected Users

The electric field from transmitter $\{h, f\}$ to a protected device m on channel c at time t ($E_{h,f,c,t}^m$) can be obtained as [43]:

$$E_{h,f,c,t}^m = \frac{Z_0^m \sqrt{p_{h,f,c,t}}}{D_{h,f}^m} \quad (3.1)$$

where $p_{h,f,c,t}$ is the transmission power of transmitter $\{h, f\}$ on channel c at time t (in watts) and $D_{h,f}^m$ is the distance between the protected user m and the transmitter $\{h, f\}$ (in meters). Z_0^m is the constant from the free-space impedance of protected device m . The unit of $(Z_0^m)^2$ is Ω (i.e., ohm). IEC 60601-1-2 [43] specifies Z_0^m between 800 MHz to 2.5 GHz equal to $7\sqrt{\Omega}$ and $23\sqrt{\Omega}$ for non-life-supporting devices and life-supporting devices, respectively.

Let us define two binary variables $A_{k,i,c,t}^{(p)}$ and $A_{l,j,c,t}^{(s)}$ which are 1, if and only if, user $\{k, i\}$ and $\{l, j\}$ are selected to transmit on channel c in time slot t . In time slot t , there are $\sum_{k=1}^{|\mathcal{K}|} \sum_{i=1}^{n_k} \sum_{c=1}^{|\mathcal{C}|} A_{k,i,c,t}^{(p)}$ simultaneous transmissions in the primary

networks and $\sum_{l=1}^{|\mathcal{L}|} \sum_{j=1}^{n_l} \sum_{c=1}^{|\mathcal{C}|} A_{l,j,c,t}^{(s)}$ transmissions in the secondary networks. The interference constraint for the protected user m is given by

$$\sum_{k=1}^{|\mathcal{K}|} \sum_{i=1}^{n_k} \sum_{c=1}^{|\mathcal{C}|} E_{k,i,c,t}^m A_{k,i,c,t}^{(p)} + \sum_{l=1}^{|\mathcal{L}|} \sum_{j=1}^{n_l} \sum_{c=1}^{|\mathcal{C}|} E_{l,j,c,t}^m A_{l,j,c,t}^{(s)} \leq \xi_m, \quad \forall m \in \{1, 2, \dots, M\}, \forall t \in \{1, 2, \dots, T\} \quad (3.2)$$

where $\sum_{k=1}^{|\mathcal{K}|} \sum_{i=1}^{n_k} \sum_{c=1}^{|\mathcal{C}|} E_{k,i,c,t}^m A_{k,i,c,t}^{(p)}$ and $\sum_{l=1}^{|\mathcal{L}|} \sum_{j=1}^{n_l} \sum_{c=1}^{|\mathcal{C}|} E_{l,j,c,t}^m A_{l,j,c,t}^{(s)}$ denote the aggregate amount of electric fields at the protected user m caused by transmitters of primary and secondary networks, respectively. ξ_m is the immunity level (in V/m) of the protected user m .

3.3.2 Interference Modeling for Primary Users

Given channel \hat{c} at time slot \hat{t} , there are $\sum_{k=1, c=\hat{c}, t=\hat{t}}^K A_{k,i,c,t}^{(p)}$ primary and $\sum_{l=1, c=\hat{c}, t=\hat{t}}^L A_{l,j,c,t}^{(s)}$ secondary networks sharing the same channel. Let us denote the receiver thermal noise power of user $\{k, i\}$ as $N_{k,i}$. The corresponding SINR at the receiving user $\{k, i\}$ can be written as: $\mu_{k,i,c,t}^{(p)} = \frac{g_{k,i}^{k,i} p_{k,i,c,t}^{(p)}}{I_{k,i,c,t}^{(p)} + N_{k,i}}$, where $I_{k,i,c,t}^{(p)}$ is the interference power at the receiving user $\{k, i\}$ from transmitters of other networks which are simultaneously transmitting data on the same channel c at time slot t . $I_{k,i,c,t}^{(p)}$ is given by

$$I_{k,i,c,t}^{(p)} = \sum_{x=1, x \neq k}^{|\mathcal{K}|} \sum_{h=1}^{n_x} g_{x,h}^{k,i} p_{x,h,c,t}^{(p)} A_{x,h,c,t}^{(p)} + \sum_{l=1}^{|\mathcal{L}|} \sum_{j=1}^{n_l} g_{l,j}^{k,i} p_{l,j,c,t}^{(s)} A_{l,j,c,t}^{(s)}. \quad (3.3)$$

Therefore, the interference constraint for receiving user $\{k, i\}$ can be written as

$$\begin{aligned} \mu_{k,i,c,t}^{(p)} &\geq \gamma_{k,i}^{(p)} A_{k,i,c,t}^{(p)}, \\ \forall k &\in \{1, 2, \dots, K\}, \forall i \in \{1, 2, \dots, n_k\}, \\ \forall c &\in \{1, 2, \dots, C\}, \forall t \in \{1, 2, \dots, T\}. \end{aligned} \quad (3.4)$$

3.3.3 QoS Modeling for Secondary Users

Simultaneous transmissions on the same channel also cause interference to the secondary users. The interference model for the secondary users is similar to that for

the primary users. The interference power at receiver $\{l, j\}$ from other transmitters is given by

$$I_{l,j,c,t}^{(s)} = \sum_{k=1}^{|\mathcal{K}|} \sum_{i=1}^{n_k} g_{k,i}^{l,j} p_{k,i,c,t}^{(p)} A_{k,i,c,t}^{(p)} + \sum_{f=1, f \neq l}^{|\mathcal{L}|} \sum_{y=1}^{n_l} g_{f,y}^{l,j} p_{f,y,c,t}^{(s)} A_{f,y,c,t}^{(s)}. \quad (3.5)$$

Then, the QoS requirement for secondary user $\{l, j\}$ can be expressed as in (3.6).

$$\mu_{l,j,c,t}^{(s)} \geq \gamma_{l,j}^{(s)} A_{l,j,c,t}^{(s)}, \forall l \in \{1, 2, \dots, L\}, \forall j \in \{1, 2, \dots, n_l\}, \forall c \in \{1, 2, \dots, C\}, \forall t \in \{1, 2, \dots, T\}. \quad (3.6)$$

3.3.4 Formulation of the Dual-Objective Optimization Problem

We formulate the problem as maximizing the utility function in term of the total number of secondary users in all secondary networks that can achieve their minimum bandwidth requirements and the total normalized transmission power in a frame while satisfying the interference and QoS constraints for the protected, primary, and secondary users (as given in (3.2), (3.4), and (3.6), respectively).

Let us define $O_{l,j}$ as a binary variable that is 1 if and only if the total bandwidth of secondary user $\{l, j\}$ over all the slots is greater than $u_{l,j}^{req}$. Due to the mix of integer and continuous variables in (3.2), (3.4), and (3.6), the problem can be formulated as a mixed integer problem as given in (3.7)-(3.10), where W_1 and W_2 denote the weights corresponding to the total number of satisfied secondary users and the total of normalized transmission power of secondary users, respectively. The condition in (3.8) is to ensure that only one user in a secondary network can transmit at a time slot on a channel. The condition in (3.9) enforces the maximum power constraint for each user. Finally, (3.10) ensures that the binary variable $O_{l,j}$ is set to 1, if and only if, the total bandwidth allocated to secondary user $\{l, j\}$ satisfies its minimum requirement.

$$\text{Maximize:} \quad W_1 \sum_{l=1}^{|\mathcal{L}|} \sum_{j=1}^{n_l} O_{l,j} - W_2 \sum_{l=1}^{|\mathcal{L}|} \sum_{j=1}^{n_l} \sum_{c=1}^{|\mathcal{C}|} \sum_{t=1}^T \frac{p_{l,j,c,t}^{(s)}}{p_{l,j}^{max}} \quad (3.7)$$

$$\text{Subject to:} \quad \sum_{c=1}^{|\mathcal{C}|} \sum_{j=1}^{n_l} A_{l,j,c,t}^{(s)} \leq 1, \forall l \in \{1, 2, \dots, L\}, \forall t \in \{1, 2, \dots, T\} \quad (3.8)$$

$$0 \leq p_{l,j,c,t}^{(s)} \leq p_{l,j}^{max}, \forall l \in \{1, 2, \dots, L\}, \forall j \in \{1, 2, \dots, n_l\}, \forall c \in \{1, 2, \dots, C\}, \forall t \in \{1, 2, \dots, T\} \quad (3.9)$$

$$\sum_{c=1}^{|\mathcal{C}|} \sum_{t=1}^T A_{l,j,c,t}^{(s)} \geq u_{l,j}^{req} O_{l,j}, \forall l \in \{1, 2, \dots, L\}, \forall j \in \{1, 2, \dots, n_l\} \quad (3.10)$$

and the constraints in (3.2), (3.4), (3.6)

Proposition 1 *The scheduling and power control problem for TDMA-based secondary networks coexisting with primary networks sharing multiple channels is an NP-complete problem.*

Proof. It was shown in [77] that the problem of scheduling and power control in a wireless ad-hoc network satisfying the SINR requirements of each user on a single channel is NP-complete. Since this problem is a special case of the problem under consideration, the latter is also an NP-complete problem. ■

For exhaustive search, the complexity of this problem is of $O\left(\prod_{l=1}^L \binom{n_l}{T} T!C\right)$. Although an exhaustive search would be practically infeasible, it can serve as the benchmark for evaluating the performance of our proposed algorithms.

3.4 Proposed Algorithms

3.4.1 Joint Scheduling and Power Control Algorithm Based on Transmit Power Minimization

A greedy algorithm (**Algorithm 2**) is used to solve our optimization problem. The proposed algorithm selects the best choice at a moment (i.e., time slot) to generate the locally optimal choice. Although the greedy method may not consistently find the optimal solutions, it is more practical to implement due to quick decisions and good approximations to the optimum solutions.

Since different primary users will be scheduled to transmit in different time slots, the optimization problem is decoupled into several local optimization problems (i.e., based on the time slots). In each time slot, the algorithm schedules an unsatisfied user from each secondary network that transmits with the minimum power subject to the constraints in (3.2), (3.4), and (3.9) in order to avoid causing interference to medical devices and minimize the power consumption of secondary users.

At each stage (i.e., time slot), the algorithm first specifies the *unsatisfied secondary users* (\mathbf{V}) whose acquired bandwidth is less than the required bandwidth. In the initial step, the algorithm calculates transmission power of each unsatisfied user by

considering the case that only one secondary user transmits on a channel at the considered time slot. When only one secondary user $\{l, j\}$ is selected to transmit on a channel c at time t , the transmission power can be obtained as follows:

$$\begin{aligned} \Omega_{l,j,c} &= \frac{\gamma_{l,j}^{(s)}}{g_{l,j}} (I_{l,j,c}^{(s)} + N_{l,j}), \quad \forall l \in \{1, 2, \dots, L\}, \\ &\quad \forall j \in \{1, 2, \dots, n_l\}, \quad \forall c \in \{1, 2, \dots, C\}. \end{aligned} \quad (3.11)$$

The transmission power calculated in (3.11) for all unsatisfied secondary users are kept in Ω where $\Omega_{l,j,c}$ denotes the transmission power of secondary user $\{l, j\}$ on channel c . The algorithm first considers user $\{\hat{l}, \hat{j}\}$ in Ω transmitting on channel \hat{c} that provides the least transmission power. The user $\{\hat{l}, \hat{j}\}$ is added to the *admissible set* (Ψ) if and only if its transmission satisfies the constraints in (3.2), (3.4), and (3.9). Once, the user $\{\hat{l}, \hat{j}\}$ is scheduled, all users in secondary network \hat{l} are removed from Ω because in each secondary network, only one user can transmit at a time on a channel.

Moreover, the transmit powers on \hat{c} in Ω are updated by considering all secondary users in Ψ that transmit on channel \hat{c} . Since the number of secondary transmissions (and hence interference to other secondary users) in channel \hat{c} increases and thus the SINR values of these secondary users decrease, the transmission power of every user in channel \hat{c} should be increased in order to achieve the target SINR threshold. Considering the constraint in (3.6), the transmit powers can be updated by the power control algorithm developed in [78]. The power control algorithm for secondary user $\{l, j\}$ uses the following iteration:

$$\Omega_{l,j,\hat{c}}(r+1) = \Omega'_{l,j,\hat{c}}(r+1) + \delta_{l,j,\hat{c}} \quad (3.12)$$

$$\Omega'_{l,j,\hat{c}}(r+1) = \frac{\gamma_{l,j}}{\mu_{l,j,\hat{c}}(r)} \Omega'_{l,j,\hat{c}}(r) \quad (3.13)$$

where $\delta_{l,j,\hat{c}}$ is the total increased transmission power of users in Ψ_t that transmit in channel \hat{c} and r is the iteration number.

After updating the power, the algorithm reconsiders the choices in Ω . For each time slot, the algorithm repeats these steps until either one user from every secondary

network is scheduled to transmit at time slot t (i.e., $|\Psi_t| = |\mathcal{L}|$) or Ω is empty (i.e., $|\Omega| = 0$).

Algorithm 2 Greedy algorithm for joint scheduling and power control

```

1: for all slot  $t$  do
2:   Initialize  $\Psi_t = \emptyset$ 
3:    $\mathbf{V} \leftarrow$  specify the set of unsatisfied SUs
4:    $\Omega \leftarrow$  find transmit powers for all  $\mathbf{V}$  on all channels by using (3.11)
5:   repeat
6:     Find secondary user  $\{\hat{l}, \hat{j}\}$  in  $\Omega$  transmitting on channel  $\hat{c}$  that uses the least
       transmission power
7:      $A_{\hat{l}, \hat{j}, \hat{c}, t} \leftarrow 1$ 
8:      $p_{\hat{l}, \hat{j}, \hat{c}, t} \leftarrow \Omega_{\hat{l}, \hat{j}, \hat{c}}$ 
9:     if Constraints in (3.2), (3.4), and (3.9) are satisfied then
10:       $\Psi_t \leftarrow \{\hat{l}, \hat{j}, \hat{c}\}$ 
11:      Remove all users of  $\hat{l}$  from  $\Omega$ 
12:      Update the transmit powers of all users transmitting on  $\hat{c}$  in  $\Omega$  by using
        (3.12)
13:       $u_{\hat{l}, \hat{j}}^{req} \leftarrow u_{\hat{l}, \hat{j}}^{req} - 1$ 
14:     else
15:      Remove  $\Omega_{\hat{l}, \hat{j}, \hat{c}}$  from  $\Omega$ 
16:       $A_{\hat{l}, \hat{j}, \hat{c}, t} \leftarrow 0$ 
17:       $p_{\hat{l}, \hat{j}, \hat{c}, t} \leftarrow 0$ 
18:     end if
19:   until  $|\Psi_t| = |\mathcal{L}|$  or  $|\Omega| = 0$ 
20: end for

```

The complexity of the algorithm is of $O\left(2TC \sum_{l=1}^L n_l\right)$. In each time slot, computations of order $C \sum_{l=1}^L n_l$ are used to calculate the minimum transmission power on each channel for every secondary user in the network. Additional computations of order $C \sum_{l=1}^L n_l$ are used to select an unsatisfied secondary user from each secondary network to transmit in that time slot.

3.4.2 Enhanced Greedy Algorithm Based on Interference Minimization

Since the greedy algorithm never reconsiders its choices (i.e., the scheduled secondary users will not be reconsidered), the decision made in each stage of **Algorithm 1** may not be close to the global optimal solution. The decision orders of the greedy algorithm are based on the sequence of time slots in a frame. The results from the greedy algorithm may be far from the globally optimal solution in some cases. For example, if the primary networks schedule their users in the order of the distance from the controller, the user who is close to the controller can transmit in the beginning time slot of the frame. The greedy algorithm also selects the secondary users who transmit with the least power (i.e., the users located close to the secondary controllers are selected first). In the later time slots of a frame, the algorithm may not be able to schedule any secondary user to transmit due to the interference problem between primary and secondary users because the distant users have to allocate more aggressive powers in order to achieve the SINR requirements. The radio spectrum is not fully utilized in this case.

To improve the radio spectrum utilization, we consider the decision orders based on the priority of secondary users instead of the time sequence in a frame. The secondary users who have higher priority are scheduled first. The enhanced greedy algorithm (**Algorithm 3**) first calculates the amount of interference that may be caused to primary and/or protected users on every channel in every time slot by a secondary user. The more the interference, the higher the priority of the secondary user is. This is because, the users who may cause high amount of interferences, may have fewer opportunities to transmit data during a frame. In this algorithm, these secondary users are first scheduled to transmit. Since these secondary users get more chance to transmit, the spectrum utilization increases.

Similar to the greedy algorithm, in the initial step, we calculate the minimum transmission power for all unsatisfied secondary users \mathbf{V} in all time slots on all channels and keep the information in $\mathbf{\Omega}$. In this case, $\mathbf{\Omega}$ have an additional dimension for time slots. We also calculate $INF_{l,j}$, which is the number of transmissions on each channel in each time slot by secondary user $\{l, j\}$ for which the constraints in (3.2) and (3.4) are not satisfied. Therefore, $INF_{l,j}$ is an indirect measure of interference.

In the scheduling process, the algorithm first considers the secondary user $\{\hat{l}, \hat{j}\}$ who has the maximum value of \mathbf{INF} . The algorithm schedules secondary user $\{\hat{l}, \hat{j}\}$ on channel \hat{c} in time slot \hat{t} in which the user can transmit with the least power.

Once a secondary user $\{\hat{l}, \hat{j}\}$ is selected to transmit on channel \hat{c} at time \hat{t} , the other secondary users in the secondary network \hat{l} are not allowed to transmit at time \hat{t} . Therefore, the transmit powers $\Omega_{\hat{l}, \dots, \hat{t}}$ are removed from Ω . To achieve the target SINR threshold, when the number of transmissions at time \hat{t} in channel \hat{c} increases, the transmit powers of users in other secondary networks at time \hat{t} on channel \hat{c} must be updated by using (3.12). The new transmission power plus the additional transmission power of secondary user $\{\hat{l}, \hat{j}\}$ is updated to $\Omega_{\dots, \hat{c}, \hat{t}}, \forall l \in \{1, 2, \dots, L\} \setminus \{\hat{l}\}$. Then, we recalculate \mathbf{INF} . The algorithm will repeat until all secondary users can satisfy their bandwidth requirements $|\mathbf{V}| = 0$, or there is no more possible transmission in Ω (i.e., $|\Omega| = 0$).

The complexity of the enhanced greedy algorithm is of $O\left(2TC \sum_{l=1}^L n_l\right)$. Here, computations of order $TC \sum_{l=1}^L n_l$ are required to calculate the minimum transmission power and find the initial values of each $INF_{l,j}$ in the initial stage. In the scheduling stage, we run $TC \sum_{l=1}^L n_l$ loops to prioritize the secondary users based on the values of \mathbf{INF} and schedule each user to transmit based on its priority. Although the number of computation loops in the worst-case scenario of both greedy and enhanced greedy algorithms is same, the enhanced greedy algorithm takes a longer computation time than the greedy algorithm in each loop due to the additional steps for prioritizing the secondary users.

3.5 Performance Evaluation

3.5.1 Simulation Parameters

We simulate a medical environment over an area of 105×86 square meters. There exist 10 primary networks and 10 secondary networks. The primary networks operate on three non-overlapping channels in the 2.4 GHz band. The wards include an operating room, two examination rooms, a neonatal care, two ICUs, a physical medicine and rehabilitation room, twelve patient rooms, an emergency room, a microbiology lab, a pathology lab, an administration room, ten physician rooms, and a main lobby and

Algorithm 3 Enhanced greedy algorithm for joint scheduling and power control

- 1: Initialize $\Psi = \emptyset$
 - 2: $\Omega \leftarrow$ find transmit powers for all SUs on all channels in all time slots by using (3.11)
 - 3: **INF** \leftarrow Interference for all SUs on all channels in all time slots
 - 4: **repeat**
 - 5: Find secondary user $\{\hat{l}, \hat{j}\}$ in \mathbf{V} that has the maximum value in **INF**
 - 6: **repeat**
 - 7: Find the channel \hat{c} and time slot \hat{t} in $\Omega_{\hat{l}\hat{j}}$ for which the transmission power is the least
 - 8: $A_{\hat{l},\hat{j},\hat{c},\hat{t}} \leftarrow 1$
 - 9: $p_{\hat{l},\hat{j},\hat{c},\hat{t}} \leftarrow \Omega_{\hat{l},\hat{j},\hat{c},\hat{t}}$
 - 10: **if** Constraints in (3.2), (3.4), and (3.9) are satisfied **then**
 - 11: $\Psi \leftarrow \{\hat{l}, \hat{j}, \hat{c}, \hat{t}\}$
 - 12: Remove all users of \hat{l} at time slot \hat{t} from Ω
 - 13: Update the transmit powers of all users transmitting on \hat{c} at time slot \hat{t} in Ω by using (3.12)
 - 14: $u_{\hat{l},\hat{j}}^{req} \leftarrow u_{\hat{l},\hat{j}}^{req} - 1$
 - 15: **else**
 - 16: Remove $\Omega_{\hat{l},\hat{j},\hat{c},\hat{t}}$ from Ω
 - 17: $A_{\hat{l},\hat{j},\hat{c},\hat{t}} \leftarrow 0$
 - 18: $p_{\hat{l},\hat{j},\hat{c},\hat{t}} \leftarrow 0$
 - 19: **end if**
 - 20: **until** $u_{\hat{l},\hat{j}}^{req} = 0$ or $|\Omega_{\hat{l}\hat{j}}| = 0$
 - 21: $INF_{\hat{l},\hat{j}} \leftarrow 0$
 - 22: Update **INF** for other SUs
 - 23: **until** $|\mathbf{V}| = 0$ or $|\Omega| = 0$
-

lounge. The locations of the protected users are shown in Table 3.2, where ECG stands for Electrocardiograph, EEG stands for Electroencephalography, and EMG stands for Electromyography. The EMI immunity level (ξ_m) for primary devices 1-16 is 3 V/m and that for devices 17-22 is 10 V/m, which comply with the IEC 60601-1-2 standard [43].

The locations of the primary and secondary users are shown in Table 3.3, where TR stands for Telemetry Receiver. The total number of required slots per frame in each secondary network is chosen to be Δ . Therefore, the frame length (T) is equal to Δ . Δ changes when the number of users and the bandwidth requirements of any user in the secondary networks change. The transmitting nodes of primary and secondary users are randomly located in the service area. The noise power at the controller is assumed to be -100 dBm. The maximum transmission power of a secondary user is $p_{l,j}^{max} = 100$ mW which is the maximum transmission power for the IEEE 802.11b-based radio devices. For each simulation run, the locations of primary and secondary users are generated randomly. The desired SINR for each primary and secondary users is chosen as $\gamma_i^{(p)} = \gamma_j^{(s)} = \gamma$. $W1$ and $W2$ in the optimization problem (3.7) are chosen to be 1000 and 1, respectively.

3.5.2 Simulation Results

Since the optimal scheduling incurs huge computation time when either the network or the total required time slots Δ is large, we compare the performance of the two proposed algorithms with that of random scheduling only. In random scheduling, one user is selected from each secondary network during a time slot. Then, the centralized controller selects the channel for that user such that the least transmission power is required. The method also checks for the EMI constraints of primary and protected users. If the transmission of the secondary user causes interference to any medical device or cannot satisfy the QoS of the secondary user, the secondary user will not be allowed to transmit. In this case, no secondary user in the secondary network transmits in that time slot. Therefore, the radio spectrum is not fully utilized.

Table 3.2. *Protected users in the simulation setup*

No.	Protected users	Ward	Location (x,y)
1	ECG monitor I	ICU	(13,7.5)
2	EEG monitor I	ICU	(14,7.5)
3	ECG monitor II	ICU	(13,25)
4	EEG monitor II	ICU	(14,25)
5	Foetal heart monitor	Neonatal care	(9,36)
6	EEG monitor III	Neonatal care	(16,36)
7	ECG monitor III	Examination room I	(14.5,51)
8	EMG monitor I	Examination room I	(15,52)
9	ECG monitor IV	Operating room	(11,79)
10	EEG monitor IV	Operating room	(15,79)
11	EMG monitor II	Physical medicine & rehabilitation	(42.5,31)
12	ECG monitor V	Physical medicine & rehabilitation	(56.5,31)
13	EMG monitor III	Examination room II	(48,51)
14	ECG monitor VI	Examination room II	(49,51)
15	ECG monitor VII	Emergency room	(75,38)
16	EEG monitor IV	Emergency room	(75,53)
17	Infusion pump I	ICU	(15,25)
18	Incubator	Neonatal care	(22,36)
19	Difribillator I	Operating room	(19,79)
20	Difribillator II	Physical medicine & rehabilitation	(46.5,31)
21	External pacemaker	Emergency room	(77,38)
22	Difribilator III	Emergency room	(77,53)

Table 3.3. *Primary and secondary users in the simulation setup*

No.	Device	Location (x,y)	Channel
	Primary users		
1	TR I	(22.5,29)	Channel 2
2	TR II	(22.5,57)	Channel 3
3	TR III	(45,15)	Channel 3
4	TR IV	(45,43)	Channel 1
5	TR V	(45,71)	Channel 2
6	TR VI	(67.5,29)	Channel 2
7	TR VII	(67.5,57)	Channel 3
8	TR VIII	(90,15)	Channel 3
9	TR IX	(90,43)	Channel 1
10	TR X	(90,71)	Channel 2
	Secondary users		
11	RAC I	(15,15)	-
12	RAC II	(15,43)	-
13	RAC III	(15,71)	-
14	RAC IV	(37.5,29)	-
15	RAC V	(37.5,57)	-
16	RAC VI	(60,15)	-
17	RAC VII	(60,43)	-
18	RAC VIII	(60,71)	-
19	RAC IX	(82.5,29)	-
20	RAC X	(82.5,57)	-

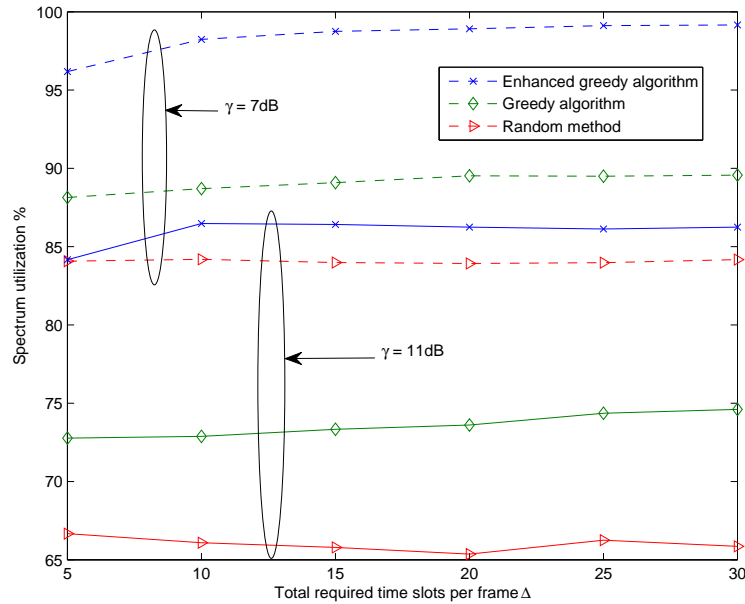


Figure 3.2. Percentage of spectrum utilization versus the total required time slots per frame.

3.5.2.1 Spectrum utilization by secondary networks

The spectrum utilization is calculated from the total time slots that secondary users can transmit over the total available time slots of all networks in a frame.

In Fig. 3.2, we show the percentage of spectrum utilization in the large-scale scenario. With $\gamma = 7$ dB, the spectrum utilization for the enhanced greedy algorithm is more than 96% and it reaches 99% when the number of required time slots is greater than 25. However, the spectrum utilization for the greedy algorithm is less than 90%. With $\gamma = 11$ dB, the spectrum utilization of the enhanced greedy algorithm decreases to 84-86.5%. Nonetheless, it is still greater than that of the greedy algorithm which achieves spectrum utilization of 73-74.6%. This is due to the fact that the enhanced greedy algorithm can provide a fairer channel access to all users when the scheduling frame lengths are longer. The enhanced greedy and the greedy algorithms can improve the spectrum utilization by 22.60% and 8.38%, respectively, when compared to the random scheduling method.

Note that we also compare the performance of our proposed algorithms with the

optimal solution obtained by exhaustive search in a small-scale network. The network consists of 7 protected users with two primary and two secondary networks. With $\gamma = 7$ dB and $\Delta = 10$, the enhanced greedy algorithm can achieve the spectrum utilization very close to the optimal solution with less than 0.33% different and the greedy algorithm has 12.07% different from the optimal solution. However, the random method can provide the least spectrum utilization with 15.65% different from the optimal solution. In addition, we compare the average of total transmission power per frame for the secondary users when all algorithms can achieve the same spectrum utilization as the optimal algorithm (i.e., spectrum utilization is same for all the schemes). The enhanced greedy algorithm has the total transmission power per frame more than the optimal solution with 1.28% while the greedy algorithm and the random method consume the total transmission power more than the optimal solution with 14.97% and 11.02%, respectively. Therefore, the enhanced greedy algorithm can achieve the performance very close to the optimal solution.

3.5.2.2 Power consumption of secondary networks

In Fig. 3.3, we show the average transmission power that the secondary users spend for transmissions in a time slot. The average transmission power in a time slot decreases as the number of required time slots per frame increases. At low SINR (i.e., $\gamma = 7$ dB), the enhanced greedy algorithm uses a lower average power than the greedy algorithm to transmit data in a time slot. This is due to the fact that the enhanced greedy algorithm tries to minimize the maximum power consumption in a frame while at the same time achieving high spectrum utilization. However, at high SINR (i.e., $\gamma = 11$ dB), the average transmission power per time slot is lower for the greedy algorithm when compared to that for the enhanced greedy algorithm. This is due to the fact that with the enhanced greedy algorithm, large transmission power has to be used in order to increase spectrum utilization under a high SINR requirement. However, the average transmission power for the enhanced greedy algorithm becomes closer to that of the greedy algorithm when the number of required time slots per frame increases.

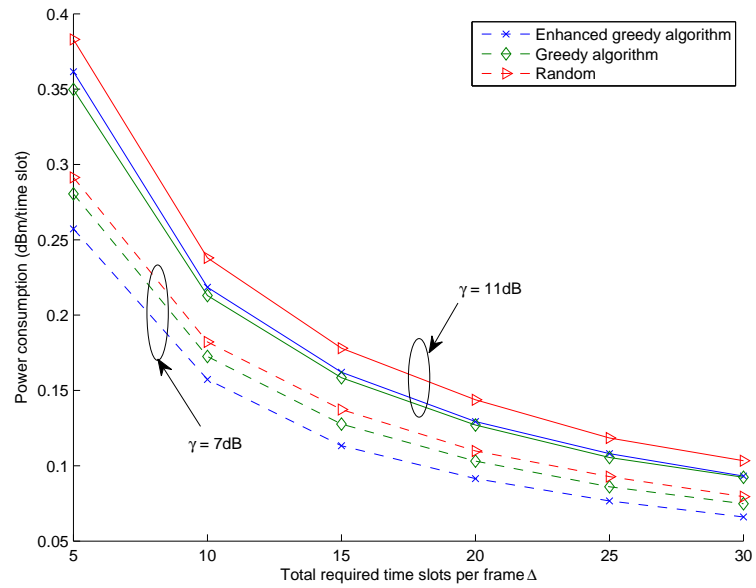


Figure 3.3. Average power consumption per time slot versus the total required time slots per frame.

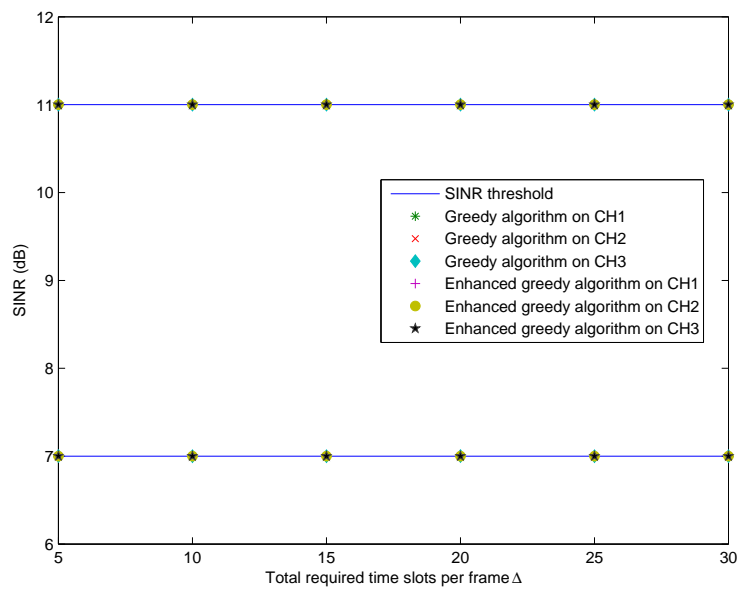


Figure 3.4. Minimum SINR of primary users.

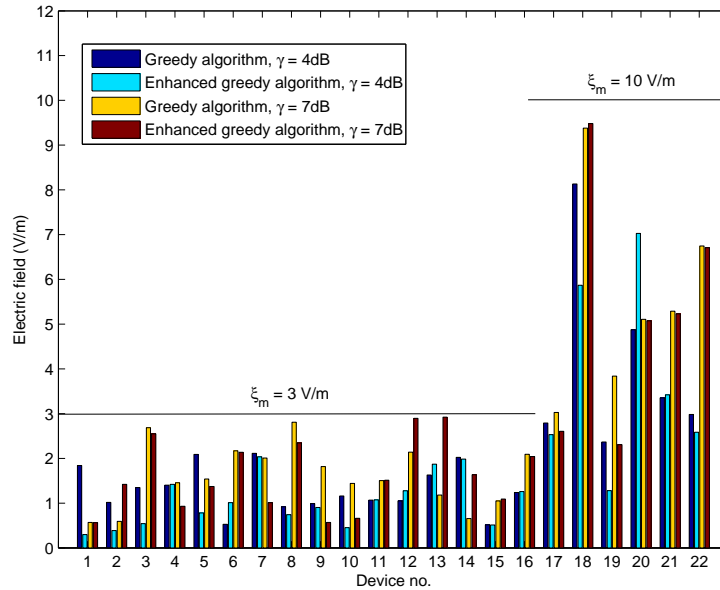


Figure 3.5. Maximum electric fields experienced by the protected users.

3.5.2.3 Electromagnetic interference level

We also observe the electromagnetic interference level from the secondary users to the primary users and from both primary and secondary users to protected users. We measure the minimum SINR of primary users on the three channels when the number of required time slots varies (as shown in Fig. 3.4). Since the algorithms are aware of the interference to primary users, the SINR values of primary users are always greater than or equal to the minimum required values in every time slot. Also, the maximum electric fields to the protected users are shown in Fig. 3.5 where devices 1 to 16 and 17 to 22 are non-life-supporting medical devices and life-supporting devices, respectively. The maximum electric fields of all passive medical devices are less than the specified EMI immunity levels.

3.5.2.4 Computation time for the proposed algorithms

We conduct our simulations on a computer with a 2.8 GHz CPU and 4 GB of RAM. The average computation times are shown in Fig. 3.6 when the number of secondary users varies from 4 to 10 users in a small-scale simulation scenario with 7 protected

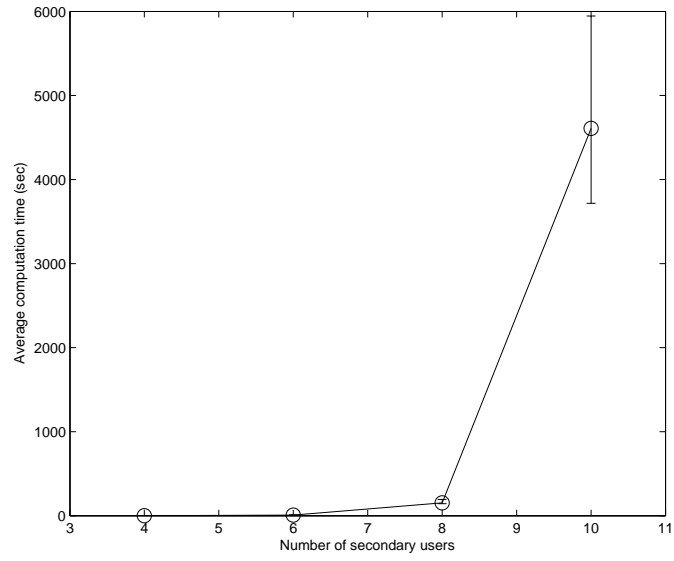
users and two primary users.

When the number of secondary users increases, the computation time increases, especially, that of the exhaustive search method increases exponentially as shown in Fig. 3.6(a). The computation time does not depend on the desired SINR. The random algorithm spends the least computation time due to its low complexity. However, its performance is poor in terms of spectrum utilization and power consumption. The enhanced greedy algorithm also takes approximately 50% longer computation time than the greedy algorithm due to the additional steps to prioritize the users based on the values of **INF**. However, the enhanced greedy algorithm can provide efficient scheduling and power control in terms of spectrum utilization and minimization of transmission power. With 10 secondary users, the enhanced greedy algorithm reduces the average runtime of exhaustive search by 99.97%.

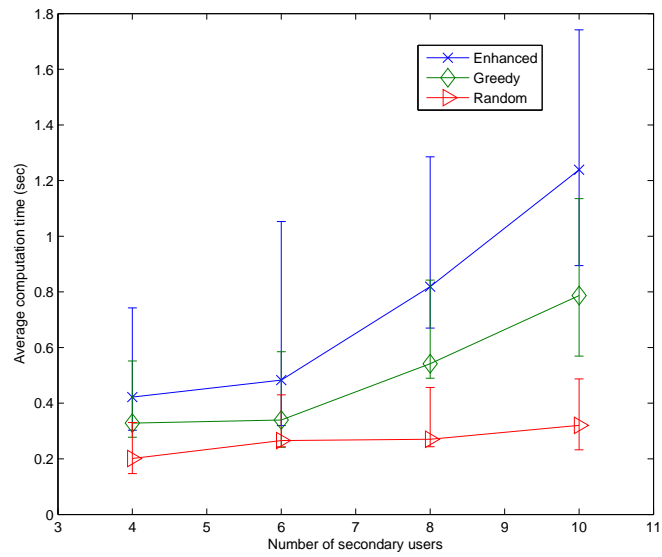
3.6 Conclusion

We have presented an approach to solve the spectrum sharing problem for wireless access in a hospital environment. In particular, a dual objective optimization problem has been formulated to maximize spectrum utilization and minimize transmission power, while guaranteeing the QoS of secondary users and satisfying the interference constraints for the protected and primary users. We have proposed two algorithms, namely the greedy and the enhanced greedy algorithms for joint scheduling and power control with low complexity.

One drawback of the centralized algorithms is their low scalability in large networks due to the increased computation time. One way to improve the scalability of the proposed algorithms is to use semi-distributed techniques for scheduling and power control. In a large network, we can divide the secondary networks into several small groups (i.e., each group has 3-4 networks located in the same vicinity). In each group, the secondary networks cooperate to schedule all secondary users in the group to transmit without causing harmful interference to medical devices in the vicinity by using either the greedy or the enhanced greedy algorithm. With the semi-distributed algorithm, the scheduling work is distributed into several small-size networks, and therefore, the computation time will decrease. However, there exists a



(a)



(b)

Figure 3.6. (a) Computation time for the exhaustive algorithm, and (b) computation time for the greedy, enhanced-greedy, and random algorithms.

tradeoff between the performance and the computation time for the semi-distributed algorithm.

Chapter 4

Robust Scheduling and Power Control for an Ad-Hoc STDMA Wireless Network

For opportunistic spectrum access and spectrum sharing in cognitive radio networks, one key problem is how to develop scheduling and power control schemes [72]-[73] for secondary users so that harmful interference to primary users can be avoided and quality-of-service (QoS) of secondary users can be guaranteed. In this chapter, we address this problem in the context of an ad-hoc STDMA network. With STDMA scheduling in a cognitive radio network, each secondary link is allocated a set of time slots in a frame to transmit simultaneously with primary links to improve the spectrum utilization in the network. The key question here in this vertical spectrum sharing scenario is how to minimize the transmission length (in terms of time slots) of secondary users in a frame, so that the traffic demand of the secondary links can be satisfied while maintaining the interference level at the primary receiving points below a maximum threshold. Note that the transmission length of the secondary users is the total number of time slots that the secondary users are active and transmit data.

The transmission length for the secondary users in a cognitive STDMA network can be minimized by using a proper joint scheduling and power control method [72]-[73], [80]-[81]. For this, a linear programming (LP)-based problem formulation can be used. However, since the possible combinations of concurrently active links can grow exponentially with the total number of links in the network, the LP formulation has to deal with a large number of variables and hence the solution has a huge computational complexity. To address this complexity issue in scheduling (along

with power control), column generation-based algorithms have been proposed both for horizontal spectrum sharing [82]-[84] and vertical spectrum sharing [85]-[86] scenarios in large-scale wireless networks. In column generation, the optimization problem is decomposed into a restricted master problem and a pricing problem. The restricted master problem is optimized to determine the values of the dual variables. The dual variables are then passed to the pricing problem to find a new column (i.e., access pattern) that can improve the current solution. However, the column generation procedure has a convergence problem (e.g., dual variables oscillate from one iteration to the next iteration) when primal degeneracy arises [87]-[88]. This convergence problem of column generation has not been addressed in the literature.

Again, robust scheduling and power control methods are required to cope with channel gain variations and traffic demand uncertainty in order to achieve the target reliability in terms of SINR and throughput requirements for secondary users, as well as the interference constraints for primary users. In this chapter, we design an efficient and robust transmission scheduling and power control framework for vertical spectrum sharing among primary and secondary users in an STDMA network.

The block diagram of the robust transmission scheduling and power control framework is shown in Fig. 4.1. Although an STDMA network is considered in this chapter, the developed framework can be applied to other networks such as hierarchical CDMA and FDMA networks (e.g., 3G and LTE femtocell networks) to provide conflict-free scheduling and improve the robustness of the schedules to channel variation due to shadow fading and traffic demand uncertainty. The solution of the problem is obtained in a centralized manner in this chapter.

The related work and the key contributions of the chapter are summarized in Section 4.1 followed by the system model and the assumptions in Section 4.2. We present the formulation of the robust scheduling and power control problem for vertical spectrum sharing in an STDMA network in Section 4.3. We introduce the column generation method and describe the stabilized column generation method for scheduling and power control in Section 4.4. In Section 4.5, we present the heuristic algorithm to solve the pricing problem. The performance evaluation results are presented in Section 4.6 followed by the conclusion in Section 4.7. Throughout the chapter, we use lower-case bold symbols to denote vectors and upper-case bold symbols to denote

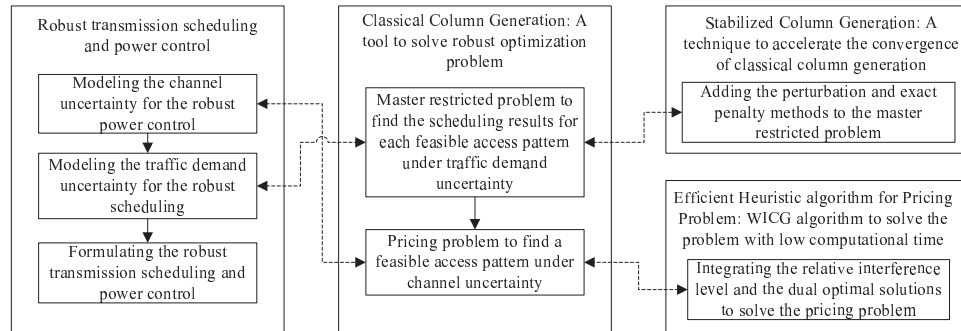


Figure 4.1. *The block diagram of the robust transmission scheduling and power control framework.*

matrices.

4.1 Related Work and Key Contributions of the Chapter

Different aspects of the power control and scheduling/channel allocation problem in wireless networks have been extensively studied in the literature (e.g., [79]-[86], [89]-[98]) considering different network architectures and power control models (e.g., infrastructure-based cellular wireless networks, ad hoc wireless networks, centralized power control, distributed power control), multiple access technique (e.g., TDMA, CDMA), different optimization objectives (e.g., maximizing network utility, minimizing power-consumption), and spectrum sharing mechanisms (e.g., horizontal spectrum sharing, vertical spectrum sharing). The problem of power allocation and scheduling in vertical (or hierarchical) spectrum sharing wireless networks as addressed in this chapter (also considered in [85]-[86], [95]-[98]) is more challenging than the traditional power control and scheduling problem in horizontal spectrum sharing networks (e.g., in [82]-[84], [89]-[94]). This is due to the fact that the QoS requirements of the primary users should always be maintained while secondary users are only allowed to exploit the remaining available network capacity. The work on power control and scheduling problem in large-scale wireless networks with horizontal spectrum sharing in [82]-[86], and those in [95]-[98] for cognitive radio networks are particularly rele-

vant to the work presented in this chapter. However, the algorithms in [82]-[86] and [95]-[98] do not take the link gain uncertainty due to the inherent stochastic nature of wireless channels into account. Consequently, the scheduling results may cause transmission failure due to improper power allocation, and subsequently result in traffic demand uncertainty.

For a horizontal spectrum sharing scenario, in [99], the authors propose a general framework of distributed robust power optimization through the ellipsoid, polyhedron, and D-norm uncertainty set, respectively. In [100], the authors employ a zero-sum game theoretic approach where the scheduler and the channel error non-cooperatively play in the scheduling process to ensure the worst-case performance bounds. The work in [101] also deals with the robust scheduling problem to minimize the frame length in spatial reuse TDMA wireless networks under log-normal fading. However, the framework in [101] does not take the traffic demand of each link into account. Moreover, the scheduling scheme does not consider the impact of transmission failure on the increase in traffic demand.

The key contributions of this chapter when compared to the existing state-of-the-art can be summarized as follows:

- *Formulation of the robust scheduling and power control problem for vertical spectrum sharing in STDMA networks:* We jointly consider three important aspects, namely, channel uncertainty, primary interference constraints, and traffic demand uncertainty of secondary users. To achieve robust scheduling and power control, we consider the worst-case scenario in modeling the channel gain uncertainty due to shadowing, which is assumed to follow a log-normal distribution and then obtain the chance constraint for the traffic demand uncertainty of secondary users. To obtain the solution, an optimization problem based on mixed-integer programming (MIP) is solved.
- *Stabilized column generation method to efficiently solve the scheduling and power control problem:* We propose a stabilized column generation approach based on the perturbation and the exact penalty methods to solve the convergence problem in the classical column generation method. This approach can stabilize and accelerate the column generation process by guiding the dual variables.
- *Efficient heuristic algorithm for the pricing problem:* The pricing problem is

formulated as an MIP problem to find an optimal access pattern along with the transmission powers of secondary users. Due to the complexity of the pricing problem, the runtime of the column generation method mainly depends on the time spent in solving the pricing problem. To overcome this complexity, we propose a greedy heuristic algorithm, namely, the Weighted Interference Criterion Greedy (WICG) algorithm, to solve the pricing problem. We integrate the relative interference level and the dual optimal solutions of the restricted master problem in the column generation method into the proposed WICG algorithm. This integration can provide efficient solutions for the pricing problem that improves the current optimal solution in the master problem with low computational complexity and low penalty (i.e., additional time slots required when compared to the optimal solution). Simulations show that our heuristic algorithm outperforms the Combined Sum Criterion Removal (CSCR) algorithm proposed in [82] and also the geometric programming approximation algorithm proposed in [102], which are the available heuristic algorithms for this problem in the existing literature.

4.2 System Model and Assumptions

4.2.1 Network and Channel Model

We consider a cognitive STDMA network with a set of primary links \mathcal{K} and a set of secondary links \mathcal{L} indexed by $k = 1, 2, \dots, |\mathcal{K}|$ and $i = 1, 2, \dots, |\mathcal{L}|$, respectively. Each secondary link i requires u_i time slots in a frame. Note that u_i is related to a minimum throughput demand π_i , where $u_i = \frac{\pi_i f}{r_i}$. Here, f is a fixed frame length and r_i is the achievable data rate of link i per unit time which depends on the SINR threshold γ_i at the receiver of link i .

Let T_i and R_i represent the transmitter and the receiver of link i . T_i transmits data with power p_i where p_i^{max} is the maximum transmission power. We use matrix \mathbf{C} to indicate the conflict among secondary links, where $c_{i,j} = 1$ if $i \neq j$ and secondary links i and j share at least one common node, otherwise $c_{i,j} = 0$. That is, there cannot be any two links in the network topology which share a common node (for which $c_{i,j}$ would be 1) implying that each node in the network has a single radio and

can communicate in half-duplex mode only.

We adopt an indoor propagation model for the link gain¹. The channel gain from T_j to R_i is given by

$$\tilde{g}_{i,j} = g_{i,j} \cdot 10^{X/10} \quad (4.1)$$

where $g_{i,j}$ is the average link gain obtained from $10^{-PL(i,j)/10}$ and X is the log-normal shadow fading gain in dB, $X \sim \mathcal{N}(0, \sigma^2)$. $PL(i, j)$ is the path-loss from T_j to R_i which is calculated from $PL(i, j)[dB] = PL(d_0)[dB] + 10n_{SF} \log\left(\frac{d_{i,j}}{d_0}\right) + FAF[dB]$. $PL(d_0)$ is the measured line-of-sight (LOS) path-loss at $d_0 = 1m$. n_{SF} is the obstructed path-loss exponent. $d_{i,j}$ is the distance of T_j to R_i . FAF is the floor attenuation factor. Note that in (4.1), the uncertainty of the channel gains in the channel gain matrix $\tilde{\mathbf{G}}$ depends on the variable X .

4.2.2 Feasible Access Patterns

Let \mathcal{S} denote the set of all feasible access patterns of secondary links indexed by $s = 1, 2, \dots, |\mathcal{S}|$. A feasible access pattern s (\mathcal{S}_s) is a subset of the secondary links \mathcal{L} that can simultaneously transmit data to achieve spatial reuse of the radio spectrum. \mathcal{S}_s has to satisfy the following four key constraints:

1. *Constraint on network topology*: No two secondary links in \mathcal{S}_s share the same node, i.e., if link $i, j \in \mathcal{S}_s$ and $i \neq j$, then $c_{i,j} = 0$.
2. *Interference constraints for primary users*: Given w_k as the maximum interference level tolerable by primary receiving point k (R_k), the interference constraint for R_k can be expressed as

$$\sum_{i \in \mathcal{S}_s} \tilde{g}_{k,i} p_i \leq w_k, \forall k \in \mathcal{K} \quad (4.2)$$

where $\tilde{g}_{k,i}$ is the channel gain between T_i to R_k .

3. *QoS constraints for secondary links*: If γ_i denotes the SINR threshold, the QoS requirement for the secondary link i can be written as

$$\mu_i \geq \gamma_i, \forall i \in \mathcal{S}_s \quad (4.3)$$

¹An outdoor propagation model can be also used for the proposed robust scheduling and power control framework.

where $\mu_i = \tilde{g}_{i,i}p_i / \left\{ \sum_{j \in \mathcal{S}_s \cup \mathcal{K}, j \neq i} \tilde{g}_{i,j}p_j + n_i \right\}$, in which the denominator is the total noise and interference power at the receiving point of secondary link i .

4. *Maximum transmission power constraints for secondary links:* The transmission power of secondary user i is limited by p_i^{max} . Therefore, $0 \leq p_i \leq p_i^{max}, \forall i \in \mathcal{L}$

Let us denote by \mathbf{Q} the binary matrix representing the activity of secondary links in \mathcal{S} (i.e., either active or inactive), where

$$q_{i,s} = \begin{cases} 1, & \text{if link } i \text{ is active in } \mathcal{S}_s \\ 0, & \text{otherwise.} \end{cases} \quad (4.4)$$

Note that the column vector \mathbf{q}_s is the s th column in \mathbf{Q} that represents \mathcal{S}_s . To specify matrix \mathbf{Q} , we have to indicate all feasible access patterns that satisfy the three constraints defined above.

Remark 1: The constraints imposed in 1) above are quite standard for wireless nodes with simple transceivers. In particular, these capture the popular half-duplexing, unicasting, and receptivity constraints [103] implying that any wireless node cannot transmit and receive simultaneously, and cannot transmit to or receive from more than one neighboring node at the same time. The constraints in 3) capture the SINR interference model.

4.3 Formulation of the Robust Transmission Scheduling and Power Control Problem

4.3.1 The Nominal Problem

The transmission scheduling and power control problem is to find the minimum transmission length (i.e., number of time slots) needed to transmit data while satisfying the minimum traffic demand of secondary users \mathbf{u} . We define \mathbf{y} as the decision variable vector to indicate the number of slots that each feasible access pattern uses in a frame, where y_s represents the number of time slots that the feasible access pattern \mathcal{S}_s is scheduled in a frame. We can formulate the scheduling problem as an integer

programming (IP) problem as follows:

$$\min_{\mathbf{y}} \quad \mathbf{1}'\mathbf{y} \quad (4.5)$$

$$\text{subject to} \quad \sum_s q_{i,s} y_s \geq u_i, \forall i \in \mathcal{L} \quad (4.6)$$

$$y_s \geq 0 \text{ and } y_s \in \mathbb{Z}, \forall s \in \mathcal{S} \quad (4.7)$$

where $\mathbf{1}'$ is a row vector of ones with dimension $1 \times |\mathcal{S}|$. Note that \mathbb{Z} here denotes a set of integers.

4.3.2 Modeling Channel Uncertainty

To generate the robust schedules, we formulate the worst-case scenario where the channel uncertainty variable X in (4.1) is modeled to result in pessimistic link gains between the secondary transmitters and receivers, and optimistic link gains between other secondary transmitters and primary receivers (i.e., the interference links). The pessimistic link gains are lower than the average link gains while the optimistic link gains are higher than the average link gains. Consequently, the pessimistic link gains can be obtained from $\tilde{g}_{i,i} = g_{i,i} \cdot 10^{X^-/10}$, where $X^- = -\alpha\tau\sigma$ and the optimistic link gains can be written as $\tilde{g}_{i,j,j \neq i} = g_{i,j} \cdot 10^{X^+/10}$, where $X^+ = \beta\tau\sigma$ with $\alpha, \beta, \tau \geq 0$, and $\sigma = \ln(10)\bar{\sigma}$ [101]. Note that the channel gains follow a log-normal distribution which is unbounded and asymmetric.

In the presence of channel uncertainty, we can formulate the robust versions of the constraints in (4.2) and (4.3) as follows:

$$\sum_{i \in \mathcal{L}} g_{k,i} \cdot 10^{X^+/10} p_i \leq w_k, \forall k \in \mathcal{K} \quad (4.8)$$

$$\frac{g_{i,i} \cdot 10^{X^-/10} p_i}{\sum_{j \in \mathcal{S}_s \cup \mathcal{K}, j \neq i} g_{i,j} \cdot 10^{X^+/10} p_j + n_i} \geq \gamma_i q_i, \forall i \in \mathcal{S}_s. \quad (4.9)$$

Note that, if the value of X is equal to zero, the model is deterministic which adopts an average link gain only and the degree of robustness (i.e., conservatism) is equal to zero. The degree of robustness can be controlled by X^+ and X^- . The SINR constraints may not be satisfied when the degree of robustness is low. Based on the

robust formulation, we can obtain an upper-bound of the probability of the event that the SINR constraint of a link is violated [101] as follows:

$$P_v = \left[1 - 10^{-\tau^2(\alpha-0.5)}\right] \cdot 10^{-\tau^2(\alpha+\beta-1)} + 10^{-\tau^2(\alpha-0.5)}. \quad (4.10)$$

4.3.3 Modeling Traffic Demand Uncertainty

Due to the channel gain uncertainty (and hence improper power allocation and subsequent SINR constraint violation), transmissions of some secondary links in a feasible access pattern s (\mathcal{S}_s) can fail. These failed links will require more time slots to retransmit the data packets, and therefore, the traffic demand of secondary users in a frame can vary from the average traffic demand. The violations of link SINRs in each time slot are independent and identically distributed following a Bernoulli distribution with probability P_v .

Let us denote by \tilde{u}_i the uncertain traffic demand of secondary link i , where $\tilde{u}_i = u_i + \hat{u}_i$. u_i is the average traffic demand and \hat{u}_i is a discrete random variable with a Binomial distribution. The traffic demand constraint of secondary links in (4.6) can be rewritten as

$$\sum_s q_{i,s} y_s - u_i - \hat{u}_i \geq 0, \forall i \in \mathcal{L}. \quad (4.11)$$

We can transform the constraint in (4.11) into a deterministic form by using the chance constraint as follows:

$$Pr \left\{ \sum_s q_{i,s} y_s - u_i - \hat{u}_i < 0 \right\} \leq \epsilon_i, \forall i \in \mathcal{L} \quad (4.12)$$

where ϵ_i is the reliability level or the robustness parameter for traffic demand. This chance constraint can be rewritten as $Pr \left\{ \sum_s q_{i,s} y_s - u_i - \hat{u}_i < 0 \right\} \leq Pr \{ \hat{u}_i > \lambda_i \} = 1 - Pr \{ \hat{u}_i \leq \lambda_i \} = 1 - (1 - \epsilon_i) = \epsilon_i$, where λ_i is the upper-bound of the number of time slots during which transmissions of link i fail due to SINR constraint violation (i.e., $Pr \{ \hat{u}_i \leq \lambda_i \} = 1 - \epsilon_i$). Then, the deterministic constraint can be obtained from

$$\sum_s q_{i,s} y_s - u_i - \lambda_i \geq 0, \forall i \in \mathcal{L} \quad (4.13)$$

where $\lambda_i = F^{-1}(1 - \epsilon_i, u_i + \lambda_i, P_v)$. $F^{-1}(\cdot)$ is the inverse distribution function of a discrete random variable with a Binomial distribution. P_v being the probability

of failure in each trial (i.e., time slot), we can consider $1 - \epsilon_i$ as the probability of observing λ_i failures in $u_i + \lambda_i$ independent trials.

4.3.4 Complexity of the Robust Scheduling and Power Control Problem

Based on the model for traffic demand uncertainty as described above, we can rewrite the robust optimization problem as follows:

$$\min_{\mathbf{y}} \quad \mathbf{1}'\mathbf{y} \quad (4.14)$$

$$\text{subject to} \quad \mathbf{Q}\mathbf{y} \succeq \mathbf{u} + \boldsymbol{\lambda} \quad (4.15)$$

$$\mathbf{y} \succeq \mathbf{0} \text{ and each element of } \mathbf{y} \text{ is an integer.} \quad (4.16)$$

Matrix \mathbf{Q} plays an important role in the solution of the robust scheduling and power control problem. The main difficulty of solving the optimization problem is to find all feasible access patterns (\mathcal{S}) and the corresponding transmission power vector that satisfy the robust constraints in (4.8) and (4.9). The complexity of the problem is stated in the following proposition.

Proposition 2 *The robust scheduling and power control problem for cognitive STDMA networks coexisting with primary networks is an NP-complete problem.*

Proof. In [103], the integrated link scheduling and power control problem to find the minimum of the schedule length in ad hoc wireless networks such that, the SINR level at the receivers is above a threshold and all links are successfully scheduled at least once, is proved to belong to the NP complexity class. The authors prove that the *edge-coloring problem* in graph theory, which is a known NP-complete problem, is reducible to the integrated link scheduling and power control problem. Therefore, the integrated link scheduling and power control problem is also NP-complete. Since this problem is a special case of the problem under consideration, which considers the interference constraints for the primary users and channel gain uncertainty in addition to the SINR constraints for secondary users, the robust scheduling and power control problem is also an NP-complete problem.



Due to this NP-completeness, there is no known polynomial-time algorithm which is able to find all feasible access patterns \mathcal{S} . Therefore, it is difficult to specify the matrix \mathbf{Q} (described by (4.4)) in advance. Moreover, the sizes of \mathcal{S} and matrix \mathbf{Q} could exponentially grow with the number of links. In this chapter, we propose an algorithm based on stabilized column generation to find an efficient solution to this problem.

4.4 A Stabilized Column Generation-Based Algorithm for Transmission Scheduling and Power Control

4.4.1 Classical Column Generation Method

Column generation [104, 105] is an efficient algorithm to solve large integer programming (IP) problems which have difficulty in retrieving all variables corresponding to all feasible access patterns (\mathbf{Q}). This method decomposes the optimization problem into a restricted master problem and a pricing problem. The restricted master problem is similar to the original problem stated in Section 4.3 except that we consider only some feasible access patterns (i.e., $\bar{\mathcal{S}} \subseteq \mathcal{S}$ and $\bar{\mathbf{Q}} \subseteq \mathbf{Q}$). $\bar{\mathbf{Q}}$ can be obtained from the pricing problem which finds only the feasible access patterns that can improve the objective function in the restricted master problem. Details of the pricing problem will be described later in Section 4.5. We can formulate the robust optimization problem by using the column generation method as follows:

$$\min_{\mathbf{y}} \quad \mathbf{1}'\mathbf{y} \tag{4.17}$$

$$\text{subject to} \quad \bar{\mathbf{Q}}\mathbf{y} \succeq \mathbf{u} + \boldsymbol{\lambda} \tag{4.18}$$

$$\mathbf{y} \succeq 0 \text{ and each element of } \mathbf{y} \text{ is an integer.} \tag{4.19}$$

The above problem is called the restricted master problem because it is a restricted version of the master problem that considers only a subset $\bar{\mathbf{Q}}$ of all the feasible access

patterns \mathbf{Q} (i.e., restricted \mathbf{Q}). This restricted master problem is solved to determine the values of dual variables. Then, the values of dual variables are passed to the pricing problem to find any feasible access pattern (i.e., any column for matrix $\bar{\mathbf{Q}}$) that can improve the current solution. If we can find such a column, the restricted master problem is re-optimized. Otherwise, the process stops and the optimization problem is solved.

However, the column generation process can have convergence problem due to the oscillation of the dual variables from one iteration to the next iteration, which results from the primal degeneracy. Consequently, the runtime of the column generation could be very long. We propose a stabilized column generation-based algorithm to solve this problem.

4.4.2 Stabilized Column Generation Method

The flowcharts for the classical column generation and stabilized column generation methods are shown in Fig. 4.2. We apply the perturbation and the exact penalty methods [88] to stabilize and accelerate the column generation method. This approach guides the dual variables for the column generation method by adding a vector of surplus and slack variables to the restricted master problem. The restricted master problem for the stabilized column generation method, which is an MIP problem, can be written as follows:

$$\min_{\mathbf{y}} \quad \mathbf{1}'\mathbf{y} - \boldsymbol{\delta}'_-\mathbf{m}_- + \boldsymbol{\delta}'_+\mathbf{m}_+ \quad (4.20)$$

$$\text{subject to} \quad \bar{\mathbf{Q}}\mathbf{y} - \mathbf{m}_- + \mathbf{m}_+ \succeq \mathbf{u} + \boldsymbol{\lambda} \quad (4.21)$$

$$\mathbf{m}_- \preceq \mathbf{e}_- \quad (4.22)$$

$$\mathbf{m}_+ \preceq \mathbf{e}_+ \quad (4.23)$$

$$\mathbf{y}, \mathbf{m}_-, \mathbf{m}_+ \succeq \mathbf{0}, \text{ and } \mathbf{y} \text{ is an integer vector} \quad (4.24)$$

where \mathbf{m}_- and \mathbf{m}_+ are vectors of surplus and slack variables which are bounded by \mathbf{e}_- and \mathbf{e}_+ , respectively. In the objective function, the surplus and slack variables are penalized by the vectors $\boldsymbol{\delta}_-$ and $\boldsymbol{\delta}_+$, respectively. Let us denote by $\boldsymbol{\zeta}$ the vector of the dual optimal solutions corresponding to the constraint in (4.21). Note that $\boldsymbol{\zeta}$ is

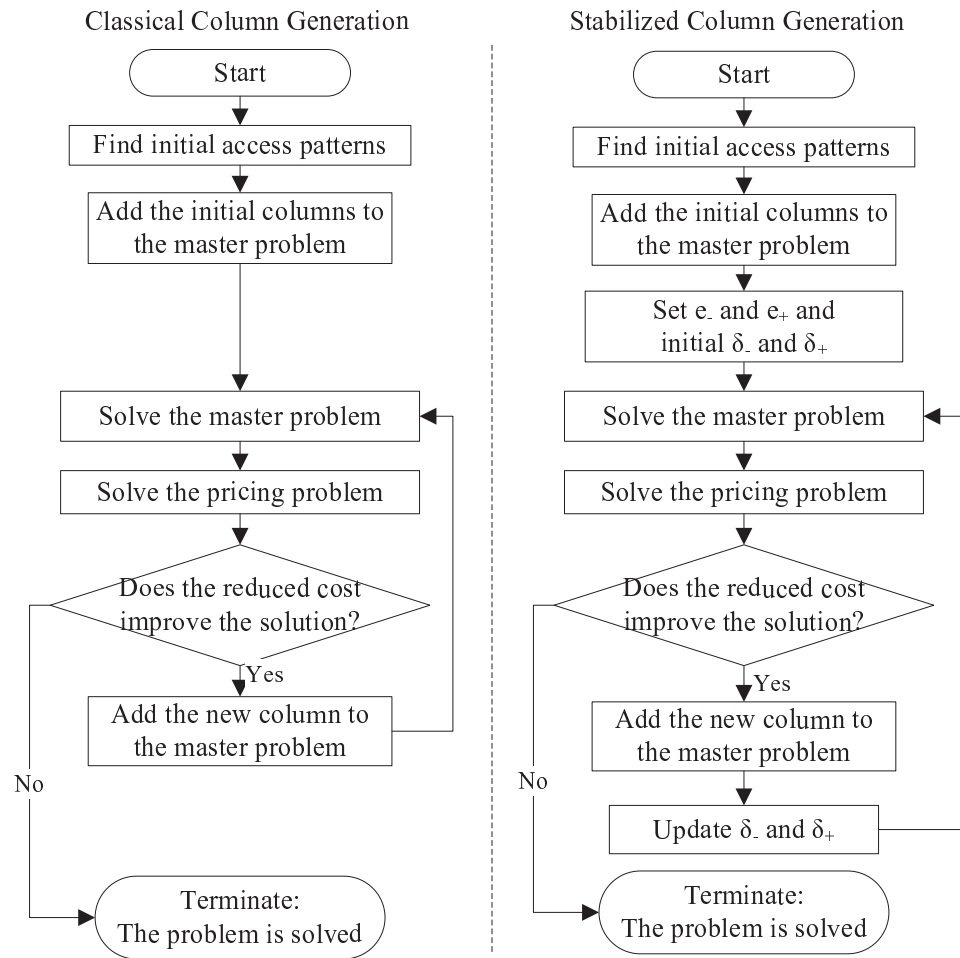


Figure 4.2. *The flowcharts for the classical column generation and stabilized column generation methods.*

the dual variable vector or shadow prices which represent the economic values. The price is the marginal cost of strengthening the constraint. Then, we can obtain the dual of the relaxed problem, which is an LP problem, as follows:

$$\max_{\zeta} \quad (\mathbf{u} + \boldsymbol{\lambda})' \boldsymbol{\zeta} - \mathbf{e}'_- \mathbf{o}_- - \mathbf{e}'_+ \mathbf{o}_+ \quad (4.25)$$

$$\text{subject to} \quad \bar{\mathbf{Q}}' \boldsymbol{\zeta} \preceq \mathbf{1} \quad (4.26)$$

$$-\boldsymbol{\zeta} - \mathbf{o}_- \preceq -\boldsymbol{\delta}_- \quad (4.27)$$

$$\boldsymbol{\zeta} - \mathbf{o}_+ \preceq \boldsymbol{\delta}_+ \quad (4.28)$$

$$\mathbf{o}_-, \mathbf{o}_+ \succeq \mathbf{0} \quad (4.29)$$

$$\boldsymbol{\zeta} \succeq \mathbf{0} \quad (4.30)$$

where \mathbf{o}_- and \mathbf{o}_+ are dual optimal solutions corresponding to the constraints in (4.22) and (4.23), respectively. The values of $\boldsymbol{\zeta}$ are penalized by \mathbf{o}_- and \mathbf{o}_+ if they lie outside the range $[\boldsymbol{\delta}_-, \boldsymbol{\delta}_+]$. Therefore, $\boldsymbol{\zeta}$ is bounded by $\boldsymbol{\delta}_- - \mathbf{o}_-$ and $\boldsymbol{\delta}_+ + \mathbf{o}_+$. Note that the optimization problem in (4.20)-(4.24) is equivalent to the problem in (4.17)-(4.19) if one of the following two conditions is met: i) $\mathbf{e}_- = \mathbf{e}_+ = \mathbf{0}$, or ii) $\boldsymbol{\delta}_- \prec \boldsymbol{\zeta}^* \prec \boldsymbol{\delta}_+$.

In each iteration, the stabilized column generation algorithm needs to update the values of $\boldsymbol{\delta}_-$ and $\boldsymbol{\delta}_+$. One way to update these values is to set $\boldsymbol{\delta}_-$ and $\boldsymbol{\delta}_+$ for the next iteration equal to the current dual solution of $\boldsymbol{\zeta}^*$ [88]. The algorithm iteratively finds an additional access pattern that can improve the current objective function and updates the values of $\boldsymbol{\delta}_-$ and $\boldsymbol{\delta}_+$ until such a column cannot be found.

We can use interior-point methods to solve a relaxed linear programming (LP) problem. The complexity-bounds for these methods when applied to solve an LP problem [106] are given by $\mathcal{O}(\sqrt{|\mathcal{S}|}Z)$ iterations and $\mathcal{O}(|\mathcal{S}|^3 Z)$ bit operations, where $Z = \dot{Z}$ (as given in (4.31)) for classical column generation method and $Z = \ddot{Z}$ (as given in (4.32), where e_{-i} and e_{+i} are the element in the vector \mathbf{e}_- and \mathbf{e}_+ , respectively, which are the bounds of the slack and surplus variables) for the stabilized column generation method.

$$\dot{Z} = \sum_{i=1}^{|\mathcal{L}|} \lceil \log_2 (|u_i + \lambda_i| + 1) + 1 \rceil + 2 \times |\mathcal{S}| + 2 \times |\mathcal{L}| \times |\mathcal{S}|. \quad (4.31)$$

$$\begin{aligned} \ddot{Z} = \dot{Z} + \sum_{i=1}^{|\mathcal{L}|} [\log_2(|e_{-i}| + 1) + 1] + \\ \sum_{i=1}^{|\mathcal{L}|} [\log_2(|e_{+i}| + 1) + 1] + 8 \times |\mathcal{L}|. \end{aligned} \quad (4.32)$$

Since the time-complexity follows a cubic function of the number of columns $|\bar{\mathcal{S}}|$ and a linear function of Z , and \ddot{Z} is larger than \dot{Z} , with the same number of columns (i.e., iterations), the stabilized column generation method has higher computational complexity. However, the number of columns generated by the classical method can be very large (i.e., infinity in the worst-case) due to the degeneracy problem. On the other hand, the perturbation and the exact penalty methods in the stabilized column generation algorithm can guide the values of the optimal dual variables and reduce the oscillation of the dual variables and then reduce the number of the generated columns (i.e., $|\bar{\mathcal{S}}|$). Therefore, the stabilized column generation algorithm can reduce the computational complexity when compared to the classical column generation algorithm. From simulations (in Section 4.6), we observe that the stabilized column generation algorithm reduces the number of iterations by $18.85\% \pm 1.2\%$ (with 95% confidence interval) when compared to the classical algorithm.

4.5 Pricing Problem for Robust Scheduling and Power Control

4.5.1 Pricing Problem

To generate matrix $\bar{\mathbf{Q}}$, we can iteratively find any feasible access pattern that can improve the current solution by solving the pricing problem. For the minimization problem, the improving price (also called the reduced price) should be the price that reduces the current objective value (i.e., has a negative value). The reduced price can be expressed as $1 - \boldsymbol{\zeta}^{*'} \mathbf{q}_s$, where $\boldsymbol{\zeta}^{*'}$ is the row vector of the optimal dual solution. If the reduced price is non-negative (i.e., $\boldsymbol{\zeta}^{*' \mathbf{q}_s} < 1$), there is no more feasible access pattern that can reduce the current objective function. Therefore, the current solution is the optimal solution.

The pricing problem here is to find a feasible access pattern \mathbf{q}_s (i.e., \mathcal{S}) that provides the most negative value of the reduced price. Let us denote by $\check{\mathbf{q}}$ a binary variable vector, where $\check{q}_i = 1$ if secondary link i is active; otherwise $\check{q}_i = 0$. This problem is equivalent to maximizing the value of $\zeta^{*\prime} \check{\mathbf{q}}$.

We define a column vector of normalized noise power, \mathbf{v} as follows:

$$v_i = \frac{\gamma_i \left(\sum_{k \in \mathcal{K}} g_{i,k} \cdot 10^{X^+/10} p_k + n_i \right)}{g_{i,i} \cdot 10^{X^-/10}} \quad (4.33)$$

and an $|\mathcal{L}| \times |\mathcal{L}|$ matrix \mathbf{A} of the relative link gains as follows:

$$a_{i,j} = \begin{cases} \frac{\gamma_i g_{i,j} \cdot 10^{X^+/10}}{g_{i,i} \cdot 10^{X^-/10}}, & \text{if } i \neq j \text{ and } c_{i,j} = 0 \\ \infty, & \text{if } i \neq j \text{ and } c_{i,j} = 1 \\ 0, & \text{if } i = j. \end{cases} \quad (4.34)$$

Considering the SINR constraints for the secondary users in (4.9), the constraints for all secondary users in the network can be written in the matrix form as follows:

$$\{I - D(\check{\mathbf{q}})\mathbf{A}D(\check{\mathbf{q}})\} \mathbf{p} \succeq D(\check{\mathbf{q}})\mathbf{v} \quad (4.35)$$

where $D(\check{\mathbf{q}})$ is a diagonal matrix whose diagonal entries are $\check{\mathbf{q}}$.

The interference constraints for the primary users in (4.8) can be rewritten in a vector form as follows:

$$\mathbf{B}D(\check{\mathbf{q}})\mathbf{p} \preceq \mathbf{w} \quad (4.36)$$

where \mathbf{B} is a $|\mathcal{K}| \times |\mathcal{L}|$ matrix whose elements are the link gains $b_{k,i}$ from secondary transmitter T_i to primary receiver R_k with $b_{k,i} = g_{k,i} \cdot 10^{X^+/10}$.

The robust pricing problem can, therefore, be formulated as follows:

$$\max_{\check{\mathbf{q}}, \mathbf{p}} \quad \zeta^{*\prime} \check{\mathbf{q}} \quad (4.37)$$

$$\text{subject to} \quad \{I - D(\check{\mathbf{q}})\mathbf{A}D(\check{\mathbf{q}})\} \mathbf{p} \succeq D(\check{\mathbf{q}})\mathbf{v} \quad (4.38)$$

$$\mathbf{B}D(\check{\mathbf{q}})\mathbf{p} \preceq \mathbf{w} \quad (4.39)$$

$$\mathbf{0} \preceq \mathbf{p} \preceq \mathbf{p}^{max} \quad (4.40)$$

where $\check{\mathbf{q}}$ is a binary vector. We can solve this nonlinear MIP problem by using a branch-and-bound algorithm [107] with relaxation of the constrained nonlinear optimization problem. The constrained nonlinear optimization problem can be solved

by using an interior point algorithm [108]. The combination of these two algorithms takes much less time than the naive exhaustive search among all secondary links \mathcal{L} . However, it still has the exponential runtime with increasing number of secondary links. The complexity of the pricing problem mainly affects the complexity of the column generation method, which is generally very high when the network is large. Therefore, we propose the Weighted Interference Criterion Greedy (WICG) algorithm to solve the pricing problem efficiently.

Remark 2: There are existing works in the literature, which consider the problem of joint discrete power control and scheduling. For example, in [83], there is a finite set of power levels and each scheduled link can choose one of these available power levels for its communications. All feasible access patterns can be enumerated with the corresponding power levels, which is a finite set. Then, the solution of the pricing problem can be found by searching over this finite set. However, for a large network, the set of feasible access patterns is extremely large, which prevents the exhaustive search from being an affordable solution. This asks for a greedy low-complexity algorithm to solve the pricing problem, which will be presented in the next section of this chapter.

4.5.2 A Heuristic Algorithm to Solve the Pricing Problem

The WICG algorithm (with the flowchart shown in Fig. 4.3) is based on a greedy heuristic. Since the pricing problem is used to find any feasible access pattern that can reduce the current solution, it is sufficient to obtain any feasible access pattern that provides the negative value of the reduced price (i.e., $\zeta^* \mathbf{q}_s > 1$). Since the dual variables are always greater than zero, a higher number of active secondary links can improve the objective function in the pricing problem. Moreover, if we can accommodate more secondary users to transmit in a time slot (i.e., in an access pattern), we can eventually reduce the frame length.

The key idea of this algorithm is to find the maximum of active secondary links that can simultaneously transmit data while satisfying the constraints for the feasible access pattern. Initially, there is no link that is active (i.e., $q_i^* = 0, \forall i \in \mathcal{L}$). We activate one link at a time (i.e., set $q_i^* = 1$) in the descending order of their weights until all secondary links are considered. A secondary link can remain active if the new

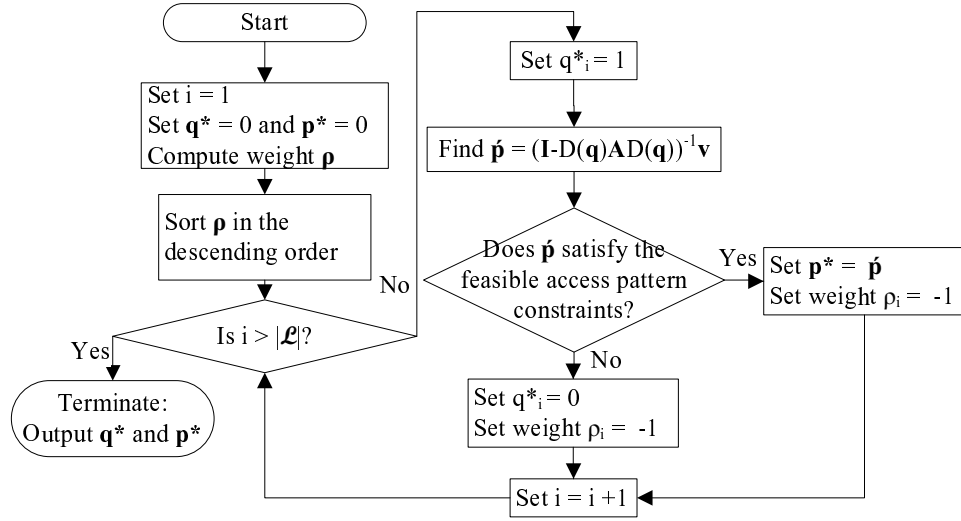


Figure 4.3. The flowchart of the Weighted Interference Criterion Greedy (WICG) algorithm.

access pattern can satisfy the constraints of the feasible access pattern. Otherwise, the secondary link will be deactivated (i.e., $q_i^* = 0$).

We define the weights based on the *relative interference level* ω_i and the optimal dual values (i.e., ζ^*). The relative interference level ω_i for link i can be obtained from

$$\omega_i = \max \left\{ \sum_j \bar{a}_{i,j}, \sum_k \bar{a}_{k,i} \right\}. \quad (4.41)$$

Here $\sum_j \bar{a}_{i,j}$ and $\sum_k \bar{a}_{k,i}$ denote, respectively, the total relative interference level that secondary link i generates to other secondary links and the total relative interference level at the receiving point of secondary link i from other secondary transmitters. Note that $\bar{a}_{i,j}$ is defined similar to $a_{i,j}$ in (4.34). However, to avoid infinite values of ω_i , we use $\bar{a}_{i,j} = \frac{\gamma_i g_{i,j} \cdot 10^{X^+/10}}{g_{i,i} \cdot 10^{X^-/10}}$ when $c_{i,j} = 1$.

Let ρ_i denote the weight of secondary link i , which can be obtained as follows:

$$\rho_i = \max(\omega) \cdot \zeta_i^* + \max(\omega) - \omega_i. \quad (4.42)$$

This weight represents the value of ζ_i^* and the relative interference level of secondary link i . Note that ζ^* expresses the marginal costs of strengthening the constraints. If the ζ_i^* is high, it means that the change by one unit of the bandwidth

allocation of user i highly impact to the objective value. Therefore, the WICG algorithm tries to find a feasible access pattern by including the links that have high values of ζ^* and low relative interference levels. Note that if ζ_i^* is high and the relative interference (ω_i) is low. The weight will be high. It is most likely to be active in the time slot. On the other hand, if ζ_i^* is low and the relative interference (ω_i) is high. It is most likely to be inactive in the time slot. Therefore, the scheduling order is based on these weights. The computational complexity of this heuristic algorithm is $\mathcal{O}(|\mathcal{L}|)$, which is acceptable.

4.5.3 Initial Feasible Access Patterns

To initialize our stabilized column generation method, we need a subset of feasible access patterns. One possible choice is the set of the feasible access patterns that have only one active link in an access pattern. This choice is simple but not efficient for initialization. A good choice of initial feasible access patterns can reduce the number of iterations required in the stabilized column generation process. We can apply the WICG algorithm to obtain a good choice of the initial feasible access patterns, which can be used by the optimal solution with high probability.

To apply the WICG algorithm in finding initial feasible access patterns, we have to modify two main points. First, the optimal dual solution (ζ^*) is not known at the initial step. Here, we can set $\zeta^* = \mathbf{1}$. Secondly, if the secondary link i cannot be added to the existing feasible access pattern, we will ignore this link in the WICG algorithm. Instead, we will create a new feasible access pattern and include this secondary link i in the new pattern.

Remark 3: The algorithmic solutions proposed in this chapter require centralized implementation in general. This means, we need a network controller that collects all required information about channel gains, traffic demand, on/off status of primary users, and target SINRs, and then calculates and distributes the solution to all network nodes. This centralized implementation may be realistic for a small or medium-size network where changes in traffic demand and primary users' activity are not very fast (e.g., in the scale of tens of minutes or hours). Examples of such networks with slow changes in primary users' activity include those on the TV bands [110]-[111].

4.6 Performance Evaluation

To evaluate the performance of the proposed stabilized column generation method for robust scheduling and power control, we conduct our simulations on a computer with a 2.8 GHz CPU and 1 GB of RAM. We solve the optimization problem by using YALMIP [109], which is a modeling language to simply model both convex and non-convex optimization problems. YALMIP has to work with external solvers (i.e., MATLAB) for actual computations. We use *fmincon* in MATLAB and *bmibnb* in YALMIP to solve the mixed integer programming problems.

In the simulation set up, we consider a single primary network, where the primary users communicate in the uplink direction with a base station located at the center of a rectangular area of 300m \times 300m. A primary transmitter is randomly located within the range of 50 m. from the base station. In the secondary network, we generate random network topologies, where the distance between a transmitter and a receiver is uniformly distributed in the range of 55 m. For the indoor propagation model, we consider $n_{SF} = 3.3$, $FAF = 16.2$ dB, and $L(d_0) = 37.7$ dB. The maximum transmission power of a secondary user (\mathbf{p}^{max}) is 100 mW. The noise power at the primary and secondary receivers (n_k and n_i) is -100 dBm. The desired SINR for primary and secondary users (γ_k and γ_i) is set to 7 dB. The maximum interference level tolerable by primary receiver k , w_k can be obtained from γ_k and n_k as $w_k = \frac{g_{k,k} \cdot 10^{X^-/10} p_k}{\gamma_k} - n_k$. The results are obtained by averaging over 100 simulations.

4.6.1 Heuristic Pricing Algorithm

First, we investigate the performance of the proposed heuristic pricing algorithm (i.e., WICG algorithm). We compare the performance of the proposed heuristic pricing algorithm with the optimal solutions obtained by using the combination of branch-and-bound and interior point algorithms proposed in [107] and [108], the CSCR (Combined Sum Criterion Removal) algorithm proposed in [82], and the geometric programming approximation algorithm in [102]. The variation in the average number of removal secondary links is shown in Fig. 4.4. As is evident from this figure, the WICG algorithm outperforms both the CSCR and geometric programming approximation algorithms. The performance of the WICG algorithm is very close to that of the optimal schedul-

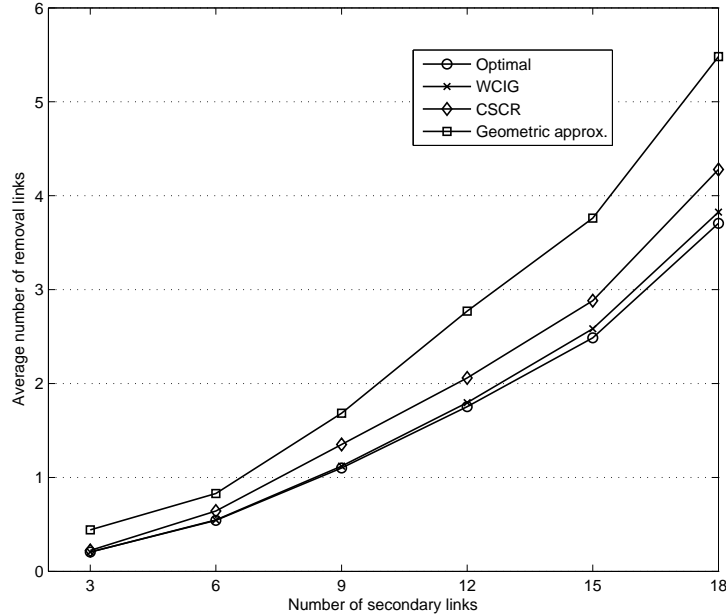


Figure 4.4. Average number of secondary removal links and the total number of secondary links.

ing algorithm with 0.39% of average cost penalty from the optimal solutions. With 18 secondary links, the cost penalty is 0.83% from the optimal solutions. Note that the average cost penalty is calculated as the ratio of the difference between the numbers of scheduled links obtained from the optimal solution and the WICG algorithm and the number of scheduled links from the optimal solution.

In Fig. 4.5, we show the average computation time of the four algorithms with 95% confidence interval. The computation time of the combination of branch-and-bound and interior point algorithms and the geometric programming approximation algorithm increases exponentially with the number of secondary links. In contrast, the computation time for the CSCR and WICG algorithms increase only slightly with the number of secondary links. Note that the WICG algorithm requires less computation time when compared to the CSCR algorithm. The WICG algorithm can reduce the computation time of the combination of branch-and-bound and interior point algorithms by 1.67×10^4 times.

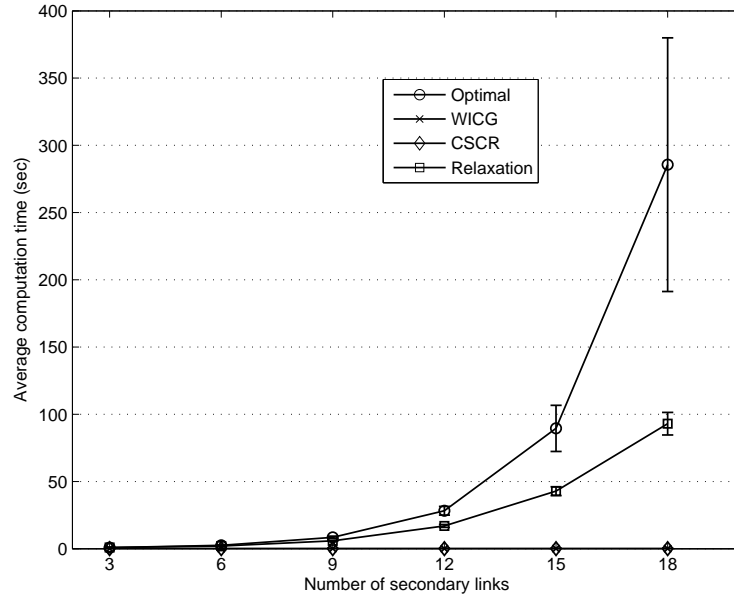


Figure 4.5. Average computation time in seconds and the total number of secondary links.

4.6.2 Stabilized Column Generation

Due to its computational efficiency, we use the WICG algorithm to solve the pricing problem for both the classical and the stabilized column generation algorithms for the scheduling and power control problem. We consider a random network with 40 secondary links. We assume the bounds of slack and surplus variables (i.e., \mathbf{e}_- and \mathbf{e}_+) to be $\mathbf{e}_- = \mathbf{e}_+ = \mathbf{e}$. Fig. 4.6 presents the average number of iterations for different values of \mathbf{e} . The average number of iterations of the stabilized column generation method is always less than that of the classical column generation method. The stabilized column generation method can reduce the number of iterations by $18.85\% \pm 1.2\%$ (with 95% confidence interval). Moreover, the performance of the stabilized column generation depends on \mathbf{e} . As \mathbf{e} increases, the number of iterations in the stabilized column generation method decreases, especially for $0.05 \preceq \mathbf{e} \preceq 5$. When \mathbf{e} increases, the bounds for the dual variables ζ^* become loose. This accelerates the column generation process. However, the number of iterations is almost the same for $0.0001 \preceq \mathbf{e} \preceq 0.05$ and $5 \preceq \mathbf{e} \preceq 500$.

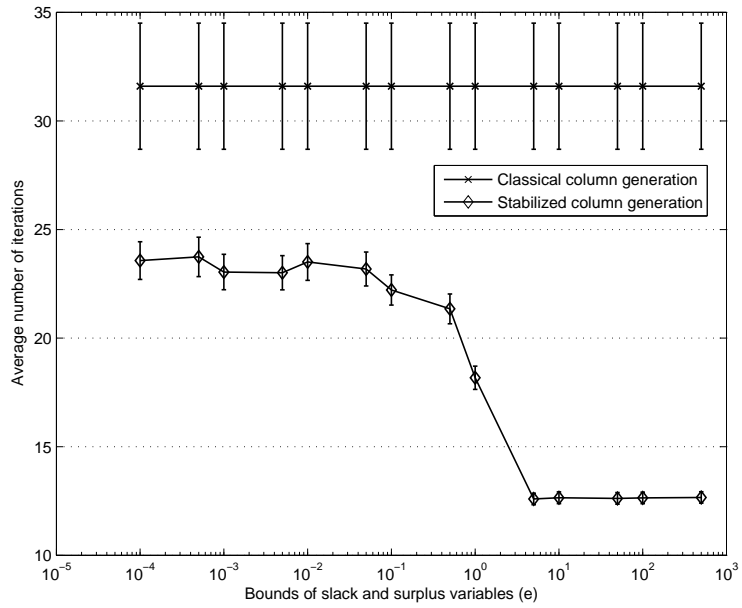


Figure 4.6. Average number of iteration and the bounds of slack and surplus variables e .

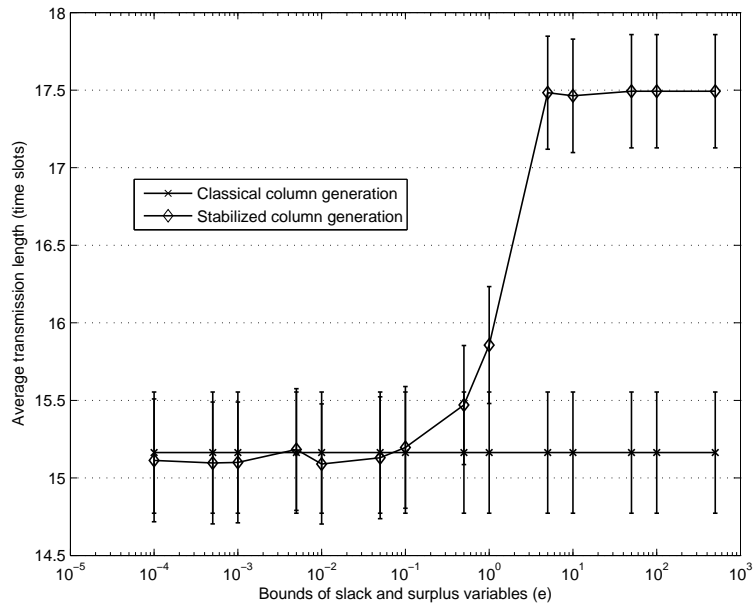


Figure 4.7. Average transmission length and the bounds of slack and surplus variables e .

In Fig. 4.7, we investigate the average transmission length obtained from the classical and the stabilized column generation methods. With $\epsilon \preceq 0.05$, the stabilized column generation method provides a smaller average transmission length than the classical column generation method. This illustrates that the stabilized column generation method is able to find more efficient feasible access patterns (through the efficient dual variables) that can improve the objective function in the restricted master problem. The stabilized column generation method can reduce the average transmission length of the classical column generation method by 0.29%.

As shown in Figs. 4.6-4.7, there is a tradeoff between the average number of iterations and the average transmission length with increasing value of e . To obtain the optimal value of e , we should select the maximum value of e such that the average transmission length is not higher than that obtained from the classical column generation method. For example, we can select $e = 0.05$ for which both the number of iterations and average transmission length are lower than those obtained from the classical column generation method.

4.6.3 Robust Scheduling and Power Control

To investigate the robustness of the proposed scheme, we set the number of secondary links equal to 40. The robustness parameters for the channel gain uncertainty are chosen as $\alpha = \beta = \sigma = 1$. We first find the optimal value of τ , which can achieve the smallest total transmission length. In Fig. 4.8, we show the variations in the average preliminary transmission length, required transmission length due to transmission failure, and total transmission length for the secondary users. The preliminary transmission length is the minimum transmission length obtained by solving the robust optimization problem in Section 4.3. Due to the channel gain variations, the SINR of secondary users can be violated. Hence, these users require more time slots to retransmit data. We refer to this as the required transmission length due to transmission failure. Finally, the total transmission length is the sum of the preliminary transmission length and the required transmission length. When τ increases, the preliminary transmission length also increases while the required transmission length decreases due to the increased robustness against channel uncertainty. The curve of the total transmission length during $0 \leq \tau \leq 1$ is dominated by the required

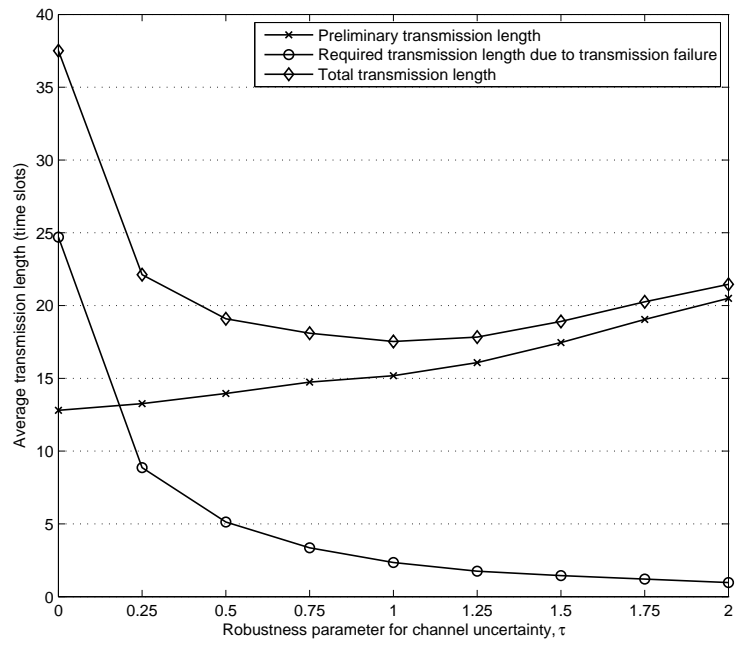


Figure 4.8. Variation in the average transmission length with the robustness parameter for channel uncertainty, τ .

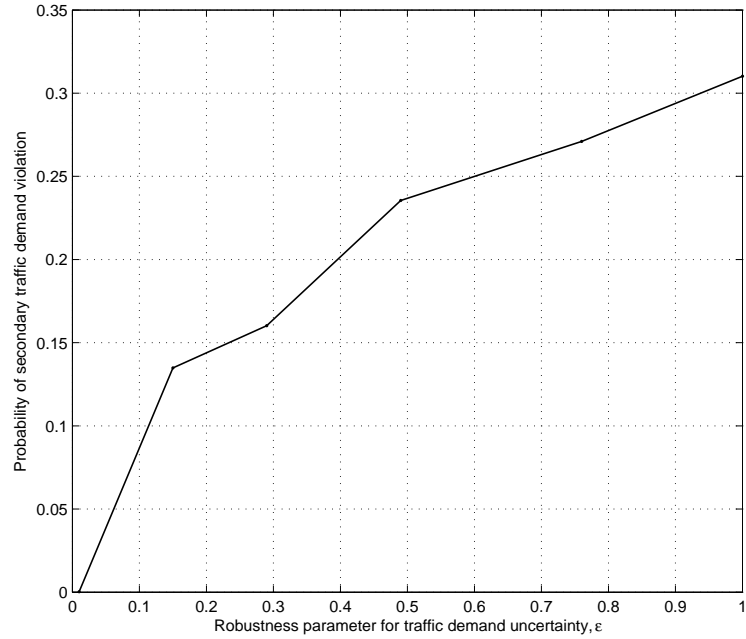


Figure 4.9. Variation in the probability of secondary traffic demand violation with the robustness parameter for traffic demand uncertainty, ϵ .

transmission length while that during $1 \leq \tau \leq 2$ is dominated by the preliminary transmission length. This is due to the fact that when τ increases, the scheduling results are more robust to channel uncertainty, and the SINR violations for secondary users are less likely. Therefore, the required transmission length due to transmission failures decreases to zero as τ increases. Moreover, we observe that the average value of total transmission length has a convex shape with a minimum value at $\tau = 1$. Therefore, we choose $\tau = 1$ for our system. Note that the interference constraints for the primary users are never violated.

In Fig. 4.9, we show the probability of secondary traffic demand violation. This probability increases when ϵ increases. When ϵ decreases, the scheduling scheme is more robust to traffic demand uncertainty, and therefore, the traffic demand violation for the secondary users decreases. The probability of traffic demand violation can be maintained below the threshold ϵ . Moreover, there is a tradeoff between the transmission length and the robustness (Fig. 4.10). When the degree of conservatism

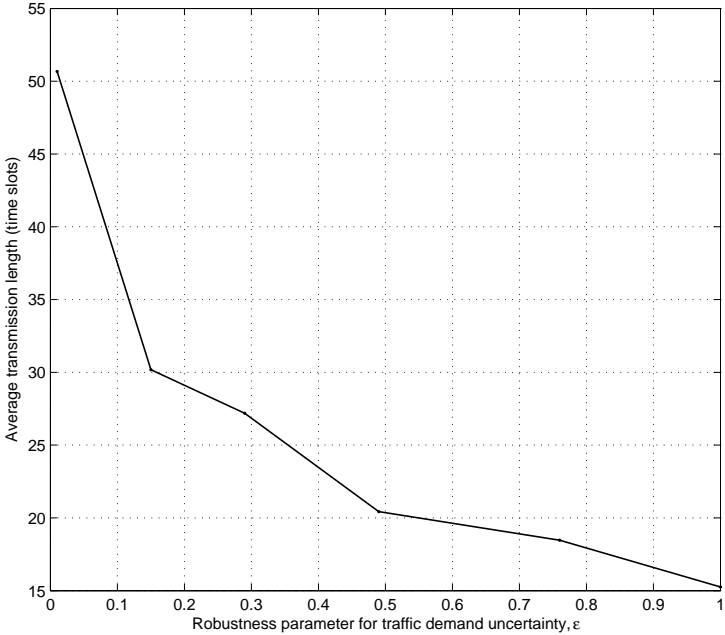


Figure 4.10. *Variation in the average transmission length with the robustness parameter for traffic demand uncertainty, ϵ .*

(i.e., robustness) is high, the transmission length increases, and vice versa.

4.7 Conclusion

We have presented a robust scheduling and power control framework for vertical spectrum sharing in STDMA-based wireless networks. In particular, a robust formulation has been presented to cope with the channel gain variations and traffic demand uncertainties. In this framework, we can control the degree of conservatism (i.e., robustness) by adjusting the robustness parameters. We have also proposed a stabilized column generation method by using the perturbation and the exact penalty methods. This method can speed up the classical column generation process. We have further proposed an efficient heuristic algorithm, namely, the Weighted Interference Criterion Greedy (WICG) algorithm for the pricing problem. Simulation results have showed that the WICG algorithm can obtain the number of removal links for the feasible access patterns very close to the optimal solution with much lower computation time. The combination of the WICG algorithm and the stabilized column generation method provides an efficient mechanism to solve the robust scheduling and power control problem for hierarchical spectrum sharing in STDMA wireless networks.

Chapter 5

Distributed Robust Scheduling and Power Control for an Ad-Hoc Cognitive STDMA Network

Although the column generation method can reduce the number of variables in a large LP problem by generating only the necessary variables in the master problem and can provide a near-optimal solution, the column generation method applied in Chapter 4 is a centralized algorithm which requires a dedicated centralized node and global information for solving the algorithms, and therefore, lacks scalability. Therefore, distributed scheduling and power control methods for ad-hoc networks were proposed based on either a fully distributed model [112]-[113] or a message-passing model [114]-[116]. [112]-[113] proposed fully distributed algorithms based on the local interference probing; however, these works did not consider the maximum power constraints for the other links. [114]-[116] proposed distributed algorithms based on a message-passing model to exchange the channel state information for the nodes. These algorithms consider only a horizontal spectrum sharing scenario.

For a vertical spectrum sharing scenario, [117] proposed a distributed admission control and power allocation method for cognitive radios in spectrum-underlay networks. The active secondary users update their transmission power by an asynchronous distributed power update method performed in a round-robin fashion. However, this scheme requires a control channel with a large number of message exchanges about the interference violation and the set of inactive links. In addition, since these existing distributed algorithms for scheduling and power control identify a subset of wireless users for only one time slot, they are not directly applicable to a cognitive

STDMA network which considers scheduling in multiple time slots to achieve the minimum transmission length of secondary users.

Furthermore, the problem of scheduling and power control in an ad-hoc network is traditionally formulated by taking only the average channel gains into account. However, the wireless link gains are stochastic by nature. Therefore, the scheduling results obtained from a traditional formulation can lead to transmission failures due to the violation of SINR constraints. The failed links require additional time slots to retransmit in order to achieve their required QoS. This motivates us to design a *distributed and robust transmission scheduling and power control framework* for vertical spectrum sharing among primary and secondary users in an STDMA-based cognitive radio network. The main contributions of this chapter are as follows:

- *Formulation of the robust scheduling and power control problem for vertical spectrum sharing in STDMA networks:* We consider the problem of transmission length minimization of secondary users subject to the traffic demand of secondary users and the interference constraints for the primary users. We jointly consider three important aspects, which are channel uncertainty, primary interference constraints, and traffic demand of secondary users. To achieve robust scheduling and power control, ellipsoidal uncertainty sets are used in the problem formulation, which capture the variations in relative channel gains between the interfering links and a transmitting link. Unlike the previous work in the literature, we present two protection functions for both guaranteeing the QoS of secondary links and protecting the primary users from harmful interference under the channel variations.
- *Distributed scheduling and power control framework:* To solve the robust scheduling and power control problem with low-complexity, we propose a novel distributed scheduling and power control framework based on a distributed column generation method. In this framework, the secondary transmitters solve an LP, which is the dual problem of the *restricted master linear-relaxation problem* (Fig. 5.1) to obtain the shadow prices (i.e., the dual optimal variables). These variables are iteratively passed to the *pricing problem* (Fig. 5.1) to find a feasible access pattern that can improve the current solution of the primal restricted master problem. For the pricing problem, we develop an efficient two-phase

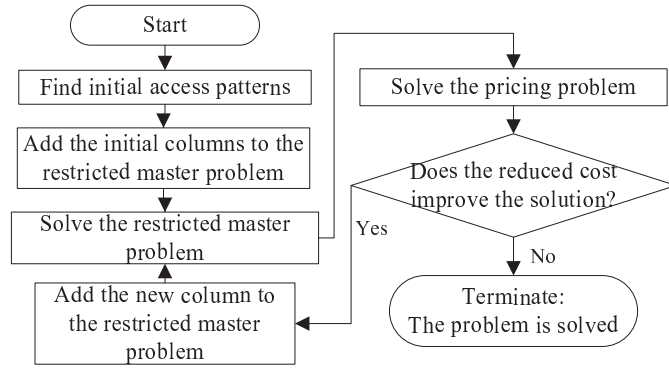


Figure 5.1. *The column generation method.*

algorithm. The first phase is used to find an initial feasible set of secondary links while the second phase is used to add as many secondary links as possible to the initial feasible set. The proposed algorithm simultaneously executes admission control with power update. Each secondary link measures SINR at the corresponding receiver and then finds its access possibility by either calculating the deactivating probability or by the interference violation notifications from the primary users. With the local SINR measurements, the secondary links can also iteratively update their transmission powers to achieve the optimal transmission powers by taking their maximum power constraints into account. The proposed algorithm can be implemented in the secondary nodes without the need for a dedicated controller and keeping track of the changes in the channel gains. Each secondary link runs the same algorithm where necessary information is exchanged by passing messages among the secondary transmitters and primary receivers. The feasible access patterns can thus be obtained in a distributed way with local SINR measurements, distributed power updates, and interference notifications from primary receivers such that the transmission length is minimized.

- *The bound on the probability of SINR constraint violation and the bound on expected transmission length:* We derive the bounds by considering the channel gain uncertainty due to shadowing, which is assumed to follow a log-normal distribution. These bounds provide guidelines for choosing the robustness parameter.

The proposed framework can be used in different network scenarios such as cognitive femtocells in the emerging fourth generation LTE-Advanced networks and spectrum sharing between wireless regional-area networks (WRANs) and wireless LANs in the TV white space.

The rest of this chapter is organized as follows. In Section 5.1, we present the system model and assumptions. Section 5.2 describes the nominal and robust formulations of the scheduling and power control problem for vertical spectrum sharing in cognitive STDMA networks. In Section 5.3, we propose a two-stage distributed algorithm based on the distributed column generation method to solve the problem. Section 5.4 presents the derivation of the probabilistic bounds on the SINR constraint violation and the expected transmission length. The performance evaluation results are presented in Section 5.5. Section 5.6 concludes the chapter. Throughout the chapter, we use lower-case bold symbols to denote vectors and upper-case bold symbols to denote matrices.

5.1 System Model and Assumptions

5.1.1 Network Model

We consider a cognitive STDMA network where a set of secondary links \mathcal{L} (indexed by $i = 1, 2, \dots, |\mathcal{L}|$) coexists with a set of *active* primary links \mathcal{K} (indexed by $k = 1, 2, \dots, |\mathcal{K}|$) as an underlay network. Each secondary link consists of a transmitter and a corresponding receiver. The secondary users are assumed to communicate in an ad-hoc fashion. Each secondary link requires a number of active time-slots (i.e., traffic demand) denoted by u_i during a frame. A fixed-length frame is divided into a fixed scheduling period for the secondary links and a transmission period as shown in Fig. 5.2. The transmission slots of the secondary users during the transmission period are underlaid with the transmissions from the primary users. Note that the proposed algorithm operates during the scheduling period to find robust schedules and transmission powers for the secondary users to be used during the transmission period. The signalling messages for the algorithm are transmitted during this scheduling period (e.g., by using some mini-slots). Let p_i^{max} represent the maximum transmission power corresponding to secondary link i . The transmission power $p_{k,s}^{(p)}$ for a primary

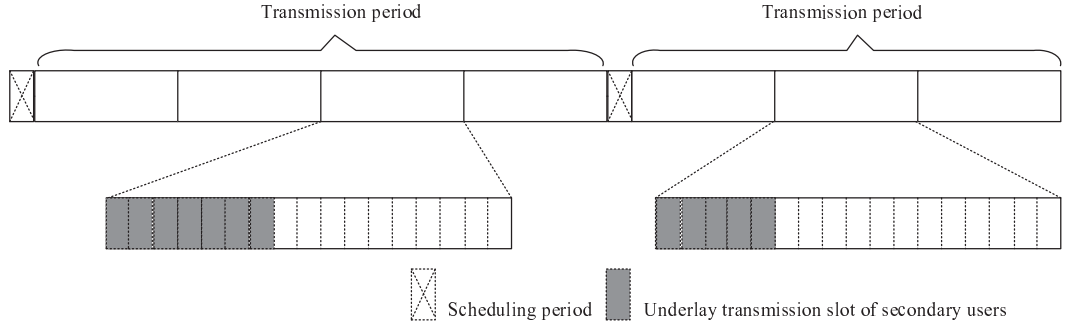


Figure 5.2. *The frame structure.*

user k , which is less than a maximum power, is assumed to be fixed over a frame. For any generic link l , we denote the transmitter by Tx_l and the receiver by Rv_l .

An indoor propagation model is considered for path-loss where the path-loss from Tx_j to Rv_i ($PL(i, j)$) can be obtained from $PL(i, j)[dB] = PL(d_0)[dB] + 10n_{SF} \log\left(\frac{d_{i,j}}{d_0}\right) + FAF[dB]$. $PL(d_0)$ is the measured line-of-sight (LOS) path-loss at $d_0 = 1\text{m}$, n_{SF} is the obstructed path-loss exponent, $d_{i,j}$ is the distance of Tx_j to Rv_i , and FAF is the floor attenuation factor. The link gain ($g_{i,j}$) between Tx_j and Rv_i is expressed by $g_{i,j} = 10^{-PL(i,j)/10}$. We consider a physical interference model where a transmitted signal is decoded successfully if the SINR at the receiver is above a certain threshold. Although an indoor propagation model is considered here, the developed framework can be used with outdoor propagation models as well.

5.1.2 Feasible Access Patterns

An access pattern represents a subset of the secondary links \mathcal{L} that simultaneously transmit data in a time-slot to achieve spatial reuse of the radio spectrum. Only the secondary links in the access pattern can have transmission powers greater than zero. An access pattern which satisfies the interference limit constraints of primary users and the minimum SINR requirements of secondary links is called a feasible access pattern. Let us denote by \mathcal{S} the set of all feasible access patterns of secondary links indexed by $s = 1, 2, \dots, |\mathcal{S}|$. A feasible access pattern \mathcal{S}_s ($\mathcal{S}_s \subseteq \mathcal{L}$) satisfies the following three constraints.

- *The primary interference limit constraints:* The total interference caused by secondary users in \mathcal{S}_s ($\eta_{k,s}$) has to be below a maximum tolerable interference limit

of primary user k , denoted by $w_{k,s}$, where $\eta_{k,s} = \sum_{j \in \mathcal{S}_s} g_{k,i} p_{i,s}$ and $p_{i,s}$ is the transmission power of secondary link i . Assuming that the SINR requirement of the primary link k is γ_k , $\mu_{k,s} \geq \gamma_k, \forall k \in \mathcal{K}$, where $\mu_{k,s} = \frac{g_{k,k} p_{k,s}^{(p)}}{\sum_{\mathcal{K}, j \neq k} g_{k,j} p_{j,s}^{(p)} + \eta_{k,s} + n_{k,s}}$, and $n_{k,s}$ is the thermal noise at the primary receiver k . Therefore, the primary link k can determine the maximum tolerable interference limit $w_{k,s}$ as follows:

$$w_{k,s} = \frac{g_{k,k} p_{k,s}^{(p)}}{\gamma_k} - \sum_{\mathcal{K}, j \neq k} g_{k,j} p_{j,s}^{(p)} - n_{k,s}, \forall k \in \mathcal{K}, \forall s \in \mathcal{S}. \quad (5.1)$$

The primary interference constraints can be expressed as $\eta_{k,s} \leq w_{k,s}, \forall k \in \mathcal{K}, \forall s \in \mathcal{S}$.

- *The minimum SINR constraints for secondary links:* At the secondary receiver Rv_i , the achievable SINR ($\mu_{i,s}$) has to be greater than the SINR threshold (γ_i) for all secondary links in \mathcal{S}_s . The QoS constraints of secondary links in terms of SINR can be written as $\mu_{i,s} \geq \gamma_i, \forall i \in \mathcal{S}_s, \forall s \in \mathcal{S}$, where $\mu_{i,s} = \frac{g_{i,i} p_{i,s}}{\sum_{\mathcal{K}} g_{i,k} p_{k,s}^{(p)} + \sum_{\mathcal{S}_s, j \neq i} g_{i,j} p_{j,s} + n_{i,s}}$, in which $n_{i,s}$ is the thermal noise power at the secondary receiver i .
- *The maximum power constraints for secondary links:* The transmission power of secondary link i should be less than p_i^{max} .

5.2 Nominal and Robust Transmission Scheduling and Power Control Problem Formulations

5.2.1 Nominal Problem Formulation

Let binary matrix \mathbf{Q} represent the activity (either active or inactive) of all secondary links in all feasible access patterns \mathcal{S} where the size of matrix \mathbf{Q} is $|\mathcal{L}| \times |\mathcal{S}|$. The elements of \mathbf{Q} are defined as: $q_{i,s} = 1$ if secondary link i is active in the feasible access pattern S_s and $q_{i,s} = 0$, otherwise. We consider the problem of transmission length minimization of secondary users subject to the traffic demand of secondary users and the constraints of feasible access patterns. Let us denote by \mathbf{y} the decision

variable vector where y_s represents the number of time-slots in which the feasible access pattern S_s is scheduled in a frame. Given the traffic demand \mathbf{u} of secondary links, we can formulate the following mixed integer programming (MIP) problem:

$$\min_{\mathbf{y}, \mathbf{Q}, \mathbf{P}} \sum_s y_s \quad (5.2)$$

$$\text{subject to } \sum_s q_{i,s} y_s \geq u_i, \forall i \in \mathcal{L} \quad (5.3)$$

$$\eta_{k,s} \leq w_{k,s}, \forall k \in \mathcal{K}, \forall s \in \mathcal{S} \quad (5.4)$$

$$\mu_{i,s} \geq q_{i,s} \gamma_i, \forall i \in \mathcal{S}_s, \forall s \in \mathcal{S} \quad (5.5)$$

$$q_{i,s} \in \{0, 1\}, \forall i \in \mathcal{L}, \forall s \in \mathcal{S} \quad (5.6)$$

$$0 \leq p_{i,s} \leq p_i^{\max}, \forall i \in \mathcal{L}, \forall s \in \mathcal{S} \quad (5.7)$$

$$y_s \geq 0 \text{ and } y_s \in \mathbb{Z}, \forall s \in \mathcal{S} \quad (5.8)$$

where \mathbb{Z} denotes a set of integers and (5.4)-(5.7) are the constraints for feasible access patterns.

5.2.2 Robust Problem Formulation with Ellipsoidal Uncertainty Set

Using (5.5), we can rewrite the SINR constraint for the secondary links as follows:

$$p_{i,s} \geq \sum_{\mathcal{K}} q_{i,s} \gamma_i \frac{g_{i,k}}{g_{i,i}} p_{k,s}^{(p)} + \sum_{\mathcal{S}_s, j \neq i} q_{i,s} q_{j,s} \gamma_i \frac{g_{i,j}}{g_{i,i}} p_{j,s} + q_{i,s} \gamma_i \frac{n_{i,s}}{g_{i,i}}, \forall i \in \mathcal{S}_s, \forall s \in \mathcal{S}. \quad (5.9)$$

Considering a feasible access pattern \mathcal{S}_s with the activity vector $\check{\mathbf{q}}$ (i.e., $\check{q}_i = q_{i,s}$) and the corresponding transmission power $\check{\mathbf{p}}$ (i.e., $\check{p}_i = p_{i,s}$), the SINR constraints for all secondary links of this access pattern can be written in the matrix form as follows:

$$(\mathbf{I} - \mathbf{F})\check{\mathbf{p}} - \mathbf{H}\mathbf{p}_s^{(p)} \succeq \mathbf{v}, \forall i \in \mathcal{L} \quad (5.10)$$

where \mathbf{I} is an identity matrix of order $|\mathcal{L}| \times |\mathcal{L}|$. \mathbf{v} is a column vector the elements of which can be written as $v_i = \check{q}_i \gamma_i \frac{\check{n}_i}{g_{i,i}}$, $i = 1, \dots, |\mathcal{L}|$. \mathbf{F} is the relative channel gain matrix among secondary links, which is of order $|\mathcal{L}| \times |\mathcal{L}|$, with the elements defined

as

$$f_{i,j} = \begin{cases} \check{q}_i \check{q}_j \gamma_i \frac{g_{i,j}}{g_{i,i}} & \text{if } i \neq j \\ 0, & \text{otherwise.} \end{cases} \quad (5.11)$$

\mathbf{H} is the relative channel gain matrix from primary transmitters to secondary receivers, which is of order $|\mathcal{L}| \times |\mathcal{K}|$, with the elements defined as $h_{i,k} = \check{q}_i \gamma_i \frac{g_{i,k}}{g_{i,i}}$, and $\mathbf{p}_s^{(p)}$ is the transmission power vector for primary transmitters with a given feasible access pattern \mathcal{S}_s .

Due to the stochastic nature of the wireless link gains, power should be allocated against channel gain uncertainty to avoid any violation of the SINR constraints. We approximate the channel gain variations using ellipsoidal uncertainty sets [118]. In particular, the uncertainties in the matrices \mathbf{F} and \mathbf{H} due to fluctuations of the wireless link gains are approximated by ellipsoids. Let $\boldsymbol{\epsilon} = [\epsilon_1, \epsilon_2, \dots, \epsilon_{|\mathcal{L}|}]$ be the maximal deviation of each entry in \mathbf{F} and \mathbf{H} . The uncertainty sets $\tilde{\mathcal{F}}_i$ and $\tilde{\mathcal{H}}_i$ for \mathbf{f}_i and \mathbf{h}_i , respectively, under the ellipsoidal approximation can be represented by

$$\begin{aligned} \tilde{\mathcal{F}}_i &= \left\{ \mathbf{f}_i + \Delta \mathbf{f}_i : \sum_{\mathcal{S}_s, j \neq i} |\Delta f_{i,j}|^2 \leq \epsilon_i^f \right\} \\ \tilde{\mathcal{H}}_i &= \left\{ \mathbf{h}_i + \Delta \mathbf{h}_i : \sum_{\mathcal{K}} |\Delta h_{i,j}|^2 \leq \epsilon_i^h \right\} \\ \epsilon_i &= \max \left\{ \epsilon_i^f, \epsilon_i^h \right\}. \end{aligned}$$

The protection function [99] associated with the uncertainty can be given as

$$\begin{aligned} \varpi_i(\check{\mathbf{p}}, \mathbf{p}_s^{(p)}) &= \check{q}_i \epsilon_i \sqrt{\sum_{\mathcal{L}, j \neq i} \check{p}_j^2 + \sum_{\mathcal{K}} \left(p_{k,s}^{(p)} \right)^2} \\ &= \check{q}_i \epsilon_i \sqrt{\|\check{\mathbf{p}}\|_2^2 + \|\mathbf{p}_s^{(p)}\|_2^2 - \check{p}_i^2}. \end{aligned} \quad (5.12)$$

We can rewrite the QoS constraint of secondary users in (5.10) to provide the robustness against the channel gain uncertainty as follows:

$$(\mathbf{I} - \mathbf{F})\check{\mathbf{p}} - \mathbf{H}\mathbf{p}_s^{(p)} \succeq \mathbf{v} + \boldsymbol{\varpi}(\check{\mathbf{p}}, \mathbf{p}_s^{(p)}), \forall i \in \mathcal{L}. \quad (5.13)$$

Similarly, to provide robustness, the interference constraint of a primary user in (5.4) can be rewritten as follows:

$$\check{\eta}_k \leq \check{w}_k - \frac{g_{k,k}}{\gamma_k} \varpi_k(\check{\mathbf{p}}, \mathbf{p}_s^{(p)}), \forall k \in \mathcal{K} \quad (5.14)$$

where $\check{\eta}_k = \eta_{k,s}$ and $\check{w}_k = w_{k,s}$.

Remark 1: The ellipsoidal channel uncertainty set can be used to approximate the channel gain variations within a bound by capturing the relative channel gain variations between the interference links and a transmitting link [99]. It was shown that the constant probability density contours of a multivariate Gaussian distribution represent an ellipsoidal set [119]. The ellipsoidal set can be regarded as a high-dimensional region inside which the parameters randomly vary with the Gaussian distribution. Moreover, the ellipsoidal uncertainty set is well-motivated by practical channel state information (CSI) error models and results in mathematical simplification [120]. In a multiple wireless access scenario, the use of ellipsoidal uncertainty set, along with the assumption that the random variables corresponding to the varying channel gains follow a multivariate Gaussian distribution enable us to calculate robust power allocation in a mathematically simple form.

The main difficulty in solving this optimization problem is to find all possible feasible access patterns \mathcal{S} because the number of feasible access patterns $|\mathcal{S}|$ grows exponentially with the number of secondary links $|\mathcal{L}|$. Therefore, the size of matrix \mathbf{Q} , \mathbf{P} , and the variables \mathbf{y} can be huge when $|\mathcal{L}|$ is large. The complexity of the problem is NP-complete as stated in Proposition 2.

It implies that the robust scheduling and power control problem cannot be solved by any algorithm without solving an NP-complete problem. Therefore, we propose an algorithm based on the distributed column generation method to obtain the near-optimal solution with low complexity.

5.3 Classical Column Generation and Distributed Column Generation Methods For Robust Transmission Scheduling and Power Control Problem

5.3.1 Classical Column Generation Method

In column generation, the problem is decomposed into two problems, namely, the *restricted master problem* and the *pricing problem*. The restricted master problem is a restricted version of the original problem that considers only a subset of the feasible access patterns (i.e., $\bar{\mathbf{Q}} \subset \mathbf{Q}$). Therefore, the restricted master problem can be written as

$$\min_{\mathbf{y}} \sum_s y_s \quad (5.15)$$

$$\text{subject to} \quad \sum_s \bar{q}_{i,s} y_s \geq u_i, \forall i \in \mathcal{L} \quad (5.16)$$

$$y_s \geq 0 \text{ and } y_s \in \mathbb{Z}, \forall s \in \mathcal{S}. \quad (5.17)$$

Note that the constraints for the feasible access patterns will be considered in the pricing problem.

The pricing problem identifies new variables, i.e., a new column in matrix $\bar{\mathbf{Q}}$. The objective function of the pricing problem is the reduced price as $1 - \boldsymbol{\zeta}^{*\prime} \mathbf{q}_s$, where $\boldsymbol{\zeta}^{*\prime}$ is the row vector of the dual variables and \mathbf{q}_s is the binary column vector of the new variables. The pricing problem can be rewritten as a maximization problem of $\boldsymbol{\zeta}^{*\prime} \mathbf{q}_s$. Let $\check{\mathbf{q}}$ denote the decision variables to indicate either the active or the inactive status of a secondary link i in a feasible access pattern and $\check{\mathbf{p}}$ be the corresponding transmission power of $\check{\mathbf{q}}$. Therefore, we can express the pricing problem as

$$\max_{\check{\mathbf{q}}, \check{\mathbf{p}}} \boldsymbol{\zeta}^{*\prime} \check{\mathbf{q}} \quad (5.18)$$

$$\text{subject to} \quad \text{constraints in (5.13), and (5.14)}$$

$$\check{q}_i \in \{0, 1\}, \forall i \in \mathcal{L} \quad (5.19)$$

$$0 \leq \check{p}_i \leq p_i^{max}, \forall i \in \mathcal{L}. \quad (5.20)$$

In this method, the restricted master problem is solved to determine the dual variables. These variables are passed to the pricing problem to generate a new column of feasible access patterns. If the objective of the pricing problem is greater than 1, the new column variables will be added to the matrix $\bar{\mathbf{Q}}$. The restricted master problem is repeatedly solved and new column variables are generated until no negative reduced price variables are identified.

5.3.2 Distributed Column Generation Method

The classical column generation method usually relies on a centralized solution from the pricing problem, which requires global information of the channel gains. This method may not be feasible to implement in a large-scale ad-hoc wireless network (e.g., due to signalling overhead and computational complexity). Therefore, we propose a distributed column generation method to solve the transmission scheduling and power control problem. The algorithm is decomposed into two main stages to solve the restricted master problem and the pricing problem.

5.3.2.1 A Distributed Algorithm to Solve the Restricted Master Problem

We consider the LP relaxation of the restricted master problem in (5.15)-(5.17), where the variable $\mathbf{y} \in \mathbb{R}$ (\mathbb{R} is a set of real numbers). The relaxation technique transforms the MIP, which is known to be an NP-hard problem, to an LP that can be solved in polynomial time. Moreover, the optimal values from the relaxed LP are no greater than those of the original MIP, and the feasible solutions to the dual problem in fact correspond to the lower-bounds for the original MIP. Given ζ , the dual variables for the primal problem in (5.15)-(5.17), the dual problem of the linear-relaxed restricted master problem can be expressed as

$$\max_{\zeta} \sum_i u_i \zeta_i \quad (5.21)$$

$$\text{subject to} \quad \sum_i \bar{q}_{s,i} \zeta_i \leq 1, \forall s \in \mathcal{S} \quad (5.22)$$

$$\zeta_i \geq 0, \forall i \in \mathcal{L}. \quad (5.23)$$

The dual problem is an LP which can be solved at each transmission node of secondary links. Since the column generation method requires the dual variables

to define new column variables in each iteration, directly solving the dual relaxed problem in (5.21)-(5.23) has lower computational complexity than the primal problem in (5.15)-(5.17). The distributed algorithm for solving the restricted master problem is shown in **Algorithm 4**. Every secondary transmitter executes **Algorithm 4** at the same time in the scheduling phase of a frame.

Algorithm 4 Distributed Algorithm to Solve the Restricted Master Problem

- 1: Transmitting node of secondary link i broadcasts its traffic demand u_i
 - 2: Initialize matrix $\bar{\mathbf{Q}}$ by considering that only one secondary link can transmit in a time-slot
 - 3: **repeat**
 - 4: Add the new column variables in the matrix $\bar{\mathbf{Q}}$
 - 5: The problem in (5.21)-(5.23) is solved for each link to obtain ζ^*
 - 6: The distributed algorithm is executed for secondary link i to solve the pricing problem to find $\check{\mathbf{q}}$ and $\check{\mathbf{p}}$
 - 7: **until** $\zeta^*/\check{\mathbf{q}} \leq 1$ or the number of iterations reaches a chosen limit
 - 8: The problem in (5.15)-(5.17) is solved for each link to obtain the final scheduling result.
-

Initially, each secondary transmitter broadcasts its traffic demand u_i . Then, the initial column for $\bar{\mathbf{Q}}$ can be obtained by considering that only one secondary link can transmit in a time-slot. Then, the secondary users solve the dual problem in (5.21)-(5.23) to obtain the optimal dual solution ζ^* . Based on the optimal dual solution, all of the secondary transmitters execute the distributed algorithm for solving the pricing problem (described in Section 5.3.2.2). Once the pricing problem is solved, the new access pattern is added to the matrix $\bar{\mathbf{Q}}$ if the value of $\zeta^*/\check{\mathbf{q}}$ (i.e., the objective function in (5.18)) is greater than 1. The secondary transmission nodes then solve the optimization problem in (5.15)-(5.17) to obtain the final schedule and power results.

5.3.2.2 A Distributed Algorithm to Solve the Pricing Problem

Each secondary link must be able to decide when to transmit or stay silent, based on its decision on local information only. The proposed algorithm is an extension of the classical distributed constrained power control (DCPC) algorithm in [121] with the

cooperation from the primary network. The primary network cooperates with the secondary network to find a feasible access pattern that does not cause any harmful interference to the primary links. The key idea of the proposed algorithm is to generate an access pattern based on the dual variables ζ^* , which satisfies the constraints for the feasible access patterns (i.e., (5.13), (5.14), (5.19), and (5.20)). If a secondary link i has a higher value of ζ_i^* , it will have a higher priority to access the channel. We propose a two-phase distributed algorithm to find a feasible access pattern. The first phase is to find an *initial feasible set*, an *undetermined set*, and an *interference set*, and the second phase is to add as many secondary links as possible to the *initial feasible set*.

Although the concept here is similar to that in [113], the details of each phase are not the same. Note that the distributed algorithm in [113] is used for joint scheduling and power control for a horizontal spectrum sharing scenario. The algorithm in [113] finds the feasible links first by measuring the interference at each receiver. When the feasible links are determined, the links in the feasible set execute the iterative power update algorithm to find their optimal power. Moreover, the algorithm in [113] does not consider the maximum power constraints for the links. In contrast, our proposed algorithm simultaneously executes the admission control with the power update. Each secondary link measures the SINR at the corresponding receiver and then finds its access possibility by either calculating the deactivating probability (i.e., the probability that a secondary link will become inactive in a time-slot) or by using the *interference violation notifications* from the primary users. Based on the SINR measurement, a secondary link also iteratively updates its transmission power while taking the maximum power constraint into account. Note that we consider not only the QoS of secondary links but also the interference limits for the primary receivers in a vertical spectrum sharing scenario. Later in the paper (in Section VI), we will compare the performance of our proposed scheme with the extension of the algorithm proposed in [113].

First phase of the distributed algorithm to solve the

pricing problem: The steps are shown in **Algorithm 5**. The deactivating probability P_i^d , which is different for different links, is used for the admission control process. P_i^d captures the value of dual variable ζ_i^* and the number of QoS violations

Algorithm 5 First Phase of the Distributed Algorithm to Solve the Pricing Problem

- 1: Set $\check{q}_i = 1$, $Const^d = Const$, $num_i^d = 0$
 - 2: Set $\check{p}_i = p_i^{init}$, $p_i^{temp} = 0$, $P_i^d = 0$
 - 3: **repeat**
 - 4: **if** $\check{q}_i = 1$ **then**
 - 5: Secondary link i broadcasts its \check{p}_i
 - 6: $p_i^{temp} = \check{p}_i$
 - 7: Update $\check{p}_i = \min \left\{ p_i^{max}, \frac{\gamma_i}{\check{\mu}_i} p_i^{temp} + \varpi_i(\mathbf{p}^{temp}, \mathbf{p}_s^{(p)}) \right\}$
 - 8: **if** $\zeta_i^* < \max \{\zeta^*\}$ **then**
 - 9: $P_i^d = \min \{1, P_i^d + (\max \{\zeta^*\} - \zeta_i^*)\}$
 - 10: **end if**
 - 11: **if** $\check{p}_i = p_i^{max}$ and $\check{\mu}_i < \gamma_i$ **then**
 - 12: $num_i^d = num_i^d + 1$
 - 13: $x = \max \left\{ P_i^d, \max \{\zeta^*\} - \zeta_i^* \cdot \min \left\{ 1, \frac{\check{\mu}_i}{\gamma_i} \right\} \right\}$
 - 14: $y = x + num_i^d \cdot Const^d$
 - 15: $P_i^d = \min \{1, y\}$
 - 16: **end if**
 - 17: Secondary link i drops with probability P_i^d
 - 18: **if** Secondary link i drops **then**
 - 19: $\check{q}_i = 0$ and $\check{p}_i = 0$
 - 20: Secondary link i joins *undetermined set*
 - 21: **end if**
 - 22: **end if**
 - 23: **until** $\check{p}_i = p_i^{temp}$ and $\check{\mu}_i \geq \gamma_i$
 - 24: Remove link i from the *initial feasible set* and add to the *interference set* if the primary interference constraint in (5.14) is violated (based on the notification from primary receiver).
-

for the secondary link (i.e., when the secondary link cannot achieve its SINR requirement even with the maximum transmission power). If the value of the dual variable is high, it means that the secondary link is able to reduce the overall transmission length and should become active. In this case, the deactivating probability of the secondary link should not increase, or if it increases, the amount of increase should be very small amount so that the link is most likely to become active. On the other hand, if the secondary link has a large number of QoS violations, this link either has low tolerance to interference from other links or it can cause high interference to other links. Therefore, this link is most likely to become inactive in order to make the access pattern feasible.

First, secondary link i starts the power update process with a certain power p_i^{init} and $P_i^d = 0$. In each power update iteration, secondary link i measures its local SINR $\check{\mu}_i$ and updates its transmission power with $\check{p}_i = \min \left\{ p_i^{max}, \frac{\gamma_i}{\check{\mu}_i} p_i^{temp} + \varpi_i(\mathbf{p}^{temp}, \mathbf{p}_s^{(p)}) \right\}$. If ζ_i^* is not the maximum value in ζ^* , secondary link i has lower priority to improve the current solution in the restricted master problem. Consequently, P_i^d is increased by $\max \{ \zeta^* \} - \zeta_i^*$. Moreover, if the transmission power of secondary link i reaches the maximum transmission power and the transmission of the secondary link i cannot achieve its SINR threshold (i.e., QoS violation occurs), some secondary links have to deactivate themselves. In this case, the deactivating probability of secondary link i increases with the ratio of $\check{\mu}_i$ and γ_i , and the rate of increase of P_i^d is smaller for higher values of $\frac{\check{\mu}_i}{\gamma_i}$. Again, P_i^d increases as the number of violations num_i^d increases. The value of P_i^d is updated as shown in steps 13-15 in **Algorithm 2**, where $Const^d$ is a constant step for updating the deactivating probability P_i^d . Then, each secondary link randomly deactivates with probability P_i^d . This process is repeated until there is no change in transmission power of each secondary transmitter and all active secondary links can satisfy their SINR requirements. The secondary links, which cannot access the channel in this phase, will join the *undetermined set* to find an opportunity in the second phase.

If the primary interference constraint in (5.14) for any primary receiver k is violated, some secondary links in the *initial feasible set* have to be deactivated. To remove the secondary links due to primary interference constraints, one of the secondary links which generates the highest interference will be notified to stay silent so

that the total interference to primary receiver k remains below $\check{w}_k - \frac{g_{k,k}}{\gamma_k} \varpi_k(\check{\mathbf{p}}, \mathbf{p}_s^{(p)})$. The primary receiver k can select the secondary link, which generates the highest interference, by using the following steps:

1. Primary receiver k receives the broadcast message containing the transmission power of each secondary link (\check{p}_i) and measures the received power (p_i^r) of the broadcast message from the secondary transmitter. Note that each secondary link broadcasts this message with the same transmission power. Therefore, the received power of the secondary link (p_i^r) can be used to obtain the channel gain from the secondary transmitter to the primary receiver.
2. Primary receiver k measures the total interference caused by the secondary links during the power update process $\check{\eta}_k$. If $\check{\eta}_k > \check{w}_k - \frac{g_{k,k}}{\gamma_k} \varpi_k(\check{\mathbf{p}}, \mathbf{p}_s^{(p)})$, primary receiver k notifies the secondary link who has the highest value of $\check{p}_i \times p_i^r$ to deactivate from the *initial feasible set* and join the *interference set*.
3. After the deactivation process, the secondary links remaining in the *initial feasible set* perform the power update process.
4. Primary receiver k and the secondary links in the *initial feasible set* repeat steps 1) to 3) until $\check{\eta}_k \leq \check{w}_k - \frac{g_{k,k}}{\gamma_k} \varpi_k(\check{\mathbf{p}}, \mathbf{p}_s^{(p)})$.

The secondary links, which are deactivated due to the primary constraint violation, have to join the *interference set* and are not allowed to participate in the second phase of the algorithm. In the first phase, the secondary links with high value of ζ_i^* and tolerable interference limit at the receivers can join the initial feasible access pattern.

Second phase of the distributed algorithm to solve the

pricing problem: The second phase is to bring as many undetermined secondary links as possible to the initial feasible access pattern in order to maximize the number of admitted links in an access pattern. In this phase, one secondary link in the *undetermined set* will join the *initial feasible set* at a time to find an opportunity to access the channel while the *initial feasible set* performs the distributed power update. To control the tradeoff between the scheduling performance and the computational time, only the secondary links which have the normalized value of ζ_i^* at least equal to ζ^{th} can participate in the second phase. A secondary link can be activated if its transmission does not cause any violation of the constraints (5.13), (5.14), (5.19), and (5.20). The *undetermined* secondary links execute the second phase in the descending

order of the value of ζ_i^* . Note that if two or more secondary links have the same value of dual variables, the links will be ordered by their identity numbers. The steps of the second phase are shown in **Algorithm 6**.

A secondary link i in the *undetermined set* starts with p_i^{init} to perform the power update along with the secondary links in the *initial feasible set*. The undetermined secondary link i has to deactivate when i) the secondary link i receives an *interference notification* from either a secondary link in the *initial feasible set* (e.g., through the message exchanges) or a primary link due to the violation of interference constraint, ii) the transmission power of link i reaches p_i^{max} and $\check{\mu}_i < \gamma_i$. Otherwise, the secondary link i can activate and join the *initial feasible set*. Other secondary links can recognize the status of secondary link i from its \check{q}_i broadcast. Note that, in this second phase, the primary links can measure the interference and transmit interference notification during the power update process.

Remark 2: When the information about the interference tolerance limits of the primary users are unknown to the secondary users, the proposed algorithm requires cooperation from the primary network during the scheduling period to avoid causing harmful interference to those primary users during the transmission period (as in [117]). The primary users will listen to the channel during the scheduling process and transmit notifications to the secondary users who cause the highest interference to the primary users only when the interference exceeds their tolerable limits. The secondary user who receives the notification can then stay silent. For the calculation of the protection function, the primary users broadcast their transmission powers to secondary users only once in a frame since the transmission power of a primary user is fixed over a frame. Therefore, the overhead involved in the primary user cooperation is limited. Note that this cooperation helps the secondary users to avoid harmful interference to the primary network without the need of global information from the primary network (i.e., channel gains and the maximum tolerable interference limit $w_{k,s}$) which may cause more overhead.

Remark 3: The worst-case complexity of the first phase of the distributed algorithm to solve the pricing problem is $O(1)$, and hence, it does not depend on the number of secondary links $|\mathcal{L}|$. Instead, the computational time of the first phase algorithm in the worst-case scenario depends on $Const^d$ which is the incremental constant step

Algorithm 6 Second Phase of the Distributed Algorithm to Solve the Pricing Problem

```

1: if secondary link  $i$  is in the initial feasible set or (in the undetermined set and the
   normalized value of  $\zeta_i^* \geq \zeta^{(th)}$ ) then
2:   if  $i$  is in the undetermined set then
3:     Set  $\check{p}_i = p_i^{init}$ 
4:     Set  $p_i^{temp} = 0$ 
5:     Set  $\check{q}_i = 1$ 
6:   end if
7:   repeat
8:     Secondary link  $i$  broadcasts its  $\check{p}_i$ 
9:      $p_i^{temp} = \check{p}_i$ 
10:    Update  $\check{p}_i = \min \left\{ p_i^{max}, \frac{\gamma_i}{\mu_i} p_i^{temp} + \varpi_i(\mathbf{p}^{temp}, \mathbf{p}_s^{(p)}) \right\}$ 
11:    if  $\check{p}_i = p_i^{max}$  and  $\check{\mu}_i < \gamma_i$  then
12:      if  $i$  is in the initial feasible set then
13:        Transmit a violation notification to the undetermined secondary link
          which is executing Algorithm 3 concurrently
14:      else
15:         $\check{q}_i = 0$  and  $\check{p}_i = 0$ 
16:      end if
17:    end if
18:    if  $i$  is in the undetermined set then
19:      if Secondary link  $i$  receives a violation notification from either primary
          links or secondary links in the initial feasible set then
20:         $\check{q}_i = 0$  and  $\check{p}_i = 0$ 
21:      end if
22:    end if
23:  until  $\check{p}_i = p_i^{temp}$  and  $\check{\mu}_i \geq \gamma_i$ 
24:  Secondary link  $i$  broadcasts its status  $\check{q}_i$ 
25: end if

```

for updating the deactivating probability when the secondary link cannot satisfy the feasible access constraints. If $Const^d$ is high, the computational time in the first phase will be small since the deactivating probability will reach to the value of 1.0 very fast. On the other hand, during the second phase of the algorithm, in the worst case, there is no secondary link in the initial feasible set and all secondary links have to be considered in the second phase. Therefore, the worst-case complexity of the second phase of the algorithm to solve the pricing problem is $O(|\mathcal{L}|)$.

5.3.3 Convergence of the Distributed Algorithms

The convergence of the proposed algorithm can be considered in three parts: **Algorithm 4** for solving the restricted master problem, **Algorithm 5** for the first phase of solving the pricing problem, and **Algorithm 6** for the second phase of solving the pricing problem.

For **Algorithm 4**, we set the maximum number of iterations to 256 (as in [82]) in the distributed column generation-based algorithm. The algorithm for solving the restricted master problem will terminate when the two-phase algorithm for solving the pricing problem (i.e., **Algorithm 5** and **Algorithm 6**) cannot obtain a better column that can improve the current solution or the maximum number of iterations have reached. With a properly chosen value for the maximum number of iterations, we can obtain the near-optimal solution and avoid the exponential runtime of the column generation-based algorithm in the worst-case.

For the pricing problem, we propose a two-phase distributed algorithm (i.e., **Algorithm 5** and **Algorithm 6**). In **Algorithm 5**, we use the distributed power update algorithm to find the *initial feasible set* of secondary links. From **Theorem 4** in [118], there exist a feasible power assignment if $\|\epsilon\|_2 + \rho(\mathbf{F}) < 1$, where $\|\epsilon\|_2$ is the induced l_2 -norm of ϵ and $\rho(\mathbf{F})$ is the maximum modulus eigenvalue (Perron-Frobenius eigenvalue) of the relative channel gain matrix among secondary links (\mathbf{F} in (5.11)). If a Pareto optimal power assignment exists, then the iterative power update algorithm

$$\check{p}_i = \min \left\{ p_i^{max}, \frac{\gamma_i}{\mu_i} p_i^{temp} + \varpi_i(\mathbf{p}^{temp}, \mathbf{p}_s^{(p)}) \right\} \quad (5.24)$$

converges to the optimal solution.

The distributed power update algorithm in (5.24) is distributed and asynchronously convergent. Note that the optimal solution is the minimum of the total transmission power that can satisfy the SINR constraints of the secondary links. However, this algorithm does not work without an effective admission control method. When the DCPC algorithm cannot converge to a fixed point, at least one secondary link will deactivate itself from the channel with a deactivating probability P_i^d . P_i^d is also monotonically increasing with the number of iterations when $Const^d > 0$. In the worst case, P_i^d ($i \in \mathcal{L}$) will reach 1.0 and all secondary links will deactivate from the channel. With the admission control process, the value of $\|\epsilon\|_2 + \rho(\mathbf{F})$ is smaller than 1 and the proposed algorithm can converge to a fixed power vector.

Algorithm 6 also employs the same DCPC algorithm with the one-by-one link admission control. If the newly activated secondary link causes harmful interference to either the secondary links in the *initial feasible set* or the primary links, or it is unable to satisfy its SINR requirement, it will deactivate from the channel and then the access pattern becomes feasible again. Therefore, the second phase certainly converges to a fixed solution.

5.4 Bounds on the SINR Constraint Violation and Expected Number of Transmission Length for Secondary Users

We can control the robustness of power control by adjusting the value of ϵ_i . Note that the robust problem reduces to the nominal problem when $\epsilon = 0$. If ϵ_i is too small (i.e., less conservative), the SINR constraint of secondary links can be easily violated. We derive the probabilistic upper-bound on the SINR constraint violation and the upper-bound on the expected number of time-slots required for the traffic demand requirement.

5.4.1 Probabilistic Bound on the SINR Constraint Violation

Given a feasible access pattern \mathcal{S}_s , $\check{\mathbf{q}}$ and $\check{\mathbf{p}}$ are the activity vector and corresponding transmission powers for the pricing problem in (5.18) where $\check{\mathbf{q}} = \mathbf{q}_s$ and $\check{\mathbf{p}} = \mathbf{p}_s$.

Let $E(i, s)$ be the event that the SINR constraint for secondary link i in the access pattern \mathcal{S}_s is violated. $E(i, s)$ can occur when the total interference due to the channel fluctuation is greater than the total interference from the average link gains plus the protection function. From (5.13), the probability of occurrence of event $E(i, s)$, $P_{i,s}^v$, can be obtained as

$$P_{i,s}^v = \Pr \left\{ \sum_{\mathcal{S}_s, j \neq i} \tilde{\mathcal{F}}_{i,j} \check{p}_j + \sum_{\mathcal{K}} \tilde{\mathcal{H}}_{i,k} p_{k,s}^{(p)} > \sum_{\mathcal{S}_s, j \neq i} f_{i,j} \check{p}_j + \sum_{\mathcal{K}} h_{i,k} p_{k,s}^{(p)} + \varpi_i(\check{\mathbf{p}}, \mathbf{p}_s^{(p)}) \right\} \quad (5.25)$$

where $\tilde{\mathcal{F}}_{i,j} = \frac{10^{(X_j/10)}}{10^{(X_i/10)}} f_{i,j} = \frac{\delta_j}{\delta_i} f_{i,j}$ and $\tilde{\mathcal{H}}_{i,j} = \frac{10^{(X_k/10)}}{10^{(X_i/10)}} h_{i,j} = \frac{\delta_k}{\delta_i} h_{i,j}$ in which X_j, X_i , and X_k are independent random variables with $X_j, X_i, X_k \sim \mathcal{N}(0, \sigma^2)$.

Note that the received signal power from a transmitter to a receiver (i.e., for either an interfering link or a transmitting link) is assumed to be characterized by log-normal distribution. The log-normal distribution however cannot capture the variations of interfering channel gains relative to the main channel gain of a user in a multiple access scenario. Therefore, the ellipsoidal uncertainty set is used to model the uncertainty set of the relative channel gain variations between the interfering links and a transmitting link where the variations are bounded. However, the SINR constraints can be violated if the instantaneous relative channel gains vary over the bound. In the following section, we derive the probabilistic bounds on the SINR constraint violation for an ellipsoidal channel uncertainty set under a log-normal channel model.

Theorem 1 *The probability of SINR constraint violation, $P_{i,s}^v$, satisfies (5.26), if i is in \mathcal{S}_s and $P_{i,s}^v = 0$, otherwise.*

$$P_{i,s}^v \leq \min \left\{ 1, \frac{10^{\frac{\ln(10)\sigma^2}{10^2}} \left(\sum_{\mathcal{S}_s, j \neq i} f_{i,j} \check{p}_j + \sum_{\mathcal{K}} h_{i,k} p_{k,s}^{(p)} \right)}{\epsilon_i \sqrt{\|\check{\mathbf{p}}\|_2^2 + \|\mathbf{p}_s^{(p)}\|_2^2} - \check{p}_i^2 + \sum_{\mathcal{S}_s, j \neq i} f_{i,j} \check{p}_j + \sum_{\mathcal{K}} h_{i,k} p_{k,s}^{(p)}} \right\}. \quad (5.26)$$

Proof. Based on (5.12) and (5.26), we can obtain the bound on the probability of

SINR violation of secondary link i in feasible access pattern \mathcal{S}_s ($P_{i,s}^v$) as follows:

$$\begin{aligned}
P_{i,s}^v &= \Pr \left\{ \sum_{\mathcal{S}_s, j \neq i} \frac{\delta_j}{\delta_i} f_{i,j} \check{p}_j + \sum_{\mathcal{K}} \frac{\delta_k}{\delta_i} h_{i,k} p_{k,s}^{(p)} > \right. \\
&\quad \left. \epsilon_i \sqrt{\|\check{\mathbf{p}}\|_2^2 + \|\mathbf{p}_s^{(p)}\|_2^2} - \check{p}_i^2 + \sum_{\mathcal{S}_s, j \neq i} f_{i,j} \check{p}_j + \sum_{\mathcal{K}} h_{i,k} p_{k,s}^{(p)} \right\} \\
&\leq \frac{\mathbb{E} \left[\left(\sum_{\mathcal{S}_s, j \neq i} \frac{\delta_j}{\delta_i} f_{i,j} \check{p}_j + \sum_{\mathcal{K}} \frac{\delta_k}{\delta_i} h_{i,k} p_{k,s}^{(p)} \right) \right]}{\left(\epsilon_i \sqrt{\|\check{\mathbf{p}}\|_2^2 + \|\mathbf{p}_s^{(p)}\|_2^2} - \check{p}_i^2 + \sum_{\mathcal{S}_s, j \neq i} f_{i,j} \check{p}_j + \sum_{\mathcal{K}} h_{i,k} p_{k,s}^{(p)} \right)}.
\end{aligned} \tag{5.27}$$

The inequality in (5.27) holds due to the Markov inequality.

We assume that $i = 1$. With λ^{th} moment of the log-normal distribution for $\delta_j, j \in \mathcal{S}_s$ and $\delta_k, k \in \mathcal{K}$, we obtain

$$\begin{aligned}
&\mathbb{E}[\delta_2]^{b_2} \cdots \mathbb{E}[\delta_{|\mathcal{S}_s|}]^{b_{|\mathcal{S}_s|}} \mathbb{E}[\delta_{|\mathcal{S}_s|+1}]^{b_{|\mathcal{S}_s|+1}} \cdots \\
&\quad \mathbb{E}[\delta_{|\mathcal{S}_s|+|\mathcal{K}|}]^{b_{|\mathcal{S}_s|+|\mathcal{K}|}} \\
&= 10^{\frac{\ln(10)\sigma^2 b_2^2}{2 \cdot 10^2}} \cdots 10^{\frac{\ln(10)\sigma^2 b_{|\mathcal{S}_s|}^2}{2 \cdot 10^2}} 10^{\frac{\ln(10)\sigma^2 b_{|\mathcal{S}_s|+1}^2}{2 \cdot 10^2}} \cdots \\
&\quad 10^{\frac{\ln(10)\sigma^2 b_{|\mathcal{S}_s|+|\mathcal{K}|}^2}{2 \cdot 10^2}} \\
&\leq 10^{\frac{\ln(10)\sigma^2}{2 \cdot 10^2} (b_2 + \cdots + b_{|\mathcal{S}_s|} + b_{|\mathcal{S}_s|+1} + \cdots + b_{|\mathcal{S}_s|+|\mathcal{K}|})^2} \\
&= 10^{\frac{\ln(10)\sigma^2 \lambda^2}{2 \cdot 10^2}}
\end{aligned} \tag{5.28}$$

where λ is any non-negative integer and $b_2 + \cdots + b_{|\mathcal{S}_s|} + b_{|\mathcal{S}_s|+1} + \cdots + b_{|\mathcal{S}_s|+|\mathcal{K}|} = \lambda$. Since $b_2, \cdots, b_{|\mathcal{S}_s|}, b_{|\mathcal{S}_s|+1}, \cdots, b_{|\mathcal{S}_s|+|\mathcal{K}|}$ are non-negative integers, the inequality of (5.28) holds.

Due to the independence of the random variables δ_i, δ_j and δ_k , we can rewrite the

numerator of (5.27) as follows:

$$\begin{aligned}
& \mathbb{E} [\delta_i]^{-\lambda} \mathbb{E} \left[\left(\sum_{\mathcal{S}_s, j \neq i} \delta_j f_{i,j} \check{p}_j + \sum_{\mathcal{K}} \delta_k h_{i,k} p_{k,s}^{(p)} \right)^\lambda \right] \\
&= 10^{\frac{\ln(10)\sigma^2\lambda^2}{2 \cdot 10^2}} \mathbb{E} \left[\sum_{b_2 + \dots + b_{|\mathcal{S}_s|} + b_{|\mathcal{S}_s|+1} + \dots + b_{|\mathcal{S}_s|+|\mathcal{K}|} = \lambda} \frac{\lambda!}{b_2! \dots b_{|\mathcal{S}_s|}! b_{|\mathcal{S}_s|+1}! \dots b_{|\mathcal{S}_s|+|\mathcal{K}|}!} \right. \\
&\quad \left. (\delta_2 f_{1,2} \check{p}_2)^{b_2} \dots (\delta_{|\mathcal{S}_s|} f_{1,|\mathcal{S}_s|} \check{p}_{|\mathcal{S}_s|})^{b_{|\mathcal{S}_s|}} (\delta_{|\mathcal{S}_s|+1} h_{1,1} p_{1,s}^{(p)})^{b_{|\mathcal{S}_s|+1}} \dots (\delta_{|\mathcal{S}_s|+|\mathcal{K}|} h_{1,|\mathcal{K}|} p_{|\mathcal{K}|,s}^{(p)})^{b_{|\mathcal{S}_s|+|\mathcal{K}|}} \right] \quad (5.29) \\
&= 10^{\frac{\ln(10)\sigma^2\lambda^2}{2 \cdot 10^2}} \sum_{\lambda} \frac{\lambda!}{b_2! \dots b_{|\mathcal{S}_s|}! b_{|\mathcal{S}_s|+1}! \dots b_{|\mathcal{S}_s|+|\mathcal{K}|}!} \\
&\quad (f_{1,2} \check{p}_2)^{b_2} \dots (f_{1,|\mathcal{S}_s|} \check{p}_{|\mathcal{S}_s|})^{b_{|\mathcal{S}_s|}} (h_{1,1} p_{1,s}^{(p)})^{b_{|\mathcal{S}_s|+1}} \dots \\
&\quad (h_{1,|\mathcal{K}|} p_{|\mathcal{K}|,s}^{(p)})^{b_{|\mathcal{S}_s|+|\mathcal{K}|}} \mathbb{E}[\delta_2]^{b_2} \dots \mathbb{E}[\delta_{|\mathcal{S}_s|}]^{b_{|\mathcal{S}_s|}} \\
&\quad \mathbb{E}[\delta_{|\mathcal{S}_s|+1}]^{b_{|\mathcal{S}_s|+1}} \dots \mathbb{E}[\delta_{|\mathcal{S}_s|+|\mathcal{K}|}]^{b_{|\mathcal{S}_s|+|\mathcal{K}|}} \quad (5.30) \\
&\leq 10^{\frac{\ln(10)\sigma^2\lambda^2}{10^2}} \left(\sum_{\mathcal{S}_s, j \neq i} f_{i,j} \check{p}_j + \sum_{\mathcal{K}} h_{i,k} p_{k,s}^{(p)} \right)^\lambda \quad (5.31)
\end{aligned}$$

where (5.29) results from the multinomial theorem and the λ^{th} moment of log-normal distribution, and (5.31) results from (5.28).

Substituting (5.31) into (5.27) and with $\lambda = 1$, we can have

$$P_{i,s}^v \leq \frac{10^{\frac{\ln(10)\sigma^2}{10^2}} \left(\sum_{\mathcal{S}_s, j \neq i} f_{i,j} \check{p}_j + \sum_{\mathcal{K}} h_{i,k} p_{k,s}^{(p)} \right)}{\epsilon_i \sqrt{\|\check{\mathbf{p}}\|_2^2 + \|\mathbf{p}_s^{(p)}\|_2^2 - \check{p}_i^2 + \sum_{\mathcal{S}_s, j \neq i} f_{i,j} \check{p}_j + \sum_{\mathcal{K}} h_{i,k} p_{k,s}^{(p)}}}. \text{ Note that } \sum_{\mathcal{S}_s, j \neq i} f_{i,j} \check{p}_j + \sum_{\mathcal{K}} h_{i,k} p_{k,s}^{(p)}$$

is the total interference to the secondary link i in \mathcal{S}_s . ■

5.4.2 Bounds on the Expected Number of Transmission Length

We derive an upper-bound on the expected transmission length (i.e., time-slots). Since the transmissions of the secondary users can fail with respect to the instantaneous channel gain realization, the failed links require additional time-slots to retransmit their data. Given a subset of feasible access patterns ($\bar{\mathcal{S}}$), the expected transmission

length ($J(\bar{\mathcal{S}})$) can be obtained as

$$J(\bar{\mathcal{S}}) = \sum_{s \in \bar{\mathcal{S}}} y_s + \hat{J}(\bar{\mathcal{S}}) \quad (5.32)$$

where $\hat{J}(\bar{\mathcal{S}})$ is the expected number of time-slots for retransmission given a subset of feasible access pattern $\bar{\mathcal{S}}$.

Theorem 2 For $\theta_s < 1$, the expected transmission length is upper bounded by

$$J(\bar{\mathcal{S}}) \leq \sum_{s \in \bar{\mathcal{S}}} \frac{y_s}{1 - \theta_s}. \quad (5.33)$$

where θ_s is the maximum probability of SINR constraint violation in the access pattern $\bar{\mathcal{S}}_s$ (i.e., $\theta_s = \max\{P_s^v\}$).

Proof. Since the retransmission occurs when at least one transmission link in an access pattern fails, the number of retransmission slots depends on the probability of SINR constraint violation where the violations of link SINRs in each time-slot are assumed to be independent. The probability that the retransmission of the feasible access pattern \mathcal{S}_s occurs is bounded by θ_s , where $P_{i,s}^v \leq \theta_s$. Consequently, the upper-bound on the number of retransmission slots given an access pattern $\bar{\mathcal{S}}_s$ can be expressed as follows:

$$\hat{J}(\bar{\mathcal{S}}_s) \leq \theta_s y_s + \theta_s^2 y_s + \theta_s^3 y_s + \dots \quad (5.34)$$

$$= y_s \left\{ \frac{\theta_s}{1 - \theta_s} \right\}, \forall s \in \bar{\mathcal{S}}. \quad (5.35)$$

Therefore, $\hat{J}(\bar{\mathcal{S}}) = \sum_{s \in \bar{\mathcal{S}}} \hat{J}(\bar{\mathcal{S}}_s) = \sum_{s \in \bar{\mathcal{S}}} y_s \left\{ \frac{\theta_s}{1 - \theta_s} \right\}$.

Recalling (5.32), we can rewrite the bound on the expected transmission length as follows:

$$J(\bar{\mathcal{S}}) \leq \sum_{s \in \bar{\mathcal{S}}} y_s + \sum_{s \in \bar{\mathcal{S}}} y_s \left\{ \frac{\theta_s}{1 - \theta_s} \right\} = \sum_{s \in \bar{\mathcal{S}}} \frac{y_s}{1 - \theta_s}. \quad (5.36)$$

■

5.5 Performance Evaluation

5.5.1 Simulation Parameters

We investigate the performance of the proposed algorithm by simulations. We simulate a single primary network coexisting with an ad-hoc network of secondary users in an indoor rectangular area of $300\text{m} \times 300\text{m}$. One primary node communicates with a base station located at the center of the area in the uplink direction, where the location of the primary transmitter is uniformly distributed within the range of 50m from the base station. In the secondary network, the secondary nodes are randomly located where the distance between a transmission node and a receiving node of a link is uniformly distributed within the range of 55m. For the indoor propagation model, we choose $n_{SF} = 3.3$, $FAF = 16.2$ dB, and $L(d_0) = 37.7$ dB. The noise power at the primary and secondary receivers (n_k and n_i) is -100 dBm. The desired SINR for primary and secondary links (γ_k and γ_i) is set to 7 dB. The maximum transmission power of a secondary link (p_i^{max}) is 100 mW. Depending on the location of the primary transmitter, the transmission power for the primary link during a frame is chosen sufficiently high so that its SINR requirement is satisfied. In the proposed algorithms, we set up $p_i^{init} = 10\zeta_i^{*2}$, $Const^d = 0.1$, and $\epsilon_i = \epsilon$.

5.5.2 Simulation Results

5.5.2.1 Impact of $\zeta^{(th)}$ on the Proposed Distributed Algorithm

We investigate the impact of $\zeta^{(th)}$ on the distributed column generation-based algorithm. The average transmission length decreases as $\zeta^{(th)}$ decreases (Fig. 5.3). When $\zeta^{(th)}$ decreases, the secondary links, which have low value of $\zeta^{(th)}$ and high interference tolerable limit at the corresponding receivers, can have more opportunities to access the channel in the second phase of solving the pricing problem. This results in a decrease in the transmission length. However, there is a trade-off between the transmission length and the computation time. The computation time decreases by 6.48% for an increase in transmission length by 2.13% on average when $\zeta^{(th)}$ increases from 0 to 0.1.

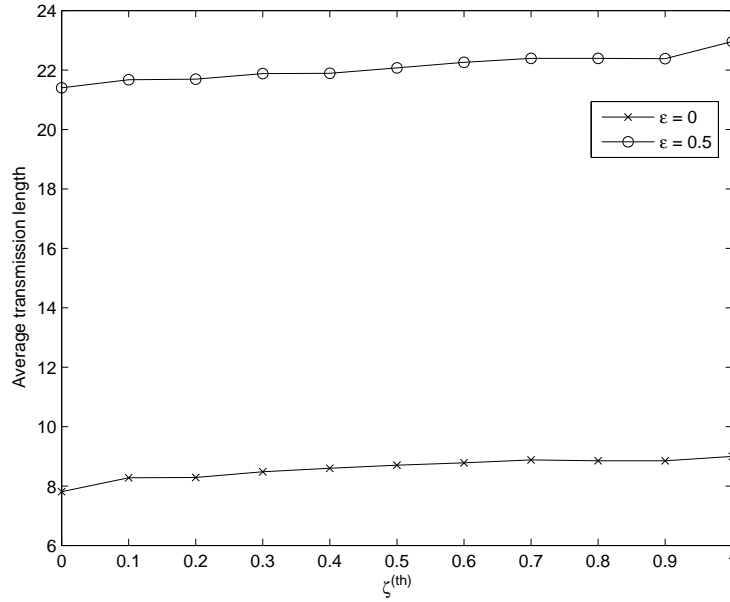


Figure 5.3. Average transmission length with $\zeta^{(th)}$.

5.5.2.2 Distributed Transmission Scheduling and Power Control Based on Column Generation Method

We compare the performance of the distributed algorithms with that of a centralized algorithm based on column generation method when $\epsilon = 0$. In the pricing problem, the centralized algorithm solves the pricing problem by using a heuristic algorithm based on a greedy method as proposed in Chapter 4. For the centralized algorithm, we need to collect information about traffic demand, SINR requirements, and channel gains of secondary users before executing the algorithm at each time-slot. The transmission length obtained from the centralized algorithm can be considered as a benchmark. In Fig. 5.4, we observe that, the proposed algorithm can provide a transmission length which is very close to that obtained from the centralized algorithm; however, with a lower computational complexity. Note that the proposed algorithm with $\zeta^{(th)} = 0$ can reduce the computation time by 47.5% with an increase in the transmission length by 3.13% compared to the centralized algorithm when the number of secondary links is 40.

We also compare the performance of the proposed scheme with two other dis-

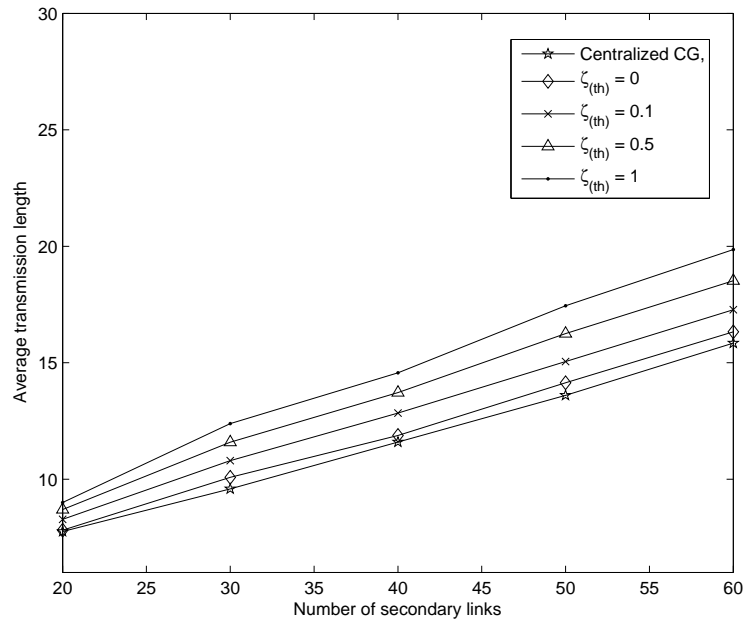


Figure 5.4. Comparison with the centralized scheduling in terms of average transmission length.

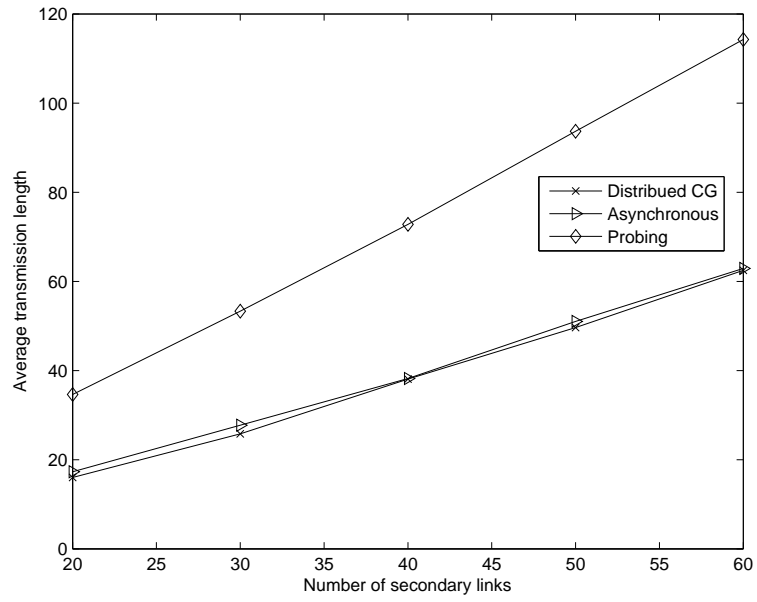


Figure 5.5. Comparison with other distributed schemes in terms of average transmission length.

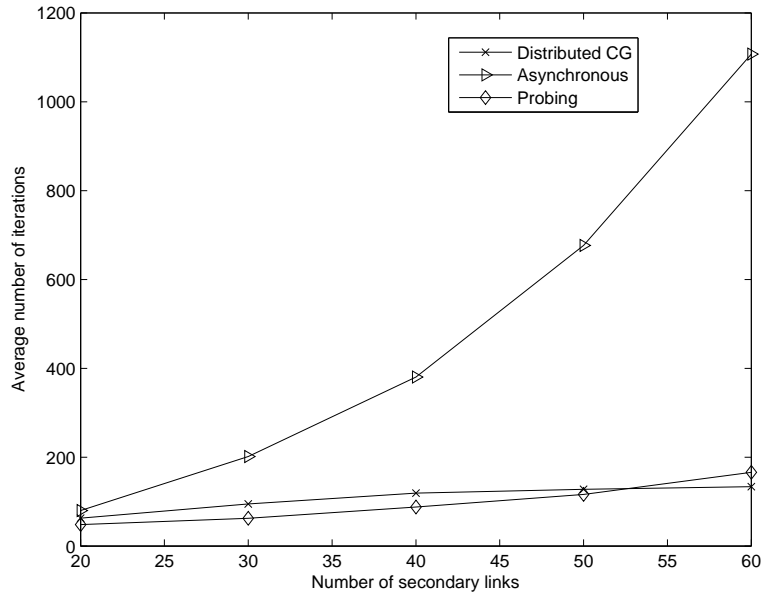


Figure 5.6. Comparison with other distributed schemes in terms of average number of iterations.

tributed algorithms to solve the pricing problem which are developed using the concepts in [117] (i.e., asynchronous power update) and [113] (i.e., interference probing). We set $\epsilon = 0.5$ and $\zeta^{(th)} = 0.1$. Fig. 5.5 shows the average transmission length of the robust schedules. The proposed algorithm can provide a transmission length lower than that for each of these two distributed algorithms. Although the transmission length obtained based on the concept in [117] is almost the same as that for the proposed algorithm, the average number of iterations required to find an access pattern is much higher than that for our proposed algorithm (Fig. 5.6). This shows that our proposed algorithm can converge to a fixed point solution much faster than the algorithm using asynchronous power update. The algorithm using the concept in [113] uses fewer number of iterations than the proposed algorithm when the number of secondary links is less than 53. However, it always provides a transmission length larger than that obtained from the proposed algorithm.

Also, in Fig. 5.7, we plot the power evolution of 10 secondary links during the first phase of solving the pricing problem. We observe that the power levels of secondary links asynchronously converge to fixed points within a small number of iterations. (e.g., 13 iterations in Fig. 5.7).

5.5.2.3 Validation of the Probabilistic Bound on the SINR Constraint Violation

We compare the bound on P^v with the probabilities calculated over 1000 Monte Carlo simulations. Fig. 5.8 shows the comparison between the bound on P^v and the simulation results with the variation of the robustness parameter, ϵ (i.e., the maximal deviation of relative channel gain). We set $\sigma = 1$. We observe that the simulation results are always upper-bounded by the analytical results. Moreover, the probability of SINR constraint violation decreases as ϵ increases. When ϵ increases, the system becomes more robust. However, the probability slowly decreases and maintains at the same level when $\epsilon > 0.3$. We also compare the analytical bounds and the simulation results by varying the standard deviation σ of log-normal shadowing (Fig. 5.9). We set $\epsilon = 0.5$. The bounds become tighter when $\sigma \leq 2.5$. Note that the SINR requirements at the primary receivers are never violated.

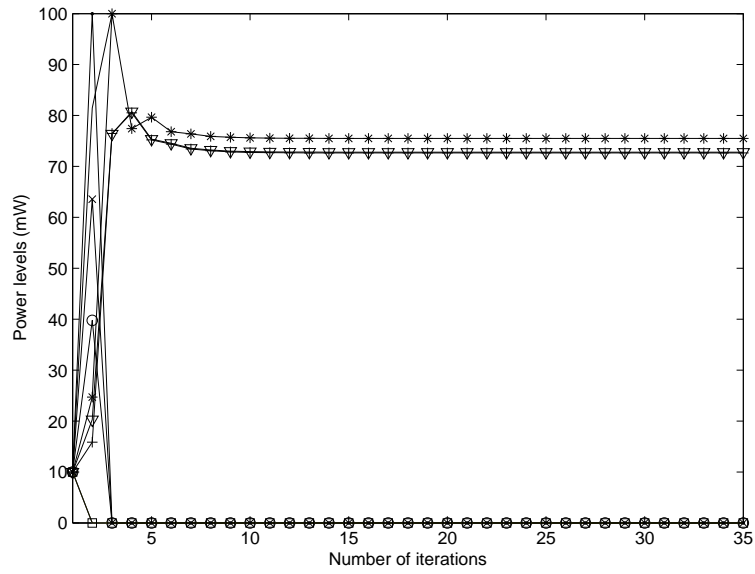


Figure 5.7. Power evolution of secondary links during the first phase for solving the pricing problem.

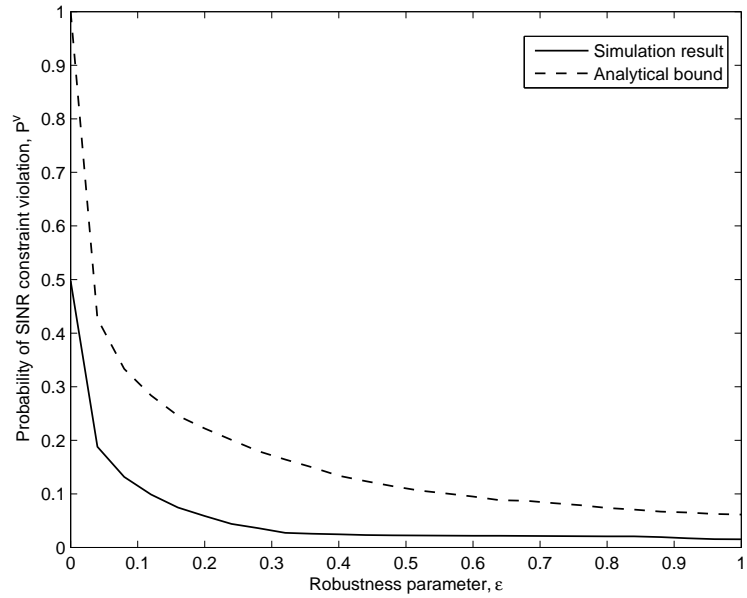


Figure 5.8. Comparison between the probabilistic bound on P^v and the simulation results with variation of ϵ .

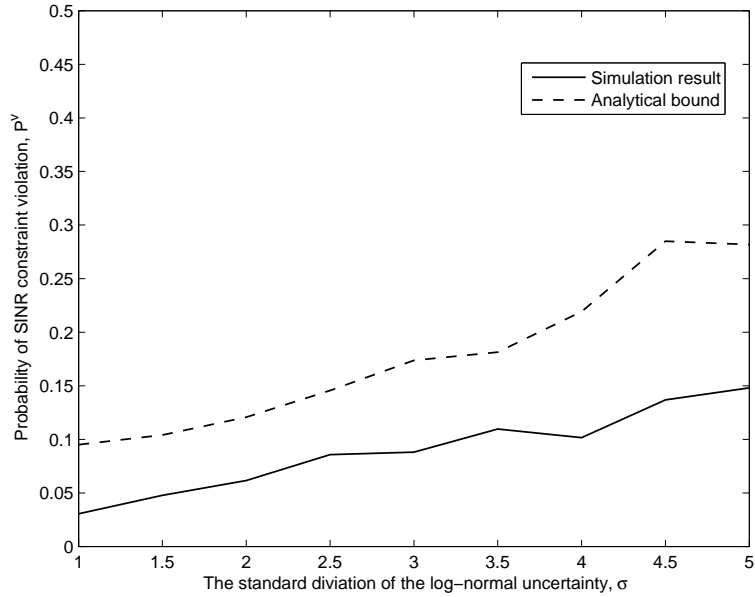


Figure 5.9. Comparison between the probabilistic bound on P^v and the simulation results with variation of σ .

5.5.2.4 Bound on the Expected Transmission Length

In Fig. 5.10, we compare the analytical bound on the expected transmission length with the simulation results obtained for 20 secondary links with $\sigma = 1$. We also show the initial transmission length which is obtained from the proposed algorithm. The initial transmission length increases as the robustness parameter ϵ increases. Note that the expected transmission length is the sum of the initial transmission length and the number of retransmissions due to the SINR constraint violation. We observe that the bound becomes tighter when $\epsilon > 0.45$.

Moreover, we plot the expected total transmission length obtained from $\sum_{s \in \mathcal{S}} \frac{y_s}{1 - \omega_s}$, where ω_s is the average value of P_s^v . The trends of variations in the analytical results on expected transmission length match well with the simulation results (Fig. 5.11). Moreover, we observe a convex shape of the expected total transmission length with the minimum value at $\epsilon = 0.15$ when the number of secondary links is equal to 20 and $\sigma = 1$, and at $\epsilon = 0.35$ when the number of secondary links is equal to 10 and $\sigma = 2$. This is due to the fact that the initial transmission length increases with increasing

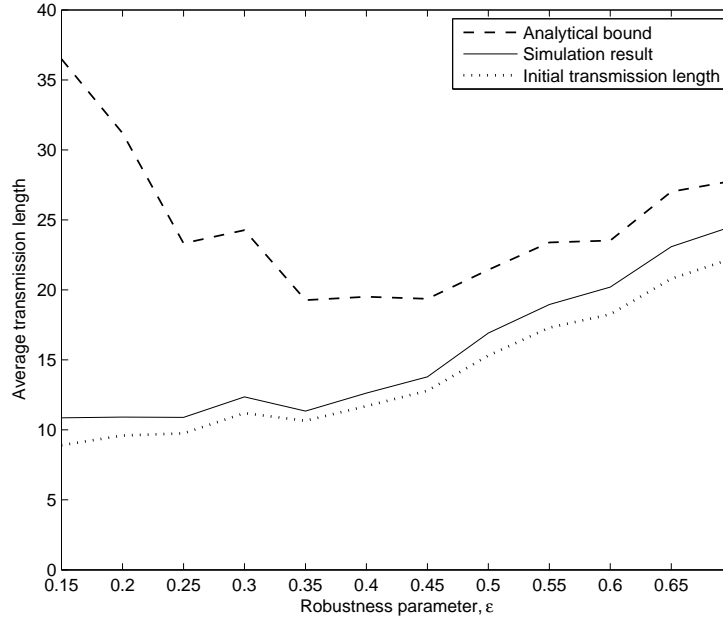


Figure 5.10. Bound on the expected transmission length and the simulation results.

ϵ and the number of retransmissions due to SINR constraint violation decreases with increasing ϵ . Therefore, we can use this analytical model as a guideline for choosing the optimal (or desired) value of the robustness parameter.

5.6 Conclusion

We have developed a framework for robust scheduling and power control for cognitive radios in an ad-hoc STDMA network. Our design objective is to minimize the transmission length of the secondary links under their QoS requirements without violating the interference constraints of primary links under channel gain uncertainty. We have approximated the uncertainty set with ellipsoid. The upper-bounds on the probability of SINR constraint violation and the expected transmission length have been obtained. The analytical results can provide guidelines for choosing the optimal robustness parameter. We have also proposed a near-optimal distributed algorithm based on the distributed column generation method. The algorithm is divided into two stages for solving the restricted master problem and the pricing problem. Our

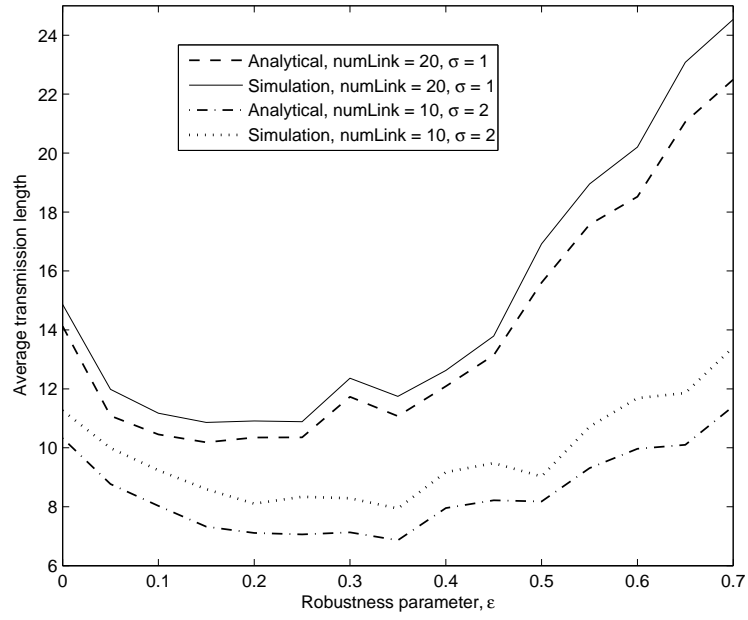


Figure 5.11. Variation in the expected transmission length and the simulation results.

algorithm is based on local information at each secondary link and local message exchanges. Also, the degree of conservatism in scheduling and power control is controllable. Simulation results have shown that the proposed algorithm can achieve the number of transmission length close to the centralized heuristic algorithm with reasonable complexity.

Chapter 6

Summary and Discussions

With ever increasing demands for ubiquitous wireless services, spectrum sharing has become a key concept to improve efficient spectrum utilization and overall network throughput. However, one major challenge in spectrum sharing is efficient control of interference specifically in healthcare environments with EMI-sensitive medical devices. In addition, resource allocation has to be performed to satisfy the QoS requirements of wireless users. This thesis presents a set of alternative solutions to address these challenges for efficient wireless access especially in eHealth services. Our results show that the proposed solutions can provide promising spectrum utilization, overall network throughput and robustness to channel gain uncertainty by guaranteeing QoS of secondary users (i.e., eHealth applications) under controlled interference to primary users (i.e., medical devices) with low computational complexity.

We summarize the contributions of this thesis (in Section 6.1) and then point out the future research directions (in Section 6.2).

6.1 Summary of Contributions

Chapter 2: EMI-Aware Prioritized Wireless Access Scheme for a Single Service Cell

- We have proposed an EMI-aware prioritized wireless access scheme to handle dynamic wireless access in a single eHealth service cell. An EMI-aware RTS/CTS protocol with a prioritized channel access scheme has been developed to jointly address the issues of EMI to medical devices and QoS provisioning to different eHealth applications. The EMI issues can be avoided by admission and power

control mechanisms during RTS/CTS process in the common control channel while the prioritized channel access can provide different QoS guarantees to different eHealth applications over the data channel.

- Based on the proposed scheme, we have developed a discrete-time Markov queuing model to analyze the performance of the proposed access scheme including the average transmission delay of high-priority users and the loss probability of low-priority users. The analytical model is further used to determine the optimal system parameters (i.e., blocking probabilities) that maximize the system throughput (in terms of the number of users who can successfully transmit their data) while satisfying the QoS requirements of eHealth applications.
- To enhance the adaptability of the proposed protocol, we have proposed an exponential moving average (EMA) prediction model to obtain the one-step-ahead values of the blocking probability. This prediction model is based on the current system parameters (i.e., number of users in the network, channel access pattern, and the presence of EMI-sensitive medical devices). Consequently, the proposed scheme can adaptively tune the blocking probability to avoid the congestion under high-load network and increase the throughput under light-load network.
- Our results show that the proposed solution can protect bio-medical devices from the harmful interference and achieve service differentiation among different eHealth applications. Moreover, the system throughput can be maximized with the optimal blocking probability obtained from the queuing model while QoS requirements of eHealth applications (i.e., delay and loss probability) can be satisfied. Finally, the proposed EMA model can accurately predict the blocking probability for adaptive performance tuning while guaranteeing QoS.

Chapter 3: EMI-Aware Transmission Scheduling and Power Control for Multiple Service Cells

- For multiple service cells, we have considered the multiple STDMA infrastructure-based wireless networks with multiple channels where multiple cells (but only one user in each cell) can transmit at the same time as long as the interference is below a limit. We have formulated joint transmission scheduling and power

control problem to maximize spectrum utilization and minimize the power consumption of secondary users while protecting the medical devices from harmful interference and guaranteeing performance of secondary users. An optimal solution includes the optimal schedules, optimal channel allocations, and optimal transmit powers of secondary users in each time slot.

- Due to high complexity of the problem, we have proposed two heuristic algorithms based on greedy methods to solve the problem. The former algorithm schedules the users with minimum transmit power in each channel based on the sequence of time slots in a frame subject to interference constraints and QoS requirements. The latter algorithm enhances the performance of the former one by finding the optimal sequence of secondary users that should be scheduled. The optimal sequence relies on the amount of the interference from a secondary user to medical devices. The users who have the higher interference levels will be first scheduled.
- Through extensive simulations, the spectrum utilization, power consumption, and the complexity of the proposed algorithms compared to a random scheduling scheme and an exhaustive search for optimal solutions are illustrated for various network settings. Moreover, the EMI levels at primary and protected users have been investigated.

Chapter 4: Robust Scheduling and Power Control for an Ad-Hoc STDMA Wireless Network

- We have addressed the robust scheduling and power control problem in the context of an ad-hoc STDMA network. The problem has been formulated as a mixed-integer programming (MIP) aimed at minimizing the transmission length in term of the number of time slots of secondary users subject to interference constraints of primary users and QoS requirements of secondary users. Considering the channel gain uncertainty, we have considered the worst-case scenario in modeling the channel gain uncertainty due to shadowing, which is assumed to follow a log-normal distribution and then obtained the chance constraint for the traffic demand uncertainty of secondary users.
- To efficiently solve the problem, we have proposed a stabilized column gener-

ation method based on perturbation and exact penalty methods to solve the convergence problem in the classical column generation method. This approach can stabilize and accelerate the column generation process by guiding the dual variables. We have further proposed an efficient heuristic algorithm, namely, the Weighted Interference Criterion Greedy (WICG) algorithm, for solving the pricing problem in the stabilized column generation approach. The proposed WICG algorithm takes into account the integration of the relative interference level and the dual optimal solutions obtained from the restricted master problem.

- Through simulations, the WICG algorithm can provide efficient solutions enhancing the current optimal solution in the master problem with very low penalty (i.e., additional required time slots when compared to the optimal solution) with much lower computation time. With integration of WICG algorithm, average number of iterations and average transmission length of the proposed stabilized column generation method compared with the classical column generation method have been further investigated. Finally, the robustness of the proposed scheme has been illustrated in terms of the average transmission length and the probability of secondary traffic demand violation for various robustness parameter settings.

Chapter 5: Distributed Robust Scheduling and Power Control for an Ad-Hoc Cognitive STDMA Network

- We have formulated the robust scheduling and power control for vertical spectrum sharing in a distributed network model. To achieve the robustness, an ellipsoid is used to model the uncertainty.
- We have then proposed a novel distributed algorithm based on distributed column generation method for solving the problem with cooperation of the primary network. The proposed algorithm can solve the problem without the need of a dedicated controller by using a message-passing model where secondary transmitters measure their local information, exchange the information among each other and receive interference notifications from the primary receivers. Furthermore, an efficient two-phase algorithm has been introduced for solving the

pricing problem (i.e., finding a feasible access pattern) in a distributed way. A feasible access pattern can be distributively obtained from local SINR measurement, distributed power updates, and interference notifications from primary receivers.

- Based on the proposed scheme, we have derived the bound on the probability of SINR constraint violation and the bound on expected transmission length. The bounds can be obtained by considering the channel gain uncertainty due to shadowing, which is assumed to follow a log-normal distribution. The analytical results can provide guidelines for choosing the optimal robustness parameter.
- Through simulations, we have illustrated average transmission length and complexity of our proposed algorithm compared with the centralized heuristic algorithm in Chapter 4 and with two existing distributed algorithms in [117] (i.e., asynchronous power update) and [113] (i.e., interference probing) to solve the pricing problem for various network settings. The analytical bounds have been also validated through simulations.

6.2 Future Work

We have developed dynamic wireless access methods for both infrastructure and ad-hoc wireless networks. Joint scheduling and power control algorithms have been proposed to address the problems of dynamic spectrum access. However, there are avenues for further research to tackle these problems. Several extensions of the presented research in this thesis are outlined below.

- **Robustness in dynamic spectrum access:** The robust formulations in Chapter 4 and Chapter 5 have considered channel gain uncertainty. In practice, other system information (e.g., number of users, SINR measurement) is typically inaccurate, time-varying, or uncertain. These uncertainties could mainly lead to poor or even infeasible solutions to the realization. The proposed framework thus can be extended to the scenarios where other uncertainties need also to be taken into account.
- **Adaptive transmission rate:** In our proposed scheme, we have fixed the transmission rate for each secondary link to the same rate for every time slot.

Alternatively, the secondary links, which have sufficiently high SINR would be able to transmit with higher transmission rates. The transmission length could then be reduced. Therefore, dynamic spectrum access with adaptive transmission rate in secondary links is one of interesting directions for future investigation.

- **Orthogonal frequency-division multiplexing (OFDM) technology:**

STDMA-based spectrum sharing has been considered in this thesis. Nevertheless, the use of orthogonal frequency-division multiplexing (OFDM) technology will be common in the next-generation wireless networks. Transmission scheduling schemes in OFDM wireless networks need to consider spectrum access not only in the time domain but also in the frequency domain. Therefore, the newly-developed wireless access methods for OFDM technology need to take into account the problem of subcarrier assignment in addition to the joint problem of transmission scheduling and power control. The research work in this thesis can be extended for OFDM-based wireless networks.

Bibliography

- [1] L. Czekierda, J. Danda, K. Loziak, M. Sikora, et.al, “Information Technology Solutions for Healthcare,” *Springer*, pp. 85–109, October 29 2007.
- [2] U. Varshney, “Pervasive Healthcare and Wireless Health Monitoring,” *Springer Science + Business Media*, July 12 2007.
- [3] H. Furuhashi, “Electromagnetic interferences of electric medical equipment from hand-held radiocommunication equipment,” *International Symposium on Electromagnetic Compatibility*, pp. 468–471, 1999.
- [4] A. Soomro and D. Cavalcanti, “Opportunities and challenges in using WPAN and WLAN technologies in medical environments,” *IEEE Communications Magazine*, vol. 45, no. 2, pp. 114–122, February 2007.
- [5] P. Hertz, “Complete Wireless Home Network,” *Prentice Hall*, The United States of America, Chapter 4, pp. 30-32, 2003
- [6] J. Mitola, III and G. Q. Maguire, Jr., “Cognitive Radio: Making Software Radios More Personal,” *IEEE Personal Communications Magazine*, vol. 6, no. 4, pp. 13-18, August 1999.
- [7] J. Mitola, III, “Cognitive Radio: An Integrated Agent Architecture for Software Defined Radio,” Thesis (PhD), Dept. of Teleinformatics, Royal Institute of Technology (KTH), Stockholm Sweden, May 2000.
- [8] J. I. Mitola, “Cognitive Radio for Flexible Mobile Multimedia Communications,” in Proc. of *IEEE International Workshop on Mobile Multimedia Communications, MoMuC '99*, San Diego CA, USA, 15-17 November 1999.
- [9] E. Hossain, L. Le, N. Devroye, and M. Vu, “Cognitive radio: From theory to practical network engineering,” invited chapter in *Advances in Wireless Communications*, (Ed. V. Tarokh), Springer, pp. 251–289, 2009.
- [10] Department of Commerce of Washington D.C., “Radio Frequency Identification: Opportunities and Challenges in Implementation,” April 2005.
- [11] Radio Spectrum Policy and Planning Resources and Networks Branch of Ministry of Economic Development of New Zealand, “Radio Frequency Identification Devices,” *An Engineering Discussion Paper on Spectrum Allocations for Short Range Devices*, pp. 14–17, August 2004.
- [12] W. C. Y. Lee, “Wireless & Cellular Telecommunications—Third Edition,” *The*

- McGraw-Hill Companies*, The United States of America, pp. 1–5, 110–130, 175–181, 187–196, 2006.
- [13] W. C. Y. Lee, “Mobile Communications Engineering—Second Edition,” *The McGraw-Hill Companies*, The United States of America, pp. 7–11, 1997.
- [14] IEEE 802.11, “Wireless LAN Medium Access Control (MAC) and Physical Layer (PHY) Specification,” 2007.
- [15] <http://www.bluetooth.com>, Last accessed: October 15, 2008.
- [16] IEEE 802.15.3, “Wireless Medium Access Control (MAC) and Physical Layer (PHY) Specs for High Rate Wireless Personal Area Networks (WPAN),” 2007.
- [17] IEEE 802.15.4, “Wireless Medium Access Control (MAC) and Physical Layer (PHY) specifications for Low-Rate Wireless Personal Area Networks (LR-WPANs),” 2006.
- [18] <http://ieee802.org/15/>, Last accessed: June 28, 2008.
- [19] <http://wireless.fcc.gov/services>, Last accessed: August 13, 2008.
- [20] Health Canada, “Recent Changes to US FCC Rules in the 460-470 MHz Band may affect Canadian Wireless Medical Telemetry Systems Located Near the US Border,” .
- [21] A. F. Graves, B. Wallace, S. Periyalwar, and C. Riccardi, “Clinical Grade - A Foundation for Healthcare Communications Networks,” in *Proceedings of 5th International Workshop on Design of Reliable Communication Networks (DRCN 2005)*, October 16-19, 2005.
- [22] IBM, “Wireless Healthcare Delivery: Adapting to Tomorrow’s Needs with Mobile Processes,” , January 2007.
- [23] B. W. Podaima and R. D. McLeod, “Point of Care Engineering and Technology,” in *Proceedings of CMBEC29*, Vancouver, BC, Canada, June 1-3, 2006.
- [24] H. Ren et al., “System Architecture of a Body Area Network and Its Web Service Based Data Publishing,” *Advanced Web and Network Technologies, and Applications*, vol. 3842, pp. 947-954, December 2005.
- [25] <http://www.welchallyn.com> Last accessed: September 8, 2008.
- [26] U. Varshney, “Pervasive Healthcare,” *Computer*, vol. 36, no. 12, pp. 138-140, December 2003.
- [27] G. Anogianakis et al., “Medical emergency aid through telematics: design, implementation guidelines and analysis of user requirements for the MERMAID project,” *International Journal of Medical Informatics*, vol. 52, issue 1, pp. 93–103, October 1999.
- [28] P. Campbell et al., “Prehospital triage of acute myocardial infarction: wireless

- transmission of electrocardiograms to the on-call cardiologist via a handheld computer,” *Journal of Electrocardiology*, vol. 38, issue 4, pp. 300-309, October 2005.
- [29] P. Fuhrer and D. Guinard, “Building a smart hospital using RFID technologies,” in *Proceedings of 1st European Conference on eHealth (ECEH06)*, Fribourg, Switzerland, pp. 1–14, Oct. 12-13, 2006.
- [30] E. Jovanov, A. Milenkovic, C. Otto, and P. C. de Groen, “A Wireless Body Area Network of Intelligent Motion Sensors for Computer Assisted Physical Rehabilitation,” *Journal of NeuroEngineering and Rehabilitation*, Vol. 2, No. 6, pp. 6–16, March 2005.
- [31] <http://www.nihonkohden.com/>, Last accessed: June 15, 2008.
- [32] <http://www.gehealthcare.com/auen/index.html>, Last accessed: June 15, 2008.
- [33] <http://www.datascope.com/ca/products.html>, Last accessed: June 15, 2008.
- [34] R. Railton, G.D. Currie, G.A. Corner, and A.L. Evans, “Malfunction of Medical Equipment as a Result of Main Borne Interference,” in *Proceedings of Eighth International Conference on Electromagnetic Compatibility, 1992*, pp. 49–53, September 21-24, 1992.
- [35] Federal Communications Commission, Office of Engineering and Technology (OET), “Questions and Answers About the Biological Effects and Potential Hazards of Radiofrequency Electromagnetic Fields,” August 1999.
- [36] L. Marchildon, “Quantum Mechanics,” *Springer*, Germany, pp. 4–6, 2002.
- [37] U.S. Department of Health and Human Services, Food and Drug Administration, Center for Devices and Radiological Health, “Draft Guidance for Industry and FDA Staff: Radio-Frequency Wireless Technology in Medical Devices,” January 3 2007.
- [38] World Health Organization (WHO), “Establishing a Dialogue on Risks from Electromagnetic Fields,” October 2002.
- [39] G. Berg et al., “Occupational Exposure to Radio Frequency/Microwave Radiation and the Risk of Brain Tumors: Interphone Study Group, Germany,” *American Journal of Epidemiology Advance Access*, July 27, 2006.
- [40] <http://www.fcc.gov/cgb/cellular.html>.
- [41] J. C. Lin, “Health aspects of wireless communication: a real and present wireless danger,” *ACM SIGMOBILE Mobile Computing and Communications Review*, vol. 4 , issue 1, pp. 17–18, January 2000.
- [42] D. Small, “Mobile Phones Should not be Used in Clinical Areas or Within a Metre of Medical Equipment in Hospitals,” *Evidence-Based Healthcare and Public health*, Volume 9, Issue 2, pp. 114–116., December 2005.
- [43] International Electrotechnical Commission, “National Standard of Canada

- CAN/CSA - C22.2 No. 60601-1-2:03 (IEC 60601-1-2:2001) Medical electrical equipment - Part 1-2: General Requirements for Safety - Collateral Standard: Electromagnetic Compatibility - Requirements and Tests", 2003.
- [44] "IEC 61000-4-2: Electromagnetic compatibility (EMC)- Part 4-2: Testing and measurement techniques - Electrostatic discharge immunity test", 2001.
- [45] "IEC 61000-4-3: Electromagnetic compatibility (EMC) - Part 4-3: Testing and measurement techniques - Radiated, radio-frequency, electromagnetic field immunity test", 2008.
- [46] "IEC 61000-4-4: Electromagnetic compatibility (EMC) - Part 4-4: Testing and measurement techniques - Electrical fast transient/burst immunity test", 2004.
- [47] "IEC 61000-4-5: Electromagnetic compatibility (EMC) - Part 4-5: Testing and measurement techniques - Surge immunity test", 2005.
- [48] "IEC 61000-4-6: Electromagnetic compatibility (EMC) - Part 4-6: Testing and measurement techniques - Immunity to conducted disturbances, induced by radio-frequency fields", 2006.
- [49] "IEC 61000-4-11: Electromagnetic compatibility (EMC) - Part 4-11: Testing and measurement techniques - Voltage dips, short interruptions and voltage variations immunity tests", 2004.
- [50] "IEC 61000-4-8: Electromagnetic compatibility (EMC) - Part 4-8: Testing and measurement techniques - Power frequency magnetic field immunity test", 2001.
- [51] D. Modi, "IEC 601-1-2 and its Impact on Medical Device Manufacturers," in *Proceedings of 19th International Conference - IEEE/EMBS*, Chicago, IL. USA, October 30 - November 2, 1997.
- [52] "Radiofrequency Interference with Medical Devices," *IEEE Engineering in Medicine and Biology Magazine* 17(3), pp. 111-114, 1998.
- [53] Federal Communications Commission, Office of Engineering and Technology (OET), "Evaluating Compliance with FCC Guidelines for Human Exposure to Radiofrequency Electromagnetic Fields," November 1997.
- [54] S. D. Baker and D. H. Hoglund, "Medical-grade, mission-critical wireless networks," *IEEE Engineering in Medicine and Biology Magazine*, pp. 86-95, March/April 2008.
- [55] F. Guo and F. Chiueh, "Software TDMA for VoIP applications over IEEE 802.11 wireless LAN," in *Proceedings of 26th IEEE International Conference on Computer Communications INFOCOM 2007*, pp. 2366-2370, May 6-12, 2007.
- [56] S. Hagihira et. al., "Infrared transmission of electronic information via LAN in the operating room," *Journal of Clinical Monitoring and Computing*, vol. 16, no. 3, pp. 171-175, February 2000.

- [57] H. Hong, Y. Ren, and C. Wang “Information illuminating system for healthcare institution,” in *Proceedings of International Conference on Bioinformatics and Biomedical Engineering*, pp. 801–804, May 16-18, 2008.
- [58] K.-J. Park, D. M. Shrestha, Y.-B. Ko, N. H. Vaidya, and L. Sha, “IEEE 802.11 WLAN for medical-grade QoS,” in *Proceedings of the First ACM International Workshop on Medical-grade Wireless Networks, co-located with ACM MobiHoc 2009*, pp. 3–8, Louisiana, USA, May 18, 2009.
- [59] S. Jiang, Y. Xue, A. Giani, and R. Bajcsy, “Providing QoS support for wireless Remote Healthcare System,” in *Proceedings of IEEE International Conference on Multimedia and Expo, 2009*, pp. 1692–1695, June 28-July 3, 2009.
- [60] T. S. Rappaport, *Wireless Communications*, Prentice Hall, New Jersey, pp. 123–133, 1996.
- [61] G. Bianchi, L. Fratta, and M. Oliveri, “Performance evaluation and enhancement of the CSMA/CA MAC protocol for 802.11 wireless LAN’s,” in *Proceedings of IEEE International Symposium on Personal, Indoor and Mobile Radio Communications (PIMRC)*, pp. 392–396, October 1996.
- [62] G. Bianchi, “Performance analysis of the IEEE 802.11 distributed coordinationfunction,” *IEEE Journal on Select Areas in Communications*, vol. 18, no. 3, pp. 535–547, March 2000.
- [63] G. Bolch, S. Greiner, H. de Meer, and K. S. Trivedi, *Queueing Networks and Markov Chains: Modeling and Performance Evaluation With Computer Science Applications*, Wiley-Interscience, August 2006.
- [64] T-H Lee, A. Marshall, and B. Zhou, “A QoS-based rate adaptation strategy for IEEE a/b/g PHY schemes using IEEE 802.11e in ad-hoc networks,” in *Proceedings of International conference on Networking and Services 2006*, Silicon Valley, CA, pp. 113–118, July 16-18, 2006.
- [65] S. B. Schoenbeck and G. D. Hocutt, “Near-death experiences in patients undergoing cardiopulmonary resuscitation,” *Journal of Near-Death Studies*, vol. 9, no. 4, pp. 211–218, June, 1991.
- [66] American Heart Association, “How your cardiologist diagnoses heart defects,” www.americanheart.org, May 19, 2009, Available Online.
- [67] Cisco, “Cisco Aironet 802.11a/b/g Wireless LAN Client Adapters (CB21AG and PI21AG) Installation and Configuration Guide,”.
- [68] G. J. M. Janssen, and R. Prasad, “Propagation measurements in an indoor radio environment at 2.4 GHz, 4.75 GHz and 11.5 GHz,” in *Proceedings of IEEE Vehicular Technology Conference (VTC)*, pp. 617–620, May 1992.
- [69] M. F. A. Rasid and B. Woodward, “Bluetooth telemedicine Processor for multi-channel biomedical signal transmission via mobile cellular networks,” *IEEE Trans-*

- actions on Information Technology in Biomedicine*, vol. 9, issue 1, pp. 35–43, March 2005.
- [70] <http://madwifi-project.org/>.
- [71] R. S. H. Istepanian and N. Y. Philip, “Healthcare-inspired cognitive radio,” in *Proceedings of IET Conference on Assisted Living 2009*, London, UK, Mar. 24–25 2009, pp. 12.
- [72] R. Patra, S. Surana, S. Nedeveschi, and E. Brewer, “Optimal scheduling and power control for TDMA based point to multipoint wireless networks,” in *Proceedings of Second ACM SIGCOMM Workshop on Networked Systems for Developing Regions*, Seattle, WA, USA, 2008, pp. 7–12.
- [73] T. ElBatt and A. Ephremides, “Joint scheduling and power control for wireless ad-hoc networks,” in *Proceedings of IEEE INFOCOM 2002*, vol. 2, Nov. 7, 2002, pp. 976–984.
- [74] D. Li, X. Dai, and H. Zhang, “Cross-layer scheduling and power control in cognitive radio networks,” in *Proceedings of International Conference on Wireless Communications, Networking and Mobile Computing, 2008*, Dalian, China, 2008, Oct. 12-14, 2008, pp. 1–3.
- [75] W. Zhu, “TDMA frame synchronization of mobile stations using a radio clock signal for short range communication,” in *Proceedings of the 1994 IEEE 44th Vehicular Technology Conference*, vol. 3, Jun 1994, pp. 1878–1882.
- [76] F. Wang, P. Zeng, and H. Yu, “Slot time synchronization for TDMA-based ad hoc networks,” in *Proceedings of International Symposium on Computer Science and Computational Technology, 2008*, Dec. 20-22, 2008, pp. 544–548.
- [77] O. Goussevskaja, Y. A. Oswald, and R. Wattenhofer, “Complexity in geometric SINR,” in *Proceedings of Mobihoc 2007*, Montreal, QC, Canada, pp. 100–109.
- [78] G. Foschini and Z. Miljanic, “A simple distributed autonomous power control algorithm and its convergence,” *IEEE Transactions on Vehicular Technology*, vol. 42, no. 4, pp. 641–646, Nov. 1993.
- [79] T. ElBatt and A. Ephremides, “Joint scheduling and power control for wireless ad hoc networks,” *IEEE Trans. Wireless Commun.*, vol. 3, no. 1, pp. 74–85, Jan. 2004.
- [80] S. A. Borbash and A. Ephremides, “Wireless link scheduling with power control and SINR constraints,” *IEEE Trans. Information Theory*, vol. 52, no. 11, pp. 5106–5111, Nov. 2006.
- [81] J. Tang, G. L. Xue, C. Chandler, and W. Zhang, “Link scheduling with power control for throughput enhancement in multihop wireless networks,” *IEEE Trans. Veh. Technol.*, vol. 55, no. 3, pp. 733–742, May. 2006.

- [82] L. Fu, S. C. Liew, and J. Huang, "Fast algorithms for joint power control and scheduling in wireless networks," *IEEE Trans. Wireless Commun.*, vol. 9, no. 3, pp. 1186–1197, Mar. 2010.
- [83] J. Luo, C. Rosenberg, and A. Girard, "Engineering wireless mesh networks: Joint scheduling, routing, power control, and rate adaptation," *IEEE/ACM Trans. Netw.*, vol. 18, no. 5, pp. 1387–1400, Oct. 2010.
- [84] M. Johansson and L. Xiao, "Cross-layer optimization of wireless networks using nonlinear column generation," *IEEE Trans. Wireless Commun.*, vol. 5, no. 2, pp. 435–445, Feb. 2006.
- [85] J. Zhang, Z. Zhang, H. Luo, and A. Huang, "A column generation approach for spectrum allocation in cognitive wireless mesh network," in *Proc. IEEE GLOBECOM*, New Orleans, LO, USA, pp. 1–5, 2008.
- [86] K. Yang and X. Wang, "Cross-layer network planning for multi-radio multi-channel cognitive wireless networks," *IEEE Trans. Commun.*, vol. 56, no. 10, pp. 1705–1714, Oct. 2008.
- [87] M. Luebbecke and J. Desrosiers, "Selected topics in column generation," *Operations Research*, vol. 53, pp. 1007–1023, 2005.
- [88] O. D. Merle, D. Villeneuve, J. Desrosiers, and P. Hansen, "Stabilized column generation," *Discrete Mathematics*, vol. 194, pp. 229–237, 1997.
- [89] J. Zander, "Performance of optimum transmitter power control in cellular radio systems," *IEEE Trans. Veh. Technol.*, vol. 41, no. 1, pp. 57–62, Feb. 1992.
- [90] R. D. Yates, "A framework for uplink power control in cellular radio systems," *IEEE J. Sel. Areas Commun.*, vol. 13, no. 7, pp. 1341–1347, Sept. 1995.
- [91] N. Bambos, S. C. Chen, and G. J. Pottie, "Channel access algorithms with active link protection for wireless communication networks with power control," *IEEE/ACM Trans. Networking*, vol. 8, no. 5, pp. 583–597, Oct. 2000.
- [92] C. U. Saraydar, N. B. Mandayam, and D. J. Goodman, "Efficient power control via pricing in wireless data networks," *IEEE Trans. Commun.*, vol. 50, no. 2, pp. 291–303, Feb. 2002.
- [93] M. Xiao, N. B. Shroff, and E. K. P. Chong, "A utility-based power control scheme in wireless cellular systems," *IEEE/ACM Trans. Netw.*, vol. 11, no. 2, pp. 210–221, Apr. 2003.
- [94] M. Rasti, A. R. Sharafat, and B. Seyfe, "Pareto-efficient and goal-driven power control in wireless networks: A game-theoretic approach with a novel pricing scheme," *IEEE/ACM Trans. Netw.*, vol. 17, no. 2, pp. 556–569, April 2009.
- [95] A. T. Hoang and Y. C. Liang, "Downlink channel assignment and power control

- for cognitive radio networks,” *IEEE Trans. Wireless Commun.*, vol. 7, no. 8, Aug. 2008.
- [96] A. T. Hoang, Y.-C. Liang, and M. H. Islam, “Power control and channel allocation in cognitive radio networks with primary users cooperation,” *IEEE Trans. Mob. Comput.*, vol. 9, no. 3, March 2010, pp. 348–360.
- [97] T. Shu and M. Krunz, “Exploiting microscopic spectrum opportunities in cognitive radio networks via coordinated channel access,” *IEEE Trans. Mob. Comput.*, vol. 9, no. 11, Nov. 2010, pp. 1522–1534.
- [98] L. Gao and S. Cui, “Power and rate control for delay-constrained cognitive radios via dynamic programming,” *IEEE Trans. Veh. Technol.*, vol. 58, no. 9, pp. 4819–4827, Nov. 2009.
- [99] K. Yang, Y. Wu, J. Huang, X. Wang, and S. Verdu, “Distributed robust optimization for communication networks,” in *Proc. IEEE INFOCOM’08*, Phoenix, AZ, USA, pp. 1157–1165, Apr. 13-18, 2008.
- [100] X. Meng, Z. Fu, and S. Lu, “Robust packet scheduling in wireless cellular networks,” *Mobile Networks and Applications*, vol. 9, no. 2, pp. 113–123, 2004.
- [101] K. Papadaki and V. Friderikos, “Robust scheduling in spatial reuse TDMA wireless networks,” *IEEE Trans. Wireless Commun.*, vol. 7, no. 12, pp. 4767–4771, 2008.
- [102] E. Karipidis, N. D. Sidiropoulos, and L. Tassiulas, “Joint QoS multicast power/admission control and base station assignment: A geometric programming approach,” in *Proc. IEEE Sensor Array and Multichannel Signal Processing Workshop*, Darmstadt, Germany, pp. 155–159, July 2008.
- [103] A. Behzad and I. Rubin “Optimum integrated link scheduling and power control for multihop wireless networks,” *IEEE Trans. Veh. Technol.*, vol. 56, no. 1, pp. 194–205, Jan. 2007.
- [104] P. Gilmore and R. Gomory, “A linear programming approach to the cutting stock problem,” *Operations Research*, vol. 9, no. 6, pp. 849–859, December 1961.
- [105] P. Gilmore and R. Gomory, “A linear programming approach to the cutting stock problem Part II,” *Operations Research*, vol. 11, no. 6, pp. 94–120, December 1963.
- [106] F.A. Potra and S.J. Wright, “Interior-Point Methods,” *Journal of Computational and Applied Mathematics*, 124(2000), pp. 281–302.
- [107] E. L. Lawler and D. E. Wood, “Branch-and-bound methods: A survey,” *Operations Research*, vol. 14, no. 4, pp. 699–719, 1966.
- [108] T. Coleman and Y. Li, “An interior, trust region approach for nonlinear mini-

- mization subject to bounds,” *SIAM Journal on Optimization*, vol. 6, pp. 418–445, 1996.
- [109] J. Löfberg, “YALMIP: A toolbox for modeling and optimization in MATLAB,” in *Proc. CACSD Conference 2004*, Taipei, Taiwan, pp. 284–289.
- [110] C. Stevenson, G. Chouinard, Z. Lei, W. Hu, S. Shellhammer, and W. Caldwell, “IEEE 802.22: The first cognitive radio wireless regional area network standard,” *IEEE Commun. Mag.*, vol. 47, no.1, pp. 130–138, Jan. 2009.
- [111] W. Hu, D. Willkomm, M. Abusubaih, J. Gross, G. Vlantis, M. Gerla, and A. Wolisz, “Cognitive radios for dynamic spectrum access—dynamic frequency hopping communities for efficient IEEE 802.22 operation,” *IEEE Commun. Mag.*, vol. 45, no. 5, pp. 80–87, May 2007.
- [112] M. Xiao, N. B. Shroff, and E. K. P. Chong, “Distributed admission control for power-controlled cellular wireless systems,” *IEEE Transactions on Networking*, vol. 9, issue 6, pp. 790–800, 2001.
- [113] C.-C. Chen and D.-S. Lee, “A joint design of distributed QoS scheduling and power control for wireless networks,” in *Proc. of INFOCOM 2006*, pp. 1–12.
- [114] K. Wang, C. F. Chiasserini, R. R. Rao, and J. G. Proakis, “A distributed joint scheduling and power control algorithm for multicasting in wireless ad hoc networks,” in *Proc. of ICC 2003*, vol. 1, pp. 725–731.
- [115] K. Wang, C. F. Chiasserini, J. G. Proakis, and R. R. Rao, “Distributed fair scheduling and power control in wireless ad hoc networks,” in *Proc. GLOBECOM 2004*, vol. 6, pp. 3556–3562.
- [116] S. H. R. Naqvi and L. M. Patnaik, “A distributed channel access protocol for ad hoc networks with feedback power control,” *IEEE Trans. on Mobile computing*, vol. 5, no. 10, pp. 1448–1459, 2006.
- [117] J. Tadrous, A. Sultan, and M. Nafie, “Admission and Power Control for Spectrum Sharing Cognitive Radio Networks,” *IEEE Trans. on Wireless Commun.*, vol.10, no.6, pp.1945-1955, June 2011
- [118] Y. Wu, K. Yang, J. Huang, X. Wang and M. Chiang, “Distributed Robust Optimization (DRO) Part II: Wireless Power Control,” submitted to *Journal of Optimization and Engineering*, Feb. 2010.
- [119] J. Singh (2006), “Variation-Aware Computer-Aided Design Techniques for VLSI digital Circuits,” (Doctoral dissertation), University of Minnesota, MN, USA, Retrieved from ProQuest Dissertations and Theses, (Accession Order No. AAI3234904), pp. 99–100.
- [120] A. Pascual-Iserte, D. P. Palomar, A. I. Perez-Neira, and M. A. Lagunas, “A robust maximin approach for MIMO communications with imperfect channel state

- information based on convex optimization,” *IEEE Trans. on Signal Processing*, vol. 54, no. 1, Jan. 2006, pp. 346–360.
- [121] S.A. Grandhi, J. Zander, and R. Yates, “Constrained power control,” *Wireless Personal Commun.*, vol.1, no. 4, pp. 257-270, 1995.

Table A.1. Events that can occur during an RTS time slot

Event	Probability
No change in the orbit and the RTS-CTS server is idle, $Prn(o_1, o_2)$	$(1-\alpha_1)^{n_1}(1-\alpha_2)^{n_2} [(1-\theta_1)^{o_1}(1-\theta_2)^{o_2} + \{z_1 - o_1\theta_1(1-\theta_1)^{o_1-1}\}(1-\theta_2)^{o_2} + (1-\theta_1)^{o_1}\{z_2 - o_2\theta_2(1-\theta_2)^{o_2-1}\} + z_1z_2]$
No change in the orbit and the RTS-CTS server serves for a high-priority user, $Prs1(o_1, o_2)$	$n_1\alpha_1(1-\alpha_1)^{n_1-1}(1-\alpha_2)^{n_2}(1-\theta_1)^{o_1}(1-\theta_2)^{o_2}$
No change in the orbit and the RTS-CTS server serves for a low-priority user, $Prs2(o_1, o_2)$	$n_2\alpha_2(1-\alpha_1)^{n_1}(1-\alpha_2)^{n_2-1}(1-\theta_1)^{o_1}(1-\theta_2)^{o_2}$
The number of high-priority users in the orbit is decreased by one and the RTS-CTS server serves for the high-priority user, $Prd1(o_1, o_2)$	$o_1\theta_1(1-\alpha_1)^{n_1}(1-\alpha_2)^{n_2}(1-\theta_1)^{o_1-1}(1-\theta_2)^{o_2}$
The number of low-priority users in the orbit is decreased by one and the RTS-CTS server serves for the low-priority user, $Prd2(o_1, o_2)$	$o_2\theta_2(1-\alpha_1)^{n_1}(1-\alpha_2)^{n_2}(1-\theta_1)^{o_1}(1-\theta_2)^{o_2-1}$
The number of high-priority users in the orbit is increased by x_1 and the RTS-CTS server is idle, $Pri1(o_1, o_2, x_1)$	$\binom{n_1}{x_1}\alpha_1^{x_1}(1-\alpha_1)^{n_1-x_1}(1-\alpha_2)^{n_2}[z_1+z_2-z_1z_2]$
The number of low-priority users in the orbit is increased by x_2 and the RTS-CTS server is idle, $Pri2(o_1, o_2, x_2)$	$\binom{n_2}{x_2}\alpha_2^{x_2}(1-\alpha_1)^{n_1}(1-\alpha_2)^{n_2-x_2}[z_1+z_2-z_1z_2]$
The number of high-priority and low-priority users in the orbits are increased by x_1 and x_2 , respectively and the RTS-CTS server is idle, $Pri12(o_1, o_2)$	$\binom{n_1}{x_1}\alpha_1^{x_1}(1-\alpha_1)^{n_1-x_1}\binom{n_2}{x_2}\alpha_2^{x_2}(1-\alpha_2)^{n_2-x_2}$

where

$$\mathbf{U1}_k^{(j)} = \begin{bmatrix} \mathbf{B}_{\mathbf{U1}_k^{(j)}} & \mathbf{C}_{\mathbf{U1}_k^{(j)}} & & & & & & & \\ \mathbf{A}_{0,\mathbf{U1}_k^{(j)}} & \mathbf{A}_{1,\mathbf{U1}_k^{(j)}} & \mathbf{A}_{2,\mathbf{U1}_k^{(j)}} & & & & & & \\ & \ddots & \ddots & \ddots & & & & & \\ & & \mathbf{A}_{0,\mathbf{U1}_k^{(j)}} & \mathbf{A}_{1,\mathbf{U1}_k^{(j)}} & \mathbf{A}_{2,\mathbf{U1}_k^{(j)}} & & & & \\ & & & \mathbf{A}_{0,\mathbf{U1}_k^{(j)}} & \mathbf{A}_{1,\mathbf{U1}_k^{(j)}} & \mathbf{A}_{2,\mathbf{U1}_k^{(j)}} & & & \\ & & & & \mathbf{A}_{0,\mathbf{U1}_k^{(j)}} & \mathbf{A}_{1,\mathbf{U1}_k^{(j)}} & & & \end{bmatrix} \quad (\text{A.2})$$

and

$$\mathbf{U2}_k^{(j)} = \begin{bmatrix} \mathbf{B}_{\mathbf{U2}_k^{(j)}} & & & & & & & & \\ \mathbf{A}_{0,\mathbf{U2}_k^{(j)}} & \mathbf{A}_{1,\mathbf{U2}_k^{(j)}} & & & & & & & \\ & \ddots & \ddots & & & & & & \\ & & \mathbf{A}_{0,\mathbf{U2}_k^{(j)}} & \mathbf{A}_{1,\mathbf{U2}_k^{(j)}} & & & & & \\ & & & \mathbf{A}_{0,\mathbf{U2}_k^{(j)}} & \mathbf{A}_{1,\mathbf{U2}_k^{(j)}} & & & & \\ & & & & \mathbf{A}_{0,\mathbf{U2}_k^{(j)}} & \mathbf{A}_{1,\mathbf{U2}_k^{(j)}} & & & \end{bmatrix}. \quad (\text{A.3})$$

Note that $\mathbf{U1B}_k^{(j)}$ captures the overflow of the low-priority users in the orbit which the structure is the same as $\mathbf{U1}_k^{(j)}$.

$$\mathbf{A}_{k,k} = \begin{bmatrix} \mathbf{V}_k^{(0,0)} & \mathbf{V}_k^{(0,1)} & \dots & \mathbf{V}_k^{(0,N-1)} & \mathbf{V}_k^{(0,N)} \\ \mathbf{V}_k^{(1,0)} & \mathbf{V}_k^{(1,1)} & \dots & \mathbf{V}_k^{(1,N-1)} & \mathbf{V}_k^{(1,N)} \\ \mathbf{0} & \mathbf{V}_k^{(2,1)} & \dots & \mathbf{V}_k^{(2,N-1)} & \mathbf{V}_k^{(2,N)} \\ \vdots & \vdots & \dots & \vdots & \vdots \\ \mathbf{0} & \mathbf{0} & \dots & \mathbf{V}_k^{(N,N-1)} & \mathbf{V}_k^{(N,N)} \end{bmatrix} \quad (\text{A.4})$$

where

$$\mathbf{V}_k^{(M)} = \begin{bmatrix} \mathbf{B}_{\mathbf{V}_k^{(M)}} & \mathbf{C}_{\mathbf{V}_k^{(M)}} & & & \\ \mathbf{A}_{0,\mathbf{V}_k^{(M)}} & \mathbf{A}_{1,\mathbf{V}_k^{(M)}} & \mathbf{A}_{2,\mathbf{V}_k^{(M)}} & & \\ & \ddots & \ddots & \ddots & \\ & & \mathbf{A}_{0,\mathbf{V}_k^{(M)}} & \mathbf{A}_{1,\mathbf{V}_k^{(M)}} & \mathbf{A}_{2,\mathbf{V}_k^{(M)}} \\ & & & \mathbf{A}_{0,\mathbf{V}_k^{(M)}} & \mathbf{A}_{1B,\mathbf{V}_k^{(M)}} \end{bmatrix} \quad (\text{A.5})$$

where $\mathbf{V}_k^{(M)} \in \{\mathbf{V}_k^{(j,j-1)}, \mathbf{V}_k^{(j,j)}, \mathbf{V}_k^{(j,j+x_2)}\}$ and $\mathbf{A}_{1B,\mathbf{V}_k^{(M)}}$ is used to capture the event that the transmission queue of high-priority users is full.

$$\mathbf{A}_{k,k+x_1} = \begin{bmatrix} \mathbf{W}_k^{(0,0)} & \mathbf{W}_k^{(0,1)} & \dots & \mathbf{W}_k^{(0,N-1)} & \mathbf{W}_k^{(0,N)} \\ \mathbf{W}_k^{(1,0)} & \mathbf{W}_k^{(1,1)} & \dots & \mathbf{W}_k^{(1,N-1)} & \mathbf{W}_k^{(1,N)} \\ \mathbf{0} & \mathbf{W}_k^{(2,1)} & \dots & \mathbf{W}_k^{(2,N-1)} & \mathbf{W}_k^{(2,N)} \\ \vdots & \vdots & \dots & \vdots & \vdots \\ \mathbf{0} & \mathbf{0} & \dots & \mathbf{W}_k^{(N,N-1)} & \mathbf{W}_k^{(N,N)} \end{bmatrix} \quad (\text{A.6})$$

where $\mathbf{W}_k^{(M)} \in \{\mathbf{W}_k^{(j,j-1)}, \mathbf{W}_k^{(j,j)}, \mathbf{W}_k^{(j,j+x_2)}\}$ and $\mathbf{W}_k^{(M)}$ has the same structure as $\mathbf{V}_k^{(M)}$.

Let each inner square matrix \mathbf{Q} represent the transition probabilities of going from one *level* to another, where *level* is defined as the number of transmission requests in the low-priority users' queue, where $Q \in \{\mathbf{B}_{\mathbf{U}2_k^{(j)}}, \mathbf{A}_{0,\mathbf{U}2_k^{(j)}}, \mathbf{A}_{1,\mathbf{U}2_k^{(j)}}\} \cup \{\mathbf{B}_{\mathbf{U}1_k^{(j)}}, \mathbf{C}_{\mathbf{U}1_k^{(j)}}, \mathbf{A}_{0,\mathbf{U}1_k^{(j)}}, \mathbf{A}_{1,\mathbf{U}1_k^{(j)}}, \mathbf{A}_{2,\mathbf{U}1_k^{(j)}}\} \cup \{\mathbf{B}_{\mathbf{U}1B^{(k,j)}}, \mathbf{C}_{\mathbf{U}1B^{(k,j)}}, \mathbf{A}_{0,\mathbf{U}1B^{(k,j)}}, \mathbf{A}_{1,\mathbf{U}1B^{(k,j)}}, \mathbf{A}_{2,\mathbf{U}1B^{(k,j)}}\} \cup \{\mathbf{B}_{\mathbf{V}_k^{(M)}}, \mathbf{C}_{\mathbf{V}_k^{(M)}}, \mathbf{A}_{0,\mathbf{V}_k^{(M)}}, \mathbf{A}_{1,\mathbf{V}_k^{(M)}}, \mathbf{A}_{2,\mathbf{V}_k^{(M)}}, \mathbf{A}_{1B,\mathbf{V}_k^{(M)}}\} \cup \{\mathbf{B}_{\mathbf{W}_k^{(M)}}, \mathbf{C}_{\mathbf{W}_k^{(M)}}, \mathbf{A}_{0,\mathbf{W}_k^{(M)}}, \mathbf{A}_{1,\mathbf{W}_k^{(M)}}, \mathbf{A}_{2,\mathbf{W}_k^{(M)}}, \mathbf{A}_{1B,\mathbf{W}_k^{(M)}}\}$. Matrix \mathbf{Q} is given as follows:

$$\mathbf{Q} = \begin{bmatrix} \mathbf{B}_Q & \mathbf{C}_Q & & & \\ \mathbf{A}_{0,Q} & \mathbf{A}_{1,Q} & \mathbf{A}_{2,Q} & & \\ & \ddots & \ddots & \ddots & \\ & & \mathbf{A}_{0,Q} & \mathbf{A}_{1,Q} & \mathbf{A}_{2,Q} \\ & & & \mathbf{A}_{0,Q} & \mathbf{A}_{1B,Q} \end{bmatrix}. \quad (\text{A.7})$$

The dimensions of \mathbf{B}_Q , \mathbf{C}_Q , $\mathbf{A}_{0,Q}$, $\mathbf{A}_{1,Q}$, $\mathbf{A}_{2,Q}$, and $\mathbf{A}_{1B,Q}$ in this matrix are 5×5 . $\mathbf{A}_{1B,Q}$ captures the events when the low-priority users' queue is full.

Table A.2. Elementary matrices of $\mathbf{U1}_k^{(j)}$

Matrix	$\mathbf{B}_{\mathbf{U1}_k^{(j)}}$	$\mathbf{C}_{\mathbf{U1}_k^{(j)}}$	$\mathbf{A}_{0,\mathbf{U1}_k^{(j)}}$	$\mathbf{A}_{1,\mathbf{U1}_k^{(j)}}$	$\mathbf{A}_{2,\mathbf{U1}_k^{(j)}}$
$\mathbf{B}_{\mathbf{Q}}$	$Prd1(k, j)\Phi$	$Prd1(k, j)P'_{d1}\tilde{\Phi}$	$Prd1(k, j)\beta_1\Phi$	$Prd1(k, j)\tilde{\Phi}$	$Prd1(k, j)\beta'_1P'_{d1}\tilde{\Phi}$
$\mathbf{C}_{\mathbf{Q}}$	$Prd1(k, j)P'_{d2}\bar{\Phi}$	$\mathbf{0}$	$Prd1(k, j)\beta_1P'_{d2}\bar{\Phi}$	$Prd1(k, j)\beta'_1P'_{d2}\bar{\Phi}$	$\mathbf{0}$
$\mathbf{A}_{0,\mathbf{Q}}$	$Prd1(k, j)\beta_2\Phi$	$Prd1(k, j)\beta_2P'_{d1}\tilde{\Phi}$	$\mathbf{0}$	$\mathbf{0}$	$\mathbf{0}$
$\mathbf{A}_{1,\mathbf{Q}}$	$Prd1(k, j)\hat{\Phi}$	$Prd1(k, j)\beta'_2P'_{d1}\tilde{\Phi}$	$Prd1(k, j)\beta_1\Phi$	$Prd1(k, j)\tilde{\Phi}$	$Prd1(k, j)\beta'_1P'_{d1}\tilde{\Phi}$
$\mathbf{A}_{2,\mathbf{Q}}$	$Prd1(k, j)\beta'_2P'_{d2}\bar{\Phi}$	$\mathbf{0}$	$Prd1(k, j)\beta_1P'_{d2}\bar{\Phi}$	$Prd1(k, j)\beta'_1P'_{d2}\bar{\Phi}$	$\mathbf{0}$
$\mathbf{A}_{1B,\mathbf{Q}}$	$Prd1(k, j)\hat{\Phi}$	$Prd1(k, j)\beta'_2P'_{d1}\tilde{\Phi}$	$Prd1(k, j)\beta_1\Phi$	$Prd1(k, j)\tilde{\Phi}$	$Prd1(k, j)\beta'_1P'_{d1}\tilde{\Phi}$

1. Description of Matrix $\mathbf{U1}_k^{(j)}$: The elements of matrix $\mathbf{U1}_k^{(j)}$ are given in Table A.2. Note that $\mathbf{0}$ is a zero square matrix with appropriate dimension. We define elementary matrices used to construct inner matrix \mathbf{Q} of matrix $\mathbf{U1}_k^{(j)}$ as follows. Let Φ be a square matrix whose second column is given by $[1, 0, 0, P_{d1}, P_{d2}]$. Similarly, let $\hat{\Phi}$ be a square matrix whose second column is given as $[\beta'_2, 0, 0, \beta'_2P_{d1}, \beta'_2P_{d2} + \beta_2P'_{d2}]$. $\tilde{\Phi}$ is a square matrix whose second column is given as $[\beta'_1, 0, 0, \beta'_1P_{d1} + \beta_1P'_{d1}, \beta'_1P_{d2}]$. Let $\bar{\Phi}$ is a square matrix whose second column is $[0, 0, 0, 0, 1]$. $\check{\Phi}$ is similar to $\bar{\Phi}$ except that 1 is at the fourth row instead of the last row.
2. Description of Matrix $\mathbf{U2}_k^{(j)}$: Matrix $\mathbf{B}_{\mathbf{U2}_k^{(j)}}$ has only the inner matrix $\mathbf{A}_{1B,\mathbf{B}_{\mathbf{U2}_k^{(j)}}}$ which is given by $Prd1(k, j)\beta'_2P'_{d2}\bar{\Phi}$. Similarly, $\mathbf{A}_{0,\mathbf{U2}_k^{(j)}}$ and $\mathbf{A}_{1,\mathbf{U2}_k^{(j)}}$ are the same as $\mathbf{B}_{\mathbf{U2}_k^{(j)}}$ except that the inner matrices $\mathbf{A}_{1B,\mathbf{A}_{0,\mathbf{U2}_k^{(j)}}}$ and $\mathbf{A}_{1B,\mathbf{A}_{1,\mathbf{U2}_k^{(j)}}}$, which are $Prd1(k, j)\beta_1P'_{d2}\bar{\Phi}$ and $Prd1(k, j)\beta'_1P'_{d2}\bar{\Phi}$, respectively.
3. Description of Matrix $\mathbf{U1B}_k^{(j)}$: Matrix $\mathbf{U1B}_k^{(j)}$ is the same as $\mathbf{U1}_k^{(j)}$ except the inner matrices $\mathbf{A}_{1B,\mathbf{B}_{\mathbf{U1B}_k^{(j)}}}$, $\mathbf{A}_{1B,\mathbf{A}_{0,\mathbf{U1B}_k^{(j)}}}$, and $\mathbf{A}_{1B,\mathbf{A}_{1,\mathbf{U1B}_k^{(j)}}}$ of $\mathbf{B}_{\mathbf{U1B}_k^{(j)}}$, $\mathbf{A}_{0,\mathbf{U1B}_k^{(j)}}$, and $\mathbf{A}_{1,\mathbf{U1B}_k^{(j)}}$, respectively which are replaced by $Prd1(k, j) \left[\hat{\Phi} + \beta'_2P'_{d2}\bar{\Phi} \right]$, $Prd1(k, j) \left[\beta_1\Phi + \beta_1P'_{d2}\bar{\Phi} \right]$, and $Prd1(k, j) \left[\tilde{\Phi} + \beta'_1P'_{d2}\bar{\Phi} \right]$, respectively.
4. Description of Matrix $\mathbf{V}_k^{(j,j-1)}$: The structure of $\mathbf{V}_k^{(j,j-1)}$ and elementary matrices used to construct $\mathbf{V}_k^{(j,j-1)}$ are similar to those of $\mathbf{U1}_k^{(j)}$ in which Ω , $\hat{\Omega}$, $\tilde{\Omega}$, $\bar{\Omega}$, and $\check{\Omega}$ are the same as Φ , $\hat{\Phi}$, $\tilde{\Phi}$, $\bar{\Phi}$, and $\check{\Phi}$, respectively, except that the elements are at the third column instead of the second column. Moreover, $Prd1(k, j)$ is substituted by $Prd2(k, j)$.

Table A.3. Elementary matrices of $\mathbf{V}_k^{(j,j)}$

Matrix	$\mathbf{B}_{\mathbf{V}_k^{(j,j)}}$	$\mathbf{C}_{\mathbf{V}_k^{(j,j)}}$	$\mathbf{A}_{0,\mathbf{V}_k^{(j,j)}}$	$\mathbf{A}_{1,\mathbf{V}_k^{(j,j)}}$	$\mathbf{A}_{2,\mathbf{V}_k^{(j,j)}}$	$\mathbf{A}_{1B,\mathbf{V}_k^{(j,j)}}$
\mathbf{B}_Q	Δ	$\check{\Delta}$	$\beta_1\Delta$	$\tilde{\Delta}$	$\beta'_1\check{\Delta}$	$\tilde{\Delta}$
\mathbf{C}_Q	$\bar{\Delta}$	$\mathbf{0}$	$\beta_1\bar{\Delta}$	$\beta'_1\bar{\Delta}$	$\mathbf{0}$	$\beta'_1\bar{\Delta}$
$\mathbf{A}_{0,Q}$	$\beta_2\Delta$	$\beta_2\check{\Delta}$	$\mathbf{0}$	$\mathbf{0}$	$\mathbf{0}$	$\mathbf{0}$
$\mathbf{A}_{1,Q}$	$\hat{\Delta}$	$\beta'_2\check{\Delta}$	$\beta_1\Delta$	$\tilde{\Delta}$	$\beta'_1\check{\Delta}$	$\tilde{\Delta}$
$\mathbf{A}_{2,Q}$	$\beta'_2\bar{\Delta}$	$\mathbf{0}$	$\beta_1\bar{\Delta}$	$\beta'_1\bar{\Delta}$	$\mathbf{0}$	$\beta'_1\bar{\Delta}$
$\mathbf{A}_{1B,Q}$	$\hat{\Delta}$	$\beta'_2\check{\Delta}$	$\beta_1\Delta$	$\tilde{\Delta}$	$\beta'_1\check{\Delta}$	$\tilde{\Delta}$

5. Description of Matrix $\mathbf{V}_k^{(j,j)}$: Table A.3 shows the elementary matrices of $\mathbf{V}_k^{(j,j)}$ where $j < N$. The elementary matrices used to construct matrix $\mathbf{V}_k^{(j,j)}$ are defined as follows. Let Δ be a square matrix which is $[Prn(k, j), Prs1(k, j), Prs2(k, j), 0, 0; 0, 0, 0, 1, 0; 0, 0, 0, 0, 1; Prn(i, j)P_{d1}, Prs1(i, j)P_{d1}, Prs2(i, j)P_{d1}, 0, 0; Prn(i, j)P_{d2}, Prs1(i, j)P_{d2}, Prs2(i, j)P_{d2}, 0, 0]$. $\hat{\Delta}$ is the same as Δ except that each element is multiplied by β'_2 in the first to the fourth rows and the last row is given as $(\beta'_2P_{d2} + \beta_2P'_{d2}) [Prn(i, j), Prs1(i, j), Prs2(i, j), 0, 0]$. $\check{\Delta}$ is also the same as Δ except that each element is multiplied by β'_1 in the first to the third rows and the last row while the fourth row is described by $(\beta'_1P_{d1} + \beta_1P'_{d1}) [Prn(i, j), Prs1(i, j), Prs2(i, j), 0, 0]$. Let $\bar{\Delta}$ be a square matrix whose last row is given by $P'_{d2} [Prn(i, j), Prs1(i, j), Prs2(i, j), 0, 0]$. $\tilde{\Delta}$ is the same as $\bar{\Delta}$ except that the last row is zero and the fourth row is described by $P'_{d1} [Prn, Prs1(i, j), Prs2(i, j), 0, 0]$.
6. Description of Matrix $\mathbf{V}_k^{(N,N)}$: Matrix $\mathbf{V}_k^{(N,N)}$ captures the status of when the low-priority orbit is full. The structure and elementary matrices used to construct matrix $\mathbf{V}_k^{(N,N)}$ are similar to those of $\mathbf{V}_k^{(j,j)}$. Ψ , $\hat{\Psi}$, $\check{\Psi}$, $\bar{\Psi}$, and $\tilde{\Psi}$ are the same as Δ , $\hat{\Delta}$, $\check{\Delta}$, $\bar{\Delta}$, and $\tilde{\Delta}$, respectively except elements in the first column. When the transmission requests of low-priority users in the orbit reaches N , transmission requests will be lost. Therefore, the first column of Ψ is described by $[Prn(k, j) + \sum_{x_2=1}^{n_2} Pri2(k, j, x_2), 0, 0, P_{d1}(Prn(k, j) + \sum_{x_2=1}^{n_2} Pri2(k, j, x_2)), P_{d2}(Prn(k, j) + \sum_{x_2=1}^{n_2} Pri2(k, j, x_2))]$. The first column of $\hat{\Psi}$ is the same as that of Ψ except the last element which is given as $(\beta'_2P_{d2} + \beta_2P'_{d2})(Prn(k, j) +$

$\sum_{x_2=1}^{n_2} Pri2(k, j, x_2)$). Similarly, the first column of $\tilde{\Psi}$ is the same as that of Ψ except that the third element which is described by $(\beta'_1 P_{d1} + \beta_1 P'_{d1})(Prn(k, j) + \sum_{x_2=1}^{n_2} Pri2(k, j, x_2))$. The last element in the first column of $\tilde{\Psi}$ is $P'_{d2}(Prn(k, j) + \sum_{x_2=1}^{n_2} Pri2(k, j, x_2))$. The fourth element in the first column of $\tilde{\Psi}$ is changed to $P'_{d1}(Prn(k, j) + \sum_{x_2=1}^{n_2} Pri2(k, j, x_2))$. Moreover, inner matrices $\mathbf{B}_{\mathbf{A}_{1B, \mathbf{V}_k^{(N, N)}}$, $\mathbf{A}_{1, \mathbf{A}_{1B, \mathbf{V}_k^{(N, N)}}$, and $\mathbf{A}_{1B, \mathbf{A}_{1B, \mathbf{V}_k^{(N, N)}}$ of matrix $\mathbf{A}_{1B, \mathbf{V}_k^{(N, N)}}$ are given as $\tilde{\Psi}^\triangleright$ which is the same as $\tilde{\Psi}$ except that the second element in the fourth row is added with $Prd1(k, j)\beta'_1 P'_{d1}$.

7. Description of Matrix $\mathbf{V}_k^{(j, j+x_2)}$: The structure and inner matrices of $\mathbf{V}_k^{(j, j+x_2)}$ are similar to those of $\mathbf{V}_k^{(j, j)}$. The differences are that the elementary matrices Δ , $\hat{\Delta}$, $\tilde{\Delta}$, $\bar{\Delta}$, and $\check{\Delta}$ are replaced by Γ , $\hat{\Gamma}$, $\tilde{\Gamma}$, $\bar{\Gamma}$, and $\check{\Gamma}$, respectively. Let Γ be a square matrix whose first column is given by $Pri2(k, j, x_2)[1, 0, 0, P_{d1}, P_{d2}]$. Similarly, let $\hat{\Gamma}$ be a square matrix whose first column is given as $Pri2(k, j, x_2)[\beta'_2, 0, 0, \beta'_2 P_{d1}, \beta'_2 P_{d2} + \beta_2 P'_{d2}]$. $\tilde{\Gamma}$ is a square matrix whose first column is described by $Pri2(k, j, x_2)[\beta'_1, 0, 0, \beta'_1 P_{d1} + \beta_1 P'_{d1}, \beta'_1 P_{d2}]$. Let $\bar{\Gamma}$ be a square matrix whose first column is $Pri2(k, j, x_2)[0, 0, 0, 0, P'_{d2}]$. $\check{\Gamma}$ is similar to $\bar{\Gamma}$ except that P'_{d1} is at the fourth row and the last row is zero. In the case of $x_2 = 1$, inner matrices $\mathbf{A}_{1B, \mathbf{B}_{\mathbf{V}_k^{(j, j+x_2)}}$, $\mathbf{A}_{1B, \mathbf{A}_{1, \mathbf{V}_k^{(j, j+x_2)}}$, and $\mathbf{A}_{1B, \mathbf{A}_{1B, \mathbf{V}_k^{(j, j+x_2)}}$ of elementary matrices $\mathbf{B}_{\mathbf{V}_k^{(j, j+x_2)}}$, $\mathbf{A}_{1, \mathbf{V}_k^{(j, j+x_2)}}$, and $\mathbf{A}_{1B, \mathbf{V}_k^{(j, j+x_2)}}$ are $\beta'_2 \hat{\Gamma}^\triangleright$, $\tilde{\Gamma}^\triangleright$, and $\check{\Gamma}^\triangleright$, respectively where $\hat{\Gamma}^\triangleright$ is $\hat{\Gamma}$ added with $P'_{d2} [Prn(k, j), Prs1(k, j), Prs2(k, j), 0, 0]$ at the last row and $\tilde{\Gamma}^\triangleright$ is $\tilde{\Gamma}$ added with $\beta'_1 P'_{d2} [Prn(k, j), Prs1(k, j), Prs2(k, j), 0, 0]$ at the last row. When $j+x_2$ reaches N , the only difference between $\mathbf{V}_k^{(j, j+x_2)}$ and $\mathbf{V}_k^{(j, j+x_2=N)}$ is the replacement of $Pri2(k, j, x_2)$ by $\sum_{x_2=(N-j)+1}^{n_2} Pri2(k, j, x_2)$ which indicates that the orbit of low-priority users is full. The transmission requests will be lost due to collision.
8. Description of Matrix $\mathbf{W}_k^{(j, j-1)}$: All elements of $\mathbf{W}_k^{(j, j-1)}$ are zero except at the lowest right corner matrix $(\mathbf{A}_{1B, \mathbf{W}_k^{(j, j-1)}}$. $\mathbf{A}_{1B, \mathbf{W}_k^{(j, j-1)}}$ is a square matrix whose main diagonal elements are $[\eta \dots \eta]$. η is also a square matrix in which the elements at the third column are $[0, 0, 0, Prd2(k, j)\beta'_1 P'_{d1}, 0]$.
9. Description of Matrix $\mathbf{W}_k^{(j, j)}$: The structure and elementary matrices of $\mathbf{W}_k^{(j, j)}$ are similar to those of $\mathbf{V}_k^{(j, j+x_2)}$ except that $Pri2(k, j, x_2)$ is replaced by $Pri1(k, j, x_1)$.

Moreover, $\mathbf{A}_{1B, \mathbf{W}_k^{(j,j)}}$ is the same as $\mathbf{A}_{1, \mathbf{W}_k^{(j,j)}}$ except the case that $x_1 = 1$. $\mathbf{A}_{1B, \mathbf{W}_k^{(j,j)}}$ is different from $\mathbf{A}_{1, \mathbf{W}_k^{(j,j)}}$ to indicate that the transmission queue of high-priority users is full. The transmission request will go to the orbit upon its arrival. Therefore, the fourth rows of matrices $\mathbf{B}_{\mathbf{A}_{1B, \mathbf{W}_k^{(j,j)}}}$, $\mathbf{A}_{1, \mathbf{A}_{1B, \mathbf{W}_k^{(j,j)}}}$ and $\mathbf{A}_{1B, \mathbf{A}_{1B, \mathbf{W}_k^{(j,j)}}}$ of $\mathbf{A}_{1B, \mathbf{W}_k^{(j,j)}}$ are added by

$\beta'_1 P'_{d1} [Prn(k, j), Prs1(k, j), Prs2(k, j), 0, 0]$. $\mathbf{W}_k^{(N,N)}$ is also the same as $\mathbf{W}_k^{(j,j)}$ except that $Pr1(k, j, x_1)$ is substituted by $Pr1(k, j, x_1) + \sum_{x_2=1}^{n_2} Pri12(k, j, x_1, x_2)$.

10. Description of Matrix $\mathbf{W}_k^{(j,j+x_2)}$: The structure and inner matrices of $\mathbf{W}_k^{(j,j+x_2)}$ are the same as those of $\mathbf{V}_k^{(j,j+x_2)}$ except that $Pri2(k, j, x_2)$ is replaced by $Pri12(k, j, x_1, x_2)$. Moreover, in the case of $x_2 = 1$, matrix $\mathbf{A}_{1B, \mathbf{B}_{\mathbf{W}_k^{(j,j+x_2)}}}$, $\mathbf{A}_{1B, \mathbf{A}_{0, \mathbf{W}_k^{(j,j+x_2)}}}$, $\mathbf{A}_{1B, \mathbf{A}_{1, \mathbf{W}_k^{(j,j+x_2)}}}$, and $\mathbf{A}_{1B, \mathbf{A}_{1B, \mathbf{W}_k^{(j,j+x_2)}}}$ of inner matrices $\mathbf{B}_{\mathbf{W}_k^{(j,j+x_2)}}$, $\mathbf{A}_{0, \mathbf{W}_k^{(j,j+x_2)}}$, $\mathbf{A}_{1, \mathbf{W}_k^{(j,j+x_2)}}$, and $\mathbf{A}_{1B, \mathbf{W}_k^{(j,j+x_2)}}$, respectively are added with $Pr1(k, j, x_1)\beta'_1 P'_{d2}$ at the last element of the first column in the block matrices.